Jahresbericht 2004

des Lehrstuhls von Prof. Dr. Winfried Petry

Physik Department E13

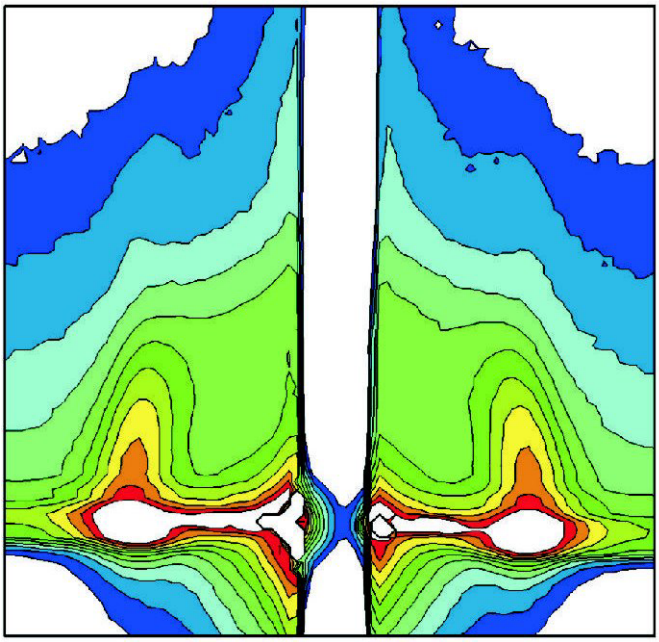

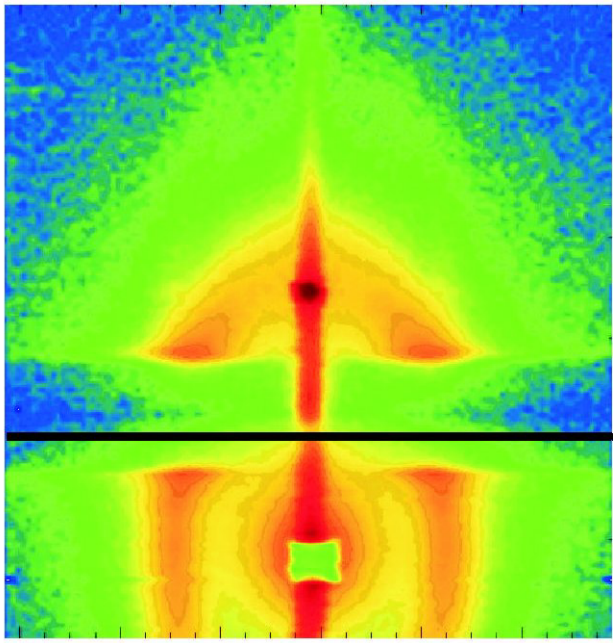

Technische Universität München

Prof. Dr. Winfried Petry
Lehrstuhl für Experimentalphysik IV
Physik Department E13

Leitung des Lehrstuhls in Vertretung für Prof. Petry:
Prof. Dr. Andreas Meyer

Physik Department E13
Technische Universität München
James-Franck-Straße
D-85748 Garching

Sekreteriat: Elke Fehsenfeld

Tel.: 089 289 12452
Fax: 089 289 12473

Email: ameyer@ph.tum.de
efehsen@ph.tum.de
http://www.e13.physik.tu-muenchen.de

Titelblatt:

Die Anwendungen von dünnen Polymerfilmen sind vielfältig. Zum Beispiel kommen multikomponentige Polymerfilme als Klebstoffe zum Einsatz. Mit dünnen Filmen aus Blockcopolymerfilmen können nanostrukturierte Oberflächen erzeugt werden. Um die Strukturen an der Oberfläche und im Filminnern zu untersuchen, sind die Röntgen- und Neutronen-Kleinwinkelstreuung unter streifendem Einfall hervorragend geeignet. Das linke Bild zeigt ein Streubild eines dünnen Diblockcopolymerfilms, das mit Röntgenkleinwinkelstreuung unter streifendem Einfall aufgenommen wurde. Die im Film vorhandenen lateral geordneten Strukturen erzeugen ähnlich zu Braggrods eine erhöhte Intensität rechts und links vom Primärstrahlfänger. Das rechte Bild wurde mit Neutronenkleinwinkelstreuung unter streifendem Einfall aufgenommen. Da der untersuchte Triblockcopolymerfilm und das Substrat transparent für Neutronen sind, konnten simultan die oberflächennahen Strukturen zusammen mit der Volumenstruktur detektiert werden. Die Streuung im Bildteil oberhalb der Linie resultiert aus der reflektierten und unterhalb der Linie aus der transmittierten Kleinwinkelstreuung. Die geordneten Strukturen sind zur Oberflächennormalen verkippt.

s. Beiträge von C. M. Papadakis und P. Müller-Buschbaum

Vorwort

Das letzte Jahr zeichnete sich durch einige einschneidende Ereignisse für unseren Lehrstuhl E13 aus:
Winfried Petry hat einen Ruf an die Universität Dresden mit Doppelfunktion als Direktor des Forschungszentrums Rossendorf abgelehnt und stattdessen den Ruf auf die Stelle des Wissenschaftlichen Direktors des FRM-II für weitere vier Jahre angenommen. Ich danke Winfried Petry und der Fakultät für das Vertrauen, das sie mir durch die Übertragung der komissarischen Leitung des Lehrstuhls für weitere vier Jahre entgegengebracht haben.
Am 2. März erreichte der FRM-II seine erste Kritikalität. Am 21. Oktober war die nukleare Inbetriebnahme des FRM-II durch Abbrand von äquivalent 52 Tagen à 20 MW erfolgreich beendet. Die Inbetriebnahme des Neutronenflugzeitspektrometers ToF-ToF von E13 schreitet gut voran. Mit Ana Gaspar haben wir weitere Verstärkung für die Testphase erhalten. Mit ersten Experimenten rechnen wir fest im April diesen Jahres.
Die Brillouin – Apparatur in unserem Lichtstreulabor wurde von Emmanuel Longueteau wieder in Betrieb genommen. Durch den Umbau konnte die Stabilität der Apparatur deutlich erhöht und die Intensität bei vergleichbarem Untergrund um eine Größenordnung gesteigert werden. Zusammen mit der Konstruktion und dem Bau eines 1300°C – Ofens mit einer Platin – Drahtschlinge als Probenhalter können jetzt an der Apparatur die Mechanismen der Ionenleitung und der strukturellen Relaxation in oxidischen Schmelzen über vier Dekaden in der Frequenz untersucht werden.
Auf dem Gebiet der kernresonanten Streuung von Synchrotronstrahlung engagieren wir uns weiterhin in der Fortentwicklung der gestörten Winkelkorrelation zur Untersuchung von Relaxationsvorgängen in Schmelzen. Cornelius Strohm vertritt diesbezüglich unser neues Projekt an der European Synchrotron Radiation Facility in Grenoble zu eisenhaltigen Silikatschmelzen.
Im März fand der erste *Workshop on Dynamics in Viscous Liquids* in München statt. Es ist uns gelungen, ohne einen einzigen eingeladenen Vortrag eine große Zahl derjenigen Wissenschaftler zum Workshop zu begrüßen, die in den letzten Jahren entscheidende Beiträge zu diesem Arbeitsgebiet geleistet haben. Das Programmkommittee konnte aus 150 Beiträgen ein sehr attraktives wissenschaftliches Programm zusammenzustellen, welches sich auch durch eine große Anzahl jüngerer Kollegen/innen ausgezeichnet hat. Der zweite Workshop on Dynamics in Viscous Liquids wird mit gleichem Konzept im März 2006 in Mainz stattfinden.

Dieser Bericht gibt Aufschluss über die hohe Qualität der Forschung an E13. Diese stellt sich dar durch eine große Anzahl hochwertiger Veröffentlichungen und eingeladener Vorträge, durch einige sehr intensive internationale Zusammenarbeiten, aber auch durch die sehr erfolgreiche Einwerbung von Drittmitteln. Wir engagieren uns auch weiter verstärkt in der Lehre, sowohl durch die Durchführung von Grund- und Nebenfachvorlesungen und Praktika, als auch in der Lehrerfortbildung durch die Organisation der Edgar-Lüscher Seminare.

Für das Jahr 2005 wünsche ich mir und den Mitarbeitern von E13 weiterhin eine so fruchtbare Forschungs- und Lehrtätigkeit wie im vergangenen Jahr.

Andreas Meyer *Januar 2005*

1 Structured polymer systems

Christine M. Papadakis

In the beginning of 2004, my group started to work at E13. Since then, we have been exploring the new (excellent) possibilities in Munich and have found a number of collaboration partners - a new home!

The work of my group is focussed on block copolymer systems, in thin film geometry, in the melt and in solution. Using grazing-incidence small-angle X-ray scattering, we have been studying thin films of lamellar diblock copolymers and have observed an unexpected dependence of the lamellar orientation on the block copolymer molar mass. The phase behavior of blends of diblock copolymers has been found to strongly influenced by the confining thin film geometry. Advanced analysis methods are necessary to quantitatively understand the scattering patterns.

In 2004, we have completed a long lasting investigation on the dynamics of block copolymer melts in different ordered morphologies using dynamic light scattering. The dynamics in the micellar, body-centered cubic state was found to be qualitatively different from the cylindric, hexagonal and the lamellar morphology.

Slow dynamics in a diblock copolymer melt in the body-centered cubic state

C.M. Papadakis, F. Rittig[1], K. Mortensen[2], K. Almdal[2], P. Štěpánek[3]

[1] BASF AG GKP/P, Ludwigshafen
[2] Danish Polymer Centre, Risø National Laboratory, Roskilde, Denmark
[3] Institute of Macromolecular Chemistry, Academy of Sciences of the Czech Republic, Prague

Besides the disordered state, diblock copolymer melts form a variety of morphologies, e.g. the lamellar, the hexagonal and the body-centered cubic (bcc) phase. This variety of structures makes block copolymer melts an ideal model system for studying the influence of the structure on the collective and translational dynamics. We have studied a series of poly(ethylene propylene)-poly(dimethylsiloxane) (PEP-PDMS) diblock copolymer melts in all these morphologies, which allows us to identify and compare the dynamic processes without changing the chemical properties of the system [1].

In the present study, we have examined a very asymmetric poly(ethylene propylene)-poly(dimethylsiloxane) (PEP-PDMS) diblock copolymer melt forming the disordered and the body-centered cubic morphology with the PEP and PDMS blocks forming the micellar cores and the matrix, respectively [2]. The PEP-PDMS system has the advantage that a large temperature range is accessible. The sample has a molar mass of 23.6 kg/mol and a volume fraction of PEP of 0.16. Small-angle neutron scattering (SANS) experiments were carried out at the PAXY instrument at the Laboratoire Léon Brillouin, CEA Saclay, France. The sample was mounted in a shear sandwich cell in a modified RSA II rheometer and was macroscopically oriented by large-amplitude oscillatory shear (Fig. 1.1a). The order-to-disorder transition is revealed by a significant drop in the dynamic shear and loss moduli measured at small shear amplitude (Fig. 1.1b). The two-dimensional SANS spectra show a number of Bragg reflections below 279°C which can be

indexed with the reciprocal lattice of a twinned body-centered cubic structure having the common $\langle\bar{1}11\rangle$-axis parallel to the shear axis (Fig. 1.1c). Above 279°C, the SANS spectrum shows a broad ring, as expected from the concentration fluctuations in the disordered state (Fig. 1.1d).

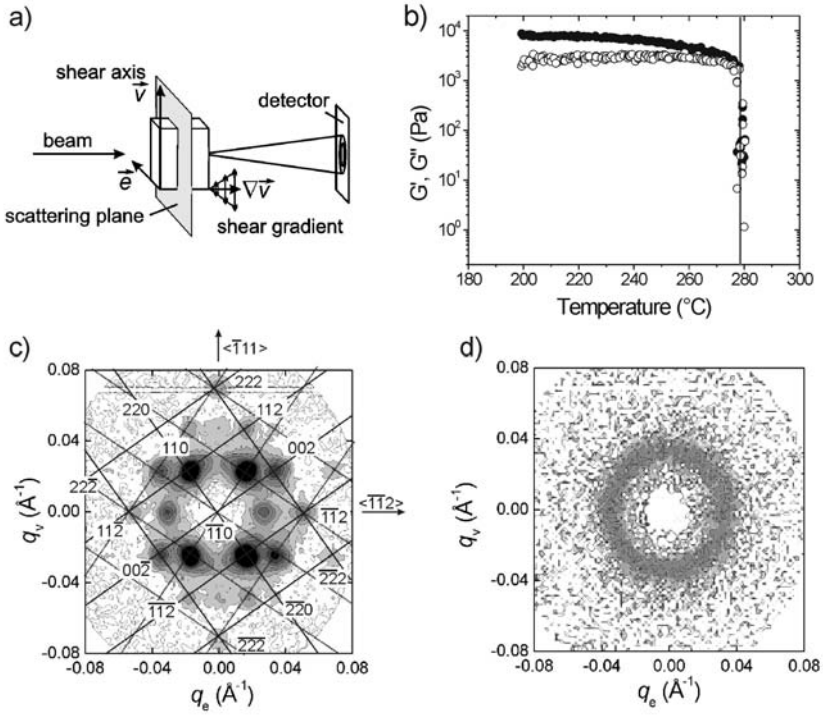

Figure 1.1:
(a) Set-up for SANS on a shear-oriented sample. The detector is an area detector. (b) Dynamic shear (●) and loss modulus (○) as a function of temperature.(c) Two-dimensional SANS spectrum measured at 24°C after shear alignment and equilibration. The full and dashed lines indicate the reciprocal lattice expected for a twinned bcc structure with the common $\langle\bar{1}11\rangle$-axis parallel to the shear axis $\vec{v}$ and the $\langle\overline{11}2\rangle$-axis parallel to the neutral axis $\vec{e}$. The indexing is given for the domain marked by full lines. (d) Two-dimensional SANS spectrum measured at 280°C. In both images, the intensity scale is logarithmic and covers three decades.

The dynamics of a quenched (i.e. non-oriented) sample were studied using dynamic light scattering (DLS). Fig. 1.2 shows the resulting distribution functions of relaxation times τ obtained by Inverse Laplace Transformation of the DLS autocorrelation functions. In the disordered state, the well-known heterogeneity mode (self-diffusion of copolymers through the melt) is observed together with the slow cluster mode. The origin of the latter is unclear. In the literature, it has been tentatively attributed to be related to long-range density fluctuations close to the glass transition; however, our results show that it is present with a significant amplitude more than 329 K above the highest glass transition temperature (PEP: -56°C), which is contradictory to a connection to the glass transition.

In the bcc state, the heterogeneity mode and the cluster mode vanish, and two modes having different characteristics appear. The fast mode has an activation energy close to the one of pure PDMS (see the Arrhenius-representation in Fig. 1.2d). We attribute it to fluctuations of the micellar distance which relax by diffusion of copolymers not bound to micelles ('free chains') through the

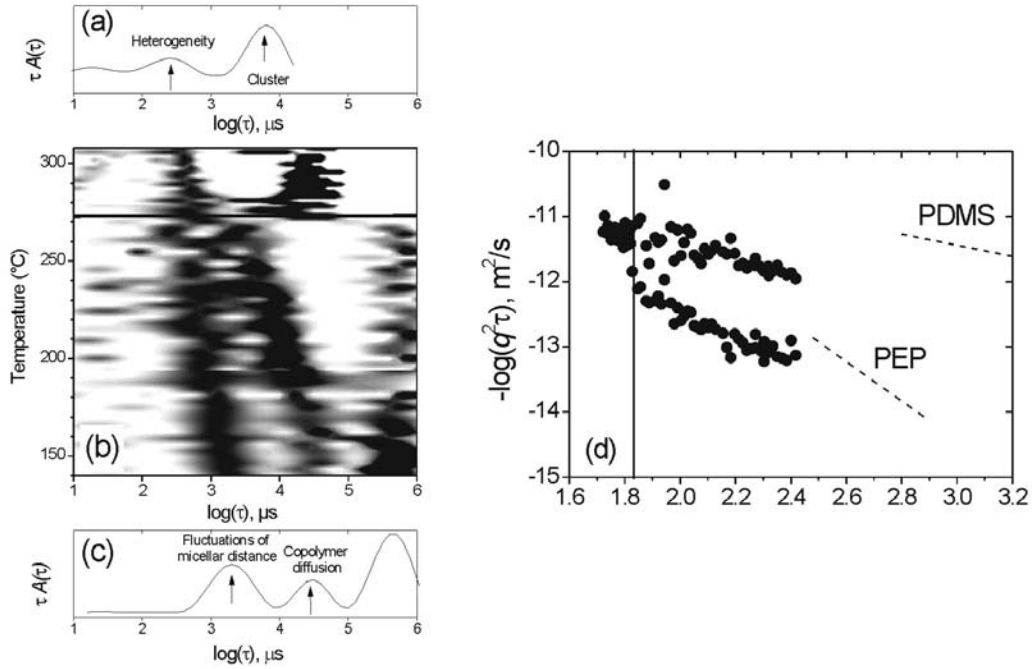

Figure 1.2:
(a) Distribution function of relaxation times τ obtained by Inverse Laplace Transformation of the DLS intensity autocorrelation function at 306°C. (b) Compilation of distribution functions as a function of decay time and temperature. The curves were normalized such that the amplitude of the fast mode both in the disordered and the bcc state is unity. The intensity scale is linear and ranges from zero (white) to one (black). The horizontal black line in (b) indicates the ODT as identified using DLS. Arrows mark the modes discussed in the text. (c) Distribution function at 140°C. (d) Arrhenius-representation of $(q^2\tau)^{-1}$ obtained from DLS (•). q is the scattering vector. The dashed lines represent the self-diffusion coefficients of the homopolymers having the same molar mass as the block copolymer. The vertical line indicates the ODT.

PDMS matrix. This process has been observed by us before on a similar sample [3]. The slow mode has a stronger temperature dependence, and the related diffusion coefficient is even lower than the one of the high friction component, PEP, having the same molar mass as the diblock copolymer. We attribute this mode to the long-range diffusion of single copolymers through the bcc structure, which involves diffusion through the matrix from micelle to micelle. Because of the increase in contact between the different blocks, when diffusing through the matrix, this motion is an activated process. The assignment is corroborated by the good agreement of the reduced diffusivities with data from the literature on chemically different systems.

This work was funded by Deutsche Forschungsgemeinschaft within the Sonderforschungsbereich 294 'Moleküle in Wechselwirkung mit Grenzflächen' at the University of Leipzig (Projects D4 and G4).

[1] C.M. Papadakis, F. Rittig, J. Phys. Cond. Matter, submitted.

[2] C.M. Papadakis, F. Rittig, K. Almdal, K. Mortensen, P. Štěpánek, Eur. Phys. J. E, **15**, 359 (2004).

[3] C.M. Papadakis, K. Almdal, K. Mortensen, F. Rittig, G. Fleischer, P. Štěpánek, Eur. Phys. J. E **1**, 275 (2000).

Aggregation behavior of amphiphilic block copolymers in aqueous solution

T. B. Bonné, R. Ivanova, K. Lüdtke [1], R. Jordan[1], P. Štěpánek[2], C. M. Papadakis

[1] Lehrstuhl für Makromolekulare Stoffe, Chemie Department, TU München
[2] Institute of Macromolecular Chemistry, Academy of Sciences of the Czech Republic, Prag

Amphiphilic block copolymers in solution exhibit a very rich phase behavior, depending on temperature, concentration, chemical composition and architecture of the copolymers and the solvent used. They can form unimers, micelles as well as ordered phases. We study a versatile system, based on oxazolines (fig. 1.3), where the hydrophobicity can be tuned by changing the length of the side chain. Furthermore, this polymer system has the advantage that fluorescence groups can be chemically attached to the polymer at different positions.

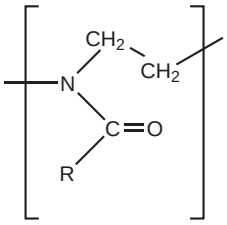

Figure 1.3:
Structure of an oxazoline monomer. R is an alkyl side chain, which can be varied in length, thereby altering the hydrophobicity.

We have studied the aggregation behavior of poly[(2-methyl-2-oxazoline)-*b*-(2-nonyl-2-oxazoline)] block copolymers in aqueous solution using fluorescence correlation spectroscopy (FCS) and dynamic light scattering (DLS) [1].

In temperature resolved DLS experiments, we found, that after dissolution at room temperature, a metastable state is formed, consisting of very large aggregates, possibly due to crystallization of the nonyl blocks in the solid state. After heating the solutions, the micelles assume their equilibrium size of $\sim$ 12 nm. The critical micelle concentration (CMC) was below the detection limit of DLS and no information about the unimers could be obtained either. FCS, a single molecule technique, offers these possibilities.

In our FCS experiments, fluorescence labeled polymers were used as tracers in aqueous solutions of otherwise identical, non fluorescence labeled polymers. In this way, a large concentration range could be accessed without over-saturating the detector and we could determine the diffusion coefficients of the labeled unimers and micelles and determine the CMC.

Figure 1.4 shows the hydrodynamic radius as a function of concentration for two diblock copolymers, having similar block lengths and being labeled on the hydrophilic part (Fig. 1.4A) and on the hydrophobic part (Fig. 1.4B). With FCS very low concentrations are accessible (down to $\sim 10^{-8}$ M) and the CMC's at $\sim 10^{-5}$ can be detected. In addition, the hydrodynamic radius of the labeled unimers can be determined and the values compare well with the molecular sizes.

Neither the CMC nor the micellar hydrodynamic radius are significantly influenced by the position of the dye.

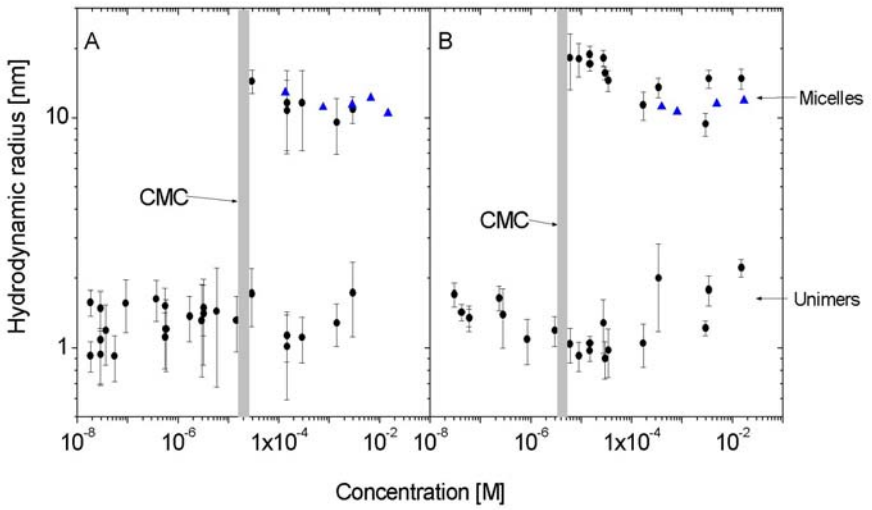

Figure 1.4:
Hydrodynamic radii from aqueous solutions of poly[(2-methyl-2-oxazoline)-*b*-(2-nonyl-2-oxazoline)] in dependence on concentration. The polymers are been labeled with the fluorescence dye TRITC on the hydrophilic end (A) and on the hydrophobic end (B), respectively. The solutions were annealed prior to measurement. Circles: results from FCS, triangles: results from DLS.

By comparing the hydrodynamic radii obtained using DLS with those from FCS on annealed samples, we have shown that the hydrodynamic radii of micelles can reliably be determined using FCS.

This work was funded by Deutsche Forschungsgemeinschaft (PA 771/2-1)

[1] T. B. Bonné, K. Lüdtke, R. Jordan, P. Štěpánek and C. M. Papadakis, Coll. Polym. Sci.**282**, 833 (2004)

Aggregation behavior of lipophilic-hydrophilic-fluorophilic triblock copolymers in aqueous solution

R. Ivanova, T. B. Bonné, T. Komenda[1], K. Lüdtke[1], R. Jordan[1] and C. M. Papadakis

[1] Fakultät für Chemie, TU München

The aggregation behavior of block copolymers containing fluorophilic moieties is currently a topic of large interest and a variety of chemical compositions and architectures are investigated [1-3]. The project described here is focused on the aggregation behavior and the micellar network formation in aqueous solutions of novel poly(2-oxazoline)-based triblock copolymers and polymer

surfactants containing lipophilic, hydrophilic and fluorophilic moieties studied by small-angle x-ray and neutron scattering. These polymers represent a versatile system with readily adjustable molecular architecture, hydrophilic-lipophilic balance and degree of block segregation [4-6]. The

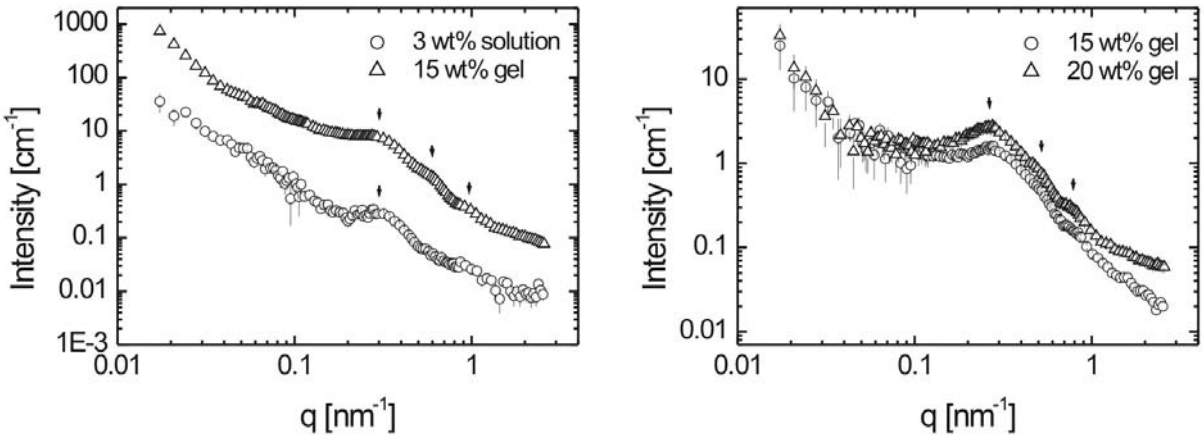

Figure 1.5:
SANS scattering profiles at 25 •C: (left) $PNOx_7$-$PMOx_{38}$-$PFOx_7$ and (right) $PNOx_{12}$-$PMOx_{64}$-$PFOx_9$. The arrows mark the characteristic peaks.

presence of a fluorophilic moiety increases strongly the degree of segregation and allows to reach the strong segregation regime at low degrees of polymerization. These novel polymers [5,6] offer the possibility to design aqueous multi-compartment systems where two kinds of solvates can be dissolved. Such systems have large practical potential, for example in the pharmaceutical industry as selective vehicles for drug delivery.

We have studied poly[(2-n-nonyl-2-oxazoline)$_n$-b-(2-methyl-2-oxazoline)$_m$-b-(2-(1'H,1'H,2'H,2'H-perfluorohexyl)-2-oxazoline)$_k$] triblock copolymers ($PNOx_n$-$PMOx_m$-$PFOx_k$). In aqueous solutions these polymers are expected to form a micellar network [3]. The central question of the present study is the structure of the micellar network, i.e. whether the network consists of separate micelles with lipophilic and fluorophilic cores linked by the hydrophilic blocks or of mixed lipophilic/fluorophilic micelles. Other issues are the micellar size and shape as well as the effect of the polymer concentration on the microstructure. The effect of the hydrophilic block length was studied using two triblock copolymers, $PNOx_7$-$PMOx_{38}$-$PFOx_7$ and $PNOx_{12}$-$PMOx_{64}$-$PFOx_9$. The polymers were selected so to have comparable main chain length of the fluorophilic and the lipophilic blocks and significantly different degree of polymerization of the hydrophilic blocks.

The triblock copolymers form micellar solutions at concentrations higher than the critical micelle concentration. At even higher concentrations, the solutions transform into gels. The scattering profiles of the solutions show one characteristic peak related to the correlations between the micelles (Fig. 1.5, left). The profiles of the gels show more than one peak, i. e. higher correlation between the micelles and/or highly ordered structure as illustrated in Fig. 1.5, left. With increasing

the polymer concentration even further, the correlation peaks become more intense and pronounced but remain at the same q position that indicates an increase of the order in the microstructure without change of the correlation length (Fig. 1.5, right).

The microstructure of the gels is expected to be that of a micellar network consisting of separate lipophilic or fluorophilic micelles [3]. This assumption is supported by our SANS experiments showing that the corresponding diblock copolymers do not form mixed lipophilic/fluorophilic micelles. In the case of $PNOx_{12}$-$PMOx_{64}$-$PFOx_9$ the gel formation starts at about 6 wt % (5.6 mmol/l), while in the case of $PNOx_7$-$PMOx_{38}$-$PFOx_7$ at about 12 wt % (17.6 mmol/l). Or in other words, the shorter the hydrophilic block (acting as a spacer separating the lipophilic and the fluorophilic micelles) the higher molecular concentration is needed in order to bridge the two types of micelles and form a gel.

In order to determine the gel microstructure and prove the formation of a micellar network consisting of separate lipophilic and fluorophilic micelles, further data evaluation such as construction of the most suitable model and fits are ongoing. The obtained measurements on an absolute scale are essential in order to create the best model of the scattering curves.

[1] Zh. Li, E. Kesselman, Y. Talmon, M. A. Hillmyer, and T. P. Lodge, Science **306**, 98 (2004)

[2] A. Kotzev, A. Laschewsky, P. Adriaensens, and J. Gelan, Macromolecules,**35**, 1091 (2002)

[3] R. Weberskirch, J. Preuschen, H. W. Spiess, and O. Nuyken Macromol. Chem. Phys. **201**, 995 (2000)

[4] R. Jordan, K. Martin, H. J. Rädler, K. K. Unger, Macromolecules **38**, 8858 (2001)

[5] T. Komenda, PhD thesis, TU München, 2004.

[6] T. Komenda, R. Jordan, Polymer Preprints **44**, 986 (2003).

Morphological transition in thin lamellar diblock copolymer films

C.M. Papadakis, P. Busch[1], D. Posselt[2], D.-M. Smilgies[3]

[1] Materials Science and Engineering, Cornell University, Ithaca NY, USA

[2] IMFUFA (Department of Mathematics and Physics), Roskilde University, Denmark

[3] Cornell High-Energy Synchrotron Source (CHESS), Cornell University, Ithaca NY, USA

Nanostructured surfaces formed by diblock copolymer films are of increasing importance for many different purposes, as described in recent reviews [1,2]. The attractive feature of block copolymers is their spontaneous tendency to self-organize into ordered structures (e.g., lamellae, cylinders on a hexagonal lattice, spheres on a body-centered cubic lattice) which can be controlled by choosing the block copolymer molar mass and the relative block volumes. The pattern repeat distance is typically of the order of 100 - 1000 Å, thus making nanolithography possible. Thin, lamellar films based on diblock copolymers may be of interest for a variety of applications, for instance as photonic band gap materials [3], as wave guides and for the confinement of particles within the lamellar layers [4].

An understanding of the mechanisms governing the structurization of thin, supported diblock copolymer films is of key importance for a controllable exploitation of such structures. A number

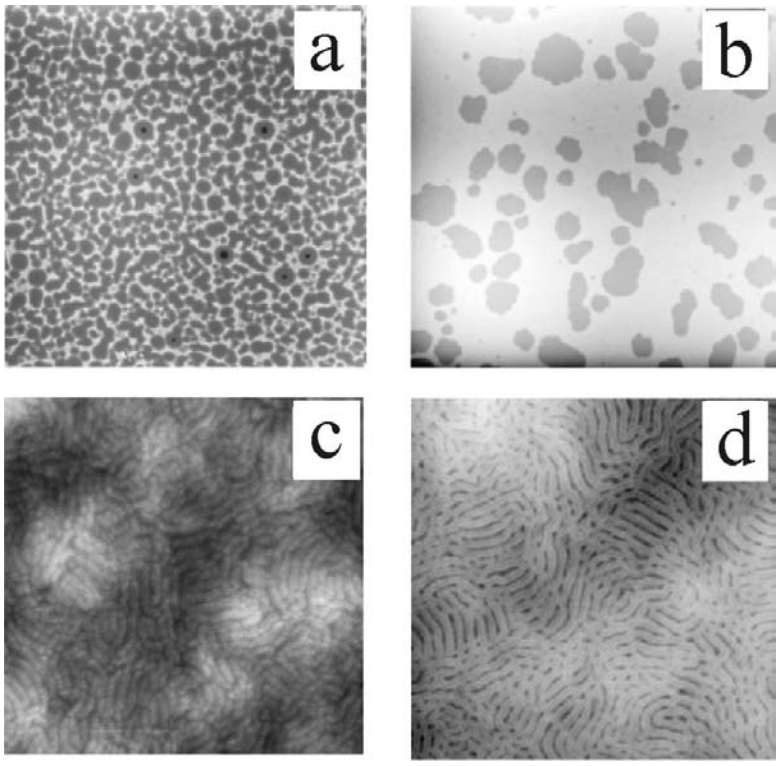

Figure 1.6:
AFM images from two low molar mass ($\bar{M}_n = 22.6$ kg/mol, $D_{\rm lam} = 197$ Å, upper row)and two high molar mass P(S-*b*-B) films (183 kg/mol, $D_{\rm lam} = 839$ Å, lower row) with different reduced film thicknesses [8,9]: (a) $D_{\rm red} = 2.1$, image size 50×50 μm^2, height scale 500 Å, (b) $D_{\rm red} = 8.0$, image size 100×100 μm^2, height scale 1200 Å, (c) $D_{\rm red} = 2.8$, image size 3×3 μm^2, height scale 200 Å, (d) $D_{\rm red} = 8.8$, image size 3×3 μm^2, height scale 400 Å. In all images, the height scale ranges from black (low) to white (high).

of experimental methods have been applied in this context, e.g., imaging in real space and scattering methods using x-rays or neutrons. We have studied thin films of lamellar poly(styrene-*b*-butadiene) (P(S-*b*-B)) diblock copolymer melts on Si substrates with a native SiO_x layer using atomic force microscopy (AFM) and grazing-incidence small-angle X-ray scattering (GISAXS, Refs. 5 – 9).

The lamellar orientation in thin, supported films of P(S-*b*-B) diblock copolymers as found using AFM shows a characteristic dependence on the block copolymer molar mass [8]. Typical images from tapping mode AFM on a low and a high molar mass sample for low and high values of the reduced film thickness $D_{\rm red} = D_{\rm film}/D_{\rm lam}$ are compiled in Fig. 1.6, $D_{\rm film}$ denoting the film thickness and $D_{\rm lam}$ the bulk lamellar thickness. The low molar mass films (upper row) display holes in the surface layer with heights similar to $D_{\rm lam}$, regardless of $D_{\rm red}$. The surfaces of the high molar mass films (lower row), on the other hand, display a lamellar texture. For samples with intermediate molar masses ($\bar{M}_{\rm n}$ = 54.5 and 69.9 kg/mol), the AFM images do not show well-defined textures, which may be caused by coexisting lamellar orientations in the film. The lamellar orientations resulting from a number of samples as observed at the film surface using AFM – parallel for 13.9–54.5 kg/mol and perpendicular for 148 and 183 kg/mol – are compiled in an orientation diagram as a function of the block copolymer molar mass and $D_{\rm red}$ in Fig. 1.7a. The

surface topographies of the low and high molar mass samples are consistent with the parallel and the perpendicular lamellar orientation; however, a unique determination of the lamellar orientation *within* the film is impossible from the AFM images alone. Hence, we have performed GISAXS measurements in order to elucidate the inner film structure.

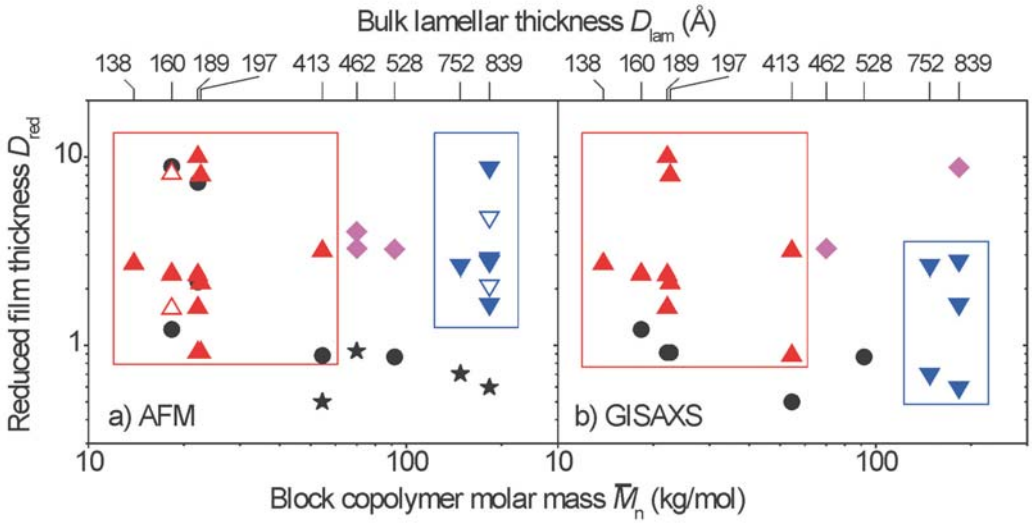

Figure 1.7:
Lamellar orientation as a function of the molar mass and D_{red}. Results from AFM (a) and from GISAXS (b). The top-axis gives the bulk lamellar thicknesses, D_{lam}. Triangles up: parallel, triangles down: perpendicular, diamonds: coexisting orientations, stars: weak surface texture, circles: no surface texture or scattering observed.

In our GISAXS experiments at beam line ID10B at the European Synchrotron Radiation Facility and at D-line at the Cornell High-Energy Synchrotron Source (CHESS), the incidence angle, α_i, was chosen to be slightly above the critical angle of external reflection of the polymer film, α_{cP}, which is typically of the order of 0.2°. Under these conditions, X-rays penetrate films up to several 1000 Å completely, absorption by the substrate is minimized, and the scattering volume is maximized. The scattering in the plane of incidence, i.e., normal to the film surface (q_z), and parallel to the film surface (q_y) is recorded simultaneously by means of a two-dimensional CCD camera. Measuring times as low as seconds lead to satisfying scattering images.

The GISAXS intensity maps display a wealth of information on the lamellar structure of the diblock copolymer films. The map of the thin, high molar mass film from Fig. 1.6c shows straight out-of-plane Bragg rods (Fig. 1.8c). Their q_y-positions are independent of q_z and correspond to 762 ± 46 Å, a value similar to the bulk lamellar thickness of 839 ± 13 Å. We conclude that the lamellae are perpendicular to the film surface throughout the film. No signs of other lamellar orientations are visible in the GISAXS intensity map. Straight Bragg rods are present in the GISAXS intensity map of the thick, high molar mass film from Fig. 1.6d as well (Fig. 1.8d). In addition to

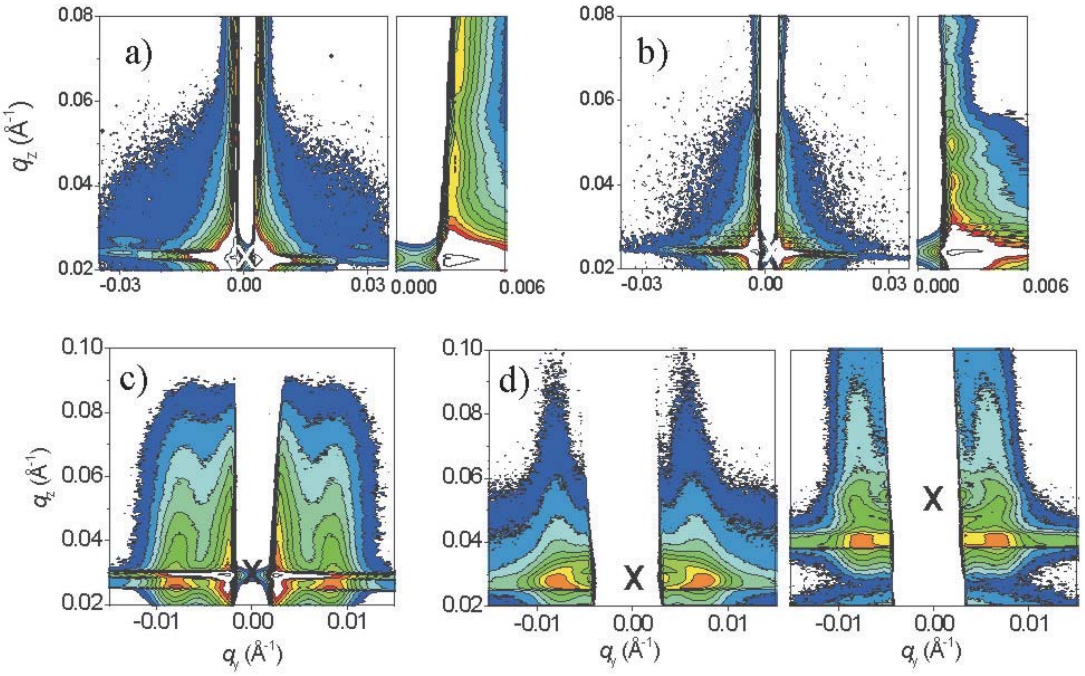

Figure 1.8:
GISAXS images from the same samples as in Fig. 1.6: $\bar{M}_n = 22.6$ kg/mol, $D_{\mathrm{lam}} = 197$ Å(upper panel), 183 kg/mol, $D_{\mathrm{lam}} = 839$ Å(lower panel). The white, vertical stripes at $q_y \approx 0$ are due to the beam stop. The crosses indicate the position of the specularly reflected beam. (a) $D_{\mathrm{red}} = 2.1$, $\alpha_i = 0.16°$, (b) $D_{\mathrm{red}} = 8.0$, $\alpha_i = 0.17°$, (c) $D_{\mathrm{red}} = 2.8$, $\alpha_i = 0.21°$, (d) $D_{\mathrm{red}} = 8.8$, $\alpha_i = 0.20°$ (left) and 0.38° (right). The narrow panels in (a) and (b) show regions of low q_y.

these straight rods, a ring of high intensity is observed. In the map measured at $\alpha_i = 0.38°$ (right image in Fig. 1.8d), it is seen that the ring is centered around the specularly reflected beam. Its radius corresponds to a repeat distance of ~ 900 Å, a value 8 % higher than D_{lam}, and we therefore attribute it to a Debye-Scherrer ring (well-known from transmission scattering from powders) around the specularly reflected beam. This indicates that lamellae with orientations other than perpendicular are present in the film.

The thick, low molar mass film from Fig. 1.6b (Fig. 1.8b) gives rise to completely different scattering: No Bragg rods are observed at the q_y-values corresponding to the bulk lamellar thickness (± 0.032 Å^{-1}); instead, the intensity at $q_z \approx 0$ shows peaks, probably due to diffuse Bragg sheets related to roughness correlations between lamellae with interfaces parallel to the film/substrate interface. For several images with $\alpha_i = 0.18$–$0.21°$, the position of the peak at $q_z = 0.05$-0.06 Å^{-1} is close to the one predicted by the Born approximation for the first-order Bragg reflection of lamellae with $D_{\mathrm{lam}} = 197$ Å. Similar scattering is observed from the thin, low molar mass film from Fig. 1.6a, also pointing to parallel lamellae (Fig. 1.8a). However, due to the low number of lamellae forming the film, the peaks at $q_z \approx 0$ are not as pronounced, and a quantitative analysis of their q_z-positions is beyond Born approximation.

The lamellar orientations within the films as deduced from the GISAXS maps are compiled in

Fig. 1.7b. For most samples, the same orientation as at the film surface (from AFM) is obtained using GISAXS: The lamellae are parallel for molar masses between 13.9-54.5 kg/mol and perpendicular for 148 and 183 kg/mol in a wide range of D_{red}-values. Only for thick, high molar mass films, the bulk limit seems to be reached, and other lamellar orientations are observed within the film.

We conclude that in thin, supported films of lamellar P(S-*b*-B) on Si/SiO_x, the lamellar orientation can be controlled by molar mass. This behavior can be explained by entropic contributions to the free energy of a lamellar block copolymer system near a hard wall. These contributions become important because both blocks are relatively non-polar and thus neither the substrate/film interface nor the film surface are strongly selective to one of the blocks. Furthermore, it is interesting that in P(S-*b*-B), the perpendicular orientation is formed spontaneously – without any prepatterning of the substrate or outer fields, leading to surfaces structured on length scales below 1000Å.

This work was funded by Deutsche Forschungsgemeinschaft (PA 771/1-1) and by NATO within a Collaborative Linkage Grant (PST.CLG.978046).

[1] I.W. Hamley, Nanotechnology **14**, R39 (2003).

[2] M. Lazzarri, M.A. López-Quintela, Adv. Mater. **15**, 1583 (2003).

[3] A. Urbas, Y. Fink, E.L. Thomas, Macromolecules **32**, 4748 (1999).

[4] V. Lauter-Pasyuk, H. Lauter, G. Gordeev, P. Müller-Buschbaum, B.P. Toperverg, W. Petry, M. Jernenkov, A. Petrenko, V. Aksenov, Physica B **350** E939 (2004).

[5] D.-M. Smilgies, P. Busch, C.M. Papadakis, D. Posselt, Synchr. Rad. News **15**, 35 (2002).

[6] P. Busch, T. Bonné, D. Smilgies, D. Posselt, C.M. Papadakis, CHESS News Magazine 2002, p. 37.

[7] P. Busch, D.-M. Smilgies, D. Posselt, F. Kremer, C.M. Papadakis, Macromol. Chem. Phys. **204**, F18 (2003).

[8] P. Busch, D. Posselt, D.-M. Smilgies, B. Rheinländer, F. Kremer, C.M. Papadakis, Macromolecules **36**, 8717 (2003).

[9] C.M. Papadakis, P. Busch, D. Posselt, D.-M. Smilgies, Adv. Solid State Phys. **44**, 327 (2004).

Inner film structures in thin films of binary blends of diblock copolymers

C.M. Papadakis, P. Busch[1], D. Posselt[2], D.-M. Smilgies[3], M. Rauscher[4]

[1] Materials Science and Engineering, Cornell University, Ithaca NY, USA
[2] IMFUFA (Department of Mathematics and Physics), Roskilde University, Denmark
[3] Cornell High-Energy Synchrotron Source (CHESS), Cornell University, Ithaca NY, USA
[4] MPI für Metallforschung, Stuttgart

The thin film geometry has frequently been used in order to study the influence of a confining geometry on the structure of polymeric systems. Thin block copolymer films represent a convenient model system because the inherent length scale in block copolymer melts - the lamellar thickness for compositionally symmetric diblock copolymers - is relatively large (typically 100-1000Å) and may be of the same order of magnitude as typical thicknesses of thin spin-coated polymer films. The effects of confinement by the thin film geometry on the mesoscopic structure – for instance

on the lamellar orientation – thus can become very pronounced. In order to understand the mechanisms leading to the formation of these structures, it is important not only to know the surface structure of the films (which is readily available using atomic force microscopy, AFM), but also the structure within the films. Grazing-incidence small-angle X-ray scattering (GISAXS) offers this possibility. The GISAXS set-up is shown schematically in Fig. 1.9.

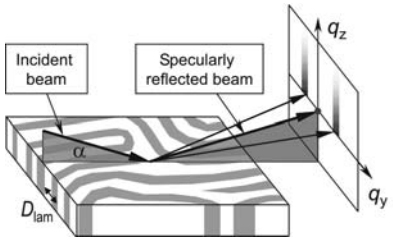

Figure 1.9:
Set-up used for GISAXS experiments. The X-ray beam hits the sample at an angle α_i slightly larger than the critical angle of external reflection. The transmitted beam serves as the primary beam for small-angle scattering from the polymer film, which is detected by a CCD camera. The beam stop protects the camera from the intense reflected beam.

We have studied thin, spin-coated films of binary blends of compositionally symmetric polystyrene-polybutadiene (PS-*b*-PB) diblock copolymers differing in overall molar mass. We had previously observed that the lamellae are parallel to the substrate surface for PS-*b*-PB diblock copolymers of low molar mass (13.9-54.5 kg/mol), whereas they are perpendicular for high molar masses (148 and 183 kg/mol, [1,2]). We have blended a high and a low molar mass (PS-*b*-PB) diblock copolymer (148 and 21.6 kg/mol, respectively) in different mixing ratios. In the bulk, these blends form (i) a one-phase lamellar morphology with a lamellar thickness between the ones of the pure copolymers (for a volume fraction of short chains $\phi_s \leq 0.35$) or (ii) for $\phi_s = 0.40$-0.95, a macrophase-separated phase consisting of two types of lamellar domains, having lamellar thicknesses of ~ 412 and ~ 194 Å [3,4].

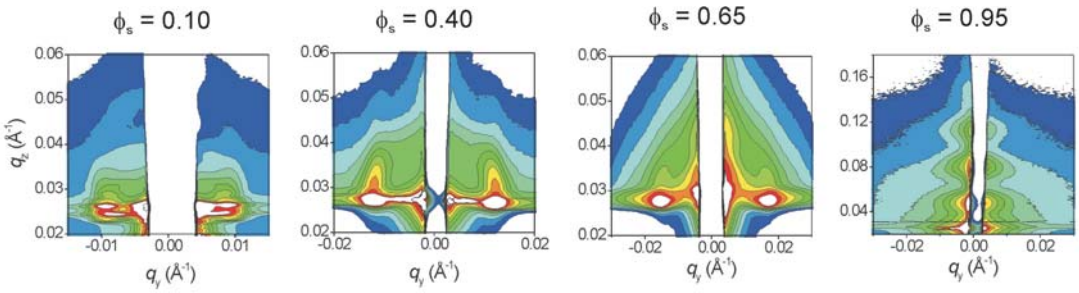

Figure 1.10:
GISAXS maps from thin films of binary blends of PS-*b*-PB films of different mixing ratios.

The results from the GISAXS measurements are compiled in Fig. 1.10. The AFM image of a blend from the lamellar one-phase state ($\phi_s = 0.10$) shows a lamellar surface texture (not shown). GISAXS reveals straight Bragg rods out of the plane of incidence at positions close to those expected from the bulk lamellar thickness, i.e. the lamellae consisting of both short and long copolymers are perpendicular to the substrate surface. This behavior reflects the one known from thin films of pure PS-*b*-PB diblock copolymers having similar lamellar thickness.

A blend containing mainly short copolymers ($\phi_s = 0.95$), on the other hand, displays strong intensity modulations in the plane of incidence, which are located near the positions predicted for lamellar of thickness 190 Å, i.e. the film contains predominantly thin lamellae parallel to the film

surface, as expected from thin films of pure (PS-*b*-PB) diblock copolymers having similar lamellar thickness.

The GISAXS maps from blends from the macrophase-separated regime are more complex. A blend, which in the bulk is in the middle of the macrophase-separated regime ($\phi_s = 0.65$), shows Bragg rods at positions expected from the larger bulk lamellar thickness (393 Å). The thicker lamellae are thus mainly perpendicular to the substrate surface, as expected from thin films of pure PS-*b*-PB diblock copolymers. The Bragg rods are not straight, but bent towards the plane of incidence, indicating the presence of other orientations as well. For a sample close to the phase boundary between the one-phase and the macrophase-separated state ($\phi_s = 0.40$), straight Bragg rods from perpendicular lamellae with thicknesses of 520 Å – thus much larger than expected from the bulk lamellar thicknesses – dominate the scattering map. This may be due to a lower fraction of short copolymers present in the domains consisting of thick lamellae than in the bulk. The mixing behavior of this sample is thus strongly influenced by the thin film geometry.

The present study shows that complex behavior may be observed in thin nanostructured polymer films, which can be studied in great detail by scattering methods.

This work was funded by Deutsche Forschungsgemeinschaft (PA 771/1-1) and by NATO within a Collaborative Linkage Grant (PST.CLG.978046).

[1] P. Busch, D. Posselt, D.-M. Smilgies, B. Rheinländer, F. Kremer, C.M. Papadakis, Macromolecules **36**, 8717 (2003).

[2] C.M. Papadakis, P. Busch, D. Posselt, D.-M. Smilgies, Adv. in Solid State Phys. **44**, 327 (2004).

[3] C.M. Papadakis, K. Mortensen, D. Posselt, Eur. Phys. J. B **4**, 325 (1998).

[4] C.M. Papadakis, K. Mortensen, D. Posselt, Macromol. Symp. **149**, 99 (2000).

Quantitative analysis of grazing-incidence small-angle scattering maps from thin films of lamellar diblock copolymers

C.M. Papadakis, P. Busch[1], M. Rauscher[2], D.-M. Smilgies[3], D. Posselt[2]

[1] Materials Science and Chemical Engineering, Cornell University, Ithaca NY, USA
[2] MPI für Metallforschung, Stuttgart
[3] Cornell High-Energy Synchrotron Source (CHESS), Cornell University, Ithaca NY, USA
[4] IMFUFA (Department of Mathematics and Physics), Roskilde University, Denmark

Nanostructured block copolymer films are promising candidates for a number of applications. In order to be able to understand and control the film structures and their stability, it is important not only to gain knowledge on the surface texture, but also on the internal structure of the films. Experimental methods such as atomic force microscopy (AFM), electron microscopy, X-ray or neutron reflectometry have been frequently applied; however, these methods only provide limited information. Grazing-incidence is a convenient tool to study the internal structure of thin, supported polymer films. The X-ray beam hits the sample at an angle α_i, and a two-dimensional image of the scattering gives simultaneous information on the lateral and vertical structures in the film. Even though in thin films of microphase-separated diblock copolymers the X-ray contrast between the blocks is relatively weak, the use of incident angles around the critical angle of total external

reflection of the polymer film, α_{cP}, enables one to investigate the internal film structures with high spatial (up to 1000 Å) and temporal resolution (a few seconds, Ref. 1).

The penetration depth of the X-rays into the polymer film can be controlled by varying α_i: Below α_{cP},the X-rays do not penetrate into the polymer film, but an evanescent wave is formed below the film surface. Above α_{cP}, the penetration depth increases sharply, and by varying α_i, the thickness of the layer giving rise to the scattering can be tuned. The critical angle of the poly(styrene-*b*-butadiene) (PS-PB) films studied by us is 0.15°, whereas the critical angle of the Si/SiO_xsubstrate is 0.22°. In our GISAXS experiments, α_i was kept fixed for a specific GISAXS map (usually below 0.4°), and the scattering was recoded over a range of exit angles of 2°.

For scattering close to α_{cP}, a purely kinematic theory such as the Born approximation is not adequate, and rather the distorted-wave Born approximation (DWBA) has to used [2]. We have applied the DWBA to the case of lamellar diblock copolymer films with the lamellar interfaces either parallel or perpendicular to the film surface [3,4]. The potential describing the sample is split up into (i) the scattering from a homogeneous film with ideal planar interfaces and (ii) the scattering from the internal, lamellar structure. Dynamical effects such as total external reflection, refraction at the film surface and reflections from the substrate are included [5].

For the perpendicular lamellar orientation, the DWBA calculations predict that the diffuse scattering cross-section factorizes into two parts: (i) the Fourier Transform of the lateral, lamellar structure (being a function of $q_{||}$ only) displaying peaks at multiplums of $2\pi/D_{\rm lam}$ ($D_{\rm lam}$ denotes the lamellar thickness) and (ii) a part depending on q_z only, containing information on the film thickness. The scattering map thus contains Bragg rods, which corresponds well with the experimental observations: The GISAXS maps of films with perpendicular lamellae show bands of high intensity (Bragg rods) on the left and right of the plane of incidence with maxima near the critical wave vectors of the substrate and the polymer film (Fig. 1.11a).

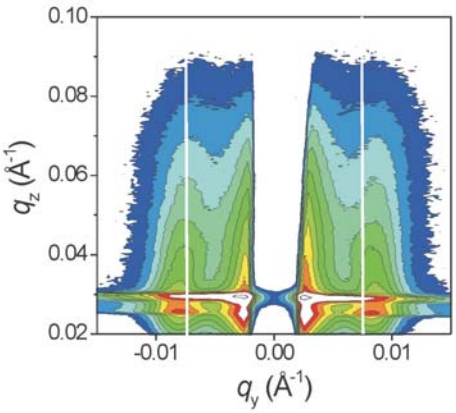

Figure 1.11:
GISAXS map of a lamellar PS-PB film with perpendicular lamellae. $D_{\rm lam} = 839$ Å. The film thickness is $2.8 \times D_{\rm lam}$. $\alpha_i = 0.19°$. The white stripe in the middle is due to the beam stop protecting the camera from the intense reflected beam. The vertical white lines indicate the positions where Bragg rods are expected.

For the parallel lamellar orientation, we have taken into account the roughness of both the lamellar interfaces and the film surface and have assumed them to be small compared to the lamellar thickness with Gaussian distributions. The lamellar interfaces are furthermore assumed to be perfectly correlated. Again, the in-plane structure of the lamellae (dependent on $q_{||}$) and the information about the stacking of the lamellae (dependent on q_z) factorizes. A calculation for a film with eight lamellae stacked (corresponding to one of our films studied experimentally) yields intensity

profiles along q_z displaying well-defined peaks. Comparison with the experimental intensity profiles obtained for several α_i shows good coincidence (Fig. 1.12). For large enough α_i, the Born approximation is recovered.

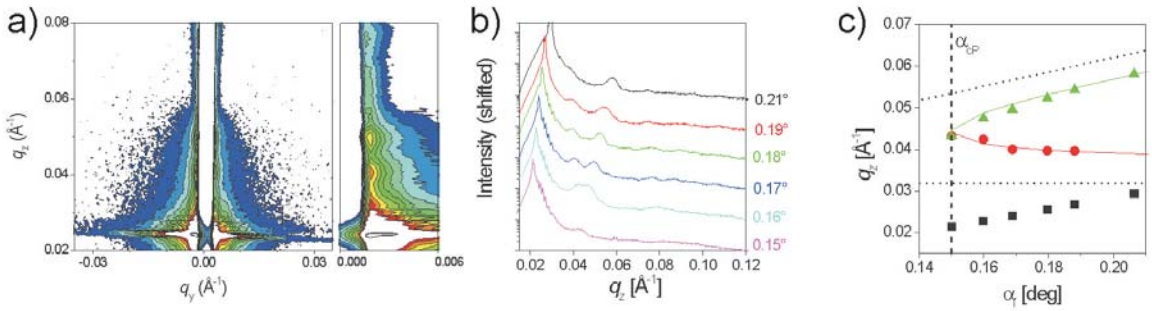

Figure 1.12:
(a) GISAXS map of a lamellar PS-PB film with parallel lamellae. $D_{\rm lam} = 197$ Å. The film thickness is $8.0 \times D_{\rm lam}$. $\alpha_i = 0.19°$. The right part is a close-up of the region close to the beamstop. (b) Integrated intensities over a stripe between $q_{||} = -0.005$ and +0.005Å^{-1} for the α_i-values given in the figure. (c) Comparison of the experimentally obtained peak positions (symbols) with the ones calculated for the same $D_{\rm lam}$-value (lines). The squares denote the positions of the specularly reflected beam, the triangles and circles the diffuse peaks. The dotted lines indicate the Born approximation.

In principle, the same information is obtained in a reflectivity measurement for parallel lamellae, but many angles of incidence and exit have to be scanned which may be time-consuming. In addition, the resulting lamellar concentration profile is not necessarily unique. Furthermore, for the weak internal contrast inherent to polymer films, the statistics obtained in X-ray reflectometry are not sufficient, and neutron reflectometry on partially deuterated samples are in order. The structures due to perpendicular lamellae cannot be monitored in reflectivity measurements. Thus, GISAXS combined with a quantitative analysis in the framework of the DWBA is a powerful tool to investigate nanostructured polymer films.

This work was funded by Deutsche Forschungsgemeinschaft (PA 771/1-1) and by NATO within a Collaborative Linkage Grant (PST.CLG.978046).

[1] D.-M. Smilgies, P. Busch, C.M. Papadakis, D. Posselt, Synchr. Rad. News **15**, 35 (2002).

[2] S. Dietrich, A. Haase, Phys. Rep. **260**, 1 (1995).

[3] P. Busch, D. Posselt, D.-M. Smilgies, B. Rheinländer, F. Kremer, C.M. Papadakis, Macromolecules **36**, 8717 (2003).

[4] P. Busch, M. Rauscher, D.-M. Smilgies, D. Posselt, C.M. Papadakis, in preparation.

[5] M. Rauscher, T. Salditt, H. Spohn, Phys.Rev. B **25**, 16855 (1995).

Inhaltsverzeichnis

2 Polymer Interfaces

Polymers offer additional characteristics in material science as compared to metals and ceramics. In this context, polymer interfaces are of importance because they largely effect the mechanical, optical or structural properties. Research is directed towards the improved understanding of the relation between structure and function. Different topics, such as surface wettability, the stabilization of thin polymer films, polymeric nanostructures, magnetic nanoparticles inside polymer matrices and polymeric adhesives have been continuously addressed. Model systems of high tech applications demanding two-dimensional polymer films are focussed. Techniques for a controlled and tailor made design of polymeric surface structures were established. With advanced scattering techniques using synchrotron radiation as well as neutrons at large scale facilities and a complementary real space analysis the interfacial structures are determined. This includes the development of characterization techniques, such as scanning sub-microbeam grazing incidence small angle scattering. Due to the unique combination of an x-ray beam with a sub-micrometer diameter and the surface sensitive scattering technique GISAXS a local structural investigation becomes accessible by scattering.

Dewetting of confined polystyrene films as a function of the applied surface clean

E. Bauer, P. Müller-Buschbaum

The wetting behavior of thin polymer films is of major interest in technical applications like dielectrics or coatings, as well as in fundamental science. Since the cleaning is the first step in every dewetting experiment to guarantee equal starting conditions we investigate the influence of the cleaning on the dewetting of thin polystyrene films [1]. To emphasis on the influence of the applied surface clean on the film stability the regime of confined films is addressed. In the confinement regime the film thickness is comparable to the radius of gyration of the unperturbed polymer chain. Films of a corresponding thickness are possible to prepare by the spin-coating technique.

Four different cleaning procedures such as rubbing with a toluene soaked KIMMWIPE, 24 hours of storage in Milli-Q-water, cleaning in an acid bath as well as in a base bath are compared. The used substrates are Si (100) wafers which are coated with an ultra thin polystyrene (PS, with a molecular weight of M_W=27500 g/mol and a narrow weight distribution M_W /M_N = 1.04) film. The substrate cleaning was applied immediately before the spin-coating of the PS film. The spin-coating conditions were optimized to result in PS films with a continuous thickness. Depending on the interfacial potential, the PS film can be meta-stable or unstable, which results in a dewetting of the initially homogenous film. In a final dewetting state the film is transformed into an arrangement of isolated polymeric drops on the bare Si surface.

As the final preparation step the samples were exposed to heat load on a heating plate at 130°C and quenched down to room temperature after the desired time. A series of different heating times for each cleaning procedure was performed to obtain the different dewetting stages beginning with the homogeneous film and ending up with droplets on the surface in two cases. Due to the initially prepared film thickness in the confinement regime and due to mass conservation, the resulting structures are well below the optical resolution limit. As a consequence, the obtained structures were probed by atomic force microscope (AFM) and by grazing incidence small angle x-ray scattering (GISAXS). The GISAXS measurements were performed at the beamline BW4

of the HASYLAB/DESY in Hamburg. The wavelength of the incident beam was 0.138 nm. The samples were placed horizontally in the GISAXS sample chamber at 12.56 m distance from the 2D detector (Gabriel). Most of the flight path, including the sample chamber were evacuated to reduce air scattering. An incident angle $\alpha = 0.325°$ slightly above the critical angle of the substrate material was selected. Thus on the one hand the important scattering features, namely the specular and the Yoneda peak, are well separated along the detector, and on the other hand the intensity is larger as compared to a further increase incident angle.

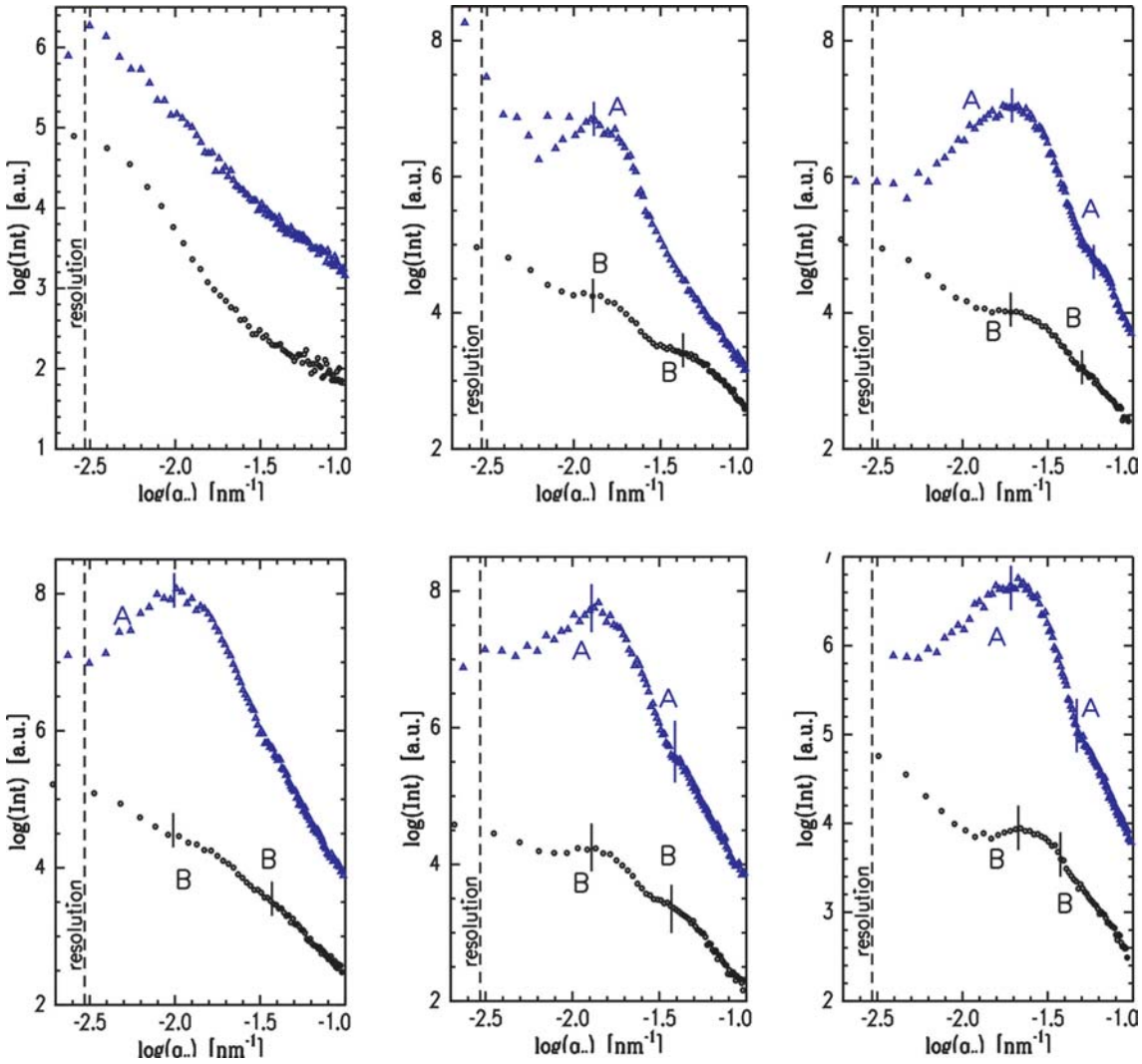

Figure 2.1:
PSD-curves of the AFM data (triangles) and horizontal cuts at the critical angle of PS of the GISAXS measurements (dots) for toluene cleaned samples. From the upper left to the lower right the annealing time increases from 0 to 180 minutes. In each graph the data are shifted vertically for clarity. The broken lines denote the resolution limit of the GISAXS measurements and A and B mark dominant length scales respectively.

From the two-dimensional intensity distribution typical vertical and horizontal cuts were performed instead of handling the full 2d information. For the position of the horizontal cuts the critical angle of PS ($\alpha_c = 0.138°$) was chosen to probe the structures created by the polymer. Of cause

the Si substrate is not effected by the annealing at the chosen temperature. As compared to the evolving polymeric structures it is flat. It was found out that the cleaning strongly alters the wetting behavior of the PS film. Time scales as well as final states differ as a function of the applied clean. The water stored and the toluene cleaned samples show patterns which are attributed to a typical dewetting scenario, starting with holes in the initially closed film which are growing with increasing heat load, forming islands and finally drops. In contrast, for the base and the acid bath cleaned samples no such behavior was found. After more than 100 hours heating just small holes had formed.

As an example in 2.1 GISAXS data of the toluene cleaned samples are displayed. To compare the length scales in reciprocal space the AFM data were 2d-Fourier transformed and the resulting power spectral density functions are included in the figure as well. A good agreement between the out-of plane data and the data calculated from the AFM measurements is observed. It has to be noted, that both techniques, scattering and AFM strongly differ in the probed surface area (more than a factor of 100), which results in a higher statistical relevance of the scattering data. Thus from the good agreement between both we can conclude that the AFM measurements have been representative for the present surface structure. Therefore the peaks have to be identified with different types of surface features: growing holes, islands with defined size and distance and finally drops [2].

So it is clear that for a better understanding of experiments and for a useful comparison detailed information about the prior cleaning should be given since the physics of the systems will strongly depend on the actual surface chemistry of the surface under investigation.

[1] P. Müller-Buschbaum; Eur. Phys. J. **12**, 443 (2003)

[2] E. Bauer, E. Maurer, P. Müller-Buschbaum; to be published

Local defects in thin polymer films: A scanning sub-microbeam grazing incidence small angle scattering investigation

P. Müller-Buschbaum, S.V. Roth [1], M. Burghammer [1], E. Bauer, S. Pfister, C. David [2], C. Riekel [1]

[1] ESRF, Grenoble (France)

[2] PSI, Villigen (Switzerland)

Solvent evaporation presents a simple route in controlling the alignment of nanostructures in thin polymer films. Evaporation of solvent is highly directional (normal to the surface) and the solvent imparts substantial mobility to the polymer. The addition of flow of the solution can be used to induce orientation. By the presence of a contact line oriented perpendicular to the flow direction two orthogonal fields result. However, flow in thin films can introduce instabilities or defects as well.

In the present investigation the structures resulting from evaporation-assisted flow of a polymeric blend of polystyrene (PS) with a molecular weight M_w= 207k (M_w/M_n=1.02) and poly-n-buthylacrylate (PnBA) with M_w=260k (M_w/M_n=3.78) are addressed. Both polymers were blended in a ratio of PS:PnBA= 3:7 wt% in a toluene solution and subjected to a flow at room temperature conditions. A three-phase contact line on the Si(100) substrate (pre-cleaned in an acid

bath prior to the deposition of the blend solution) oriented perpendicular to the flow direction was established. In the dry state, a special defect type resulting from an instability is observed. Several micro-cracks aligned parallel to the initial contact line resulted. The surface topography resulting after solvent evaporation was probed with atomic force microscopy (AFM) using tapping mode.

Fig. 2.2 shows typical examples of a micro-crack in the elsewhere continuous blend film. The surface of the blend film is dominated by the phase separation structure. The black regions in fig. 2.2a display the micro-crack. Its lateral extension is on the order of 5 μm. It is oriented perpendicular to the original flow direction and parallel to the three-phase contact line. However, on a very local scale it slightly deviates from this main crack orientation as typically observable in cracks in polymeric material. These deviations result from local heterogeneities due to phase separation in the blend film. Fig. 2.2b shows the corresponding 3d visualization of the AFM data. The film-substrate interface was positioned with respect to the mean blend film thickness of 800 nm (as determined by ellipsometry). Thus the crack nearly extends down to the substrate. Inside the crack region a few PS islands remained. While on a local scale the surface structure is nicely pictured by AFM, scattering is usually applied to obtain a mean statistical information. With grazing incidence small-angle x-ray scattering (GISAXS) a length regime comparable to AFM is addressed [1]. A local scattering information becomes accessible by combining GISAXS with a micro-sized x-ray beam [2, 3]. We demonstrate the actual possibilities of this technique by locally probing the micro-crack with a beam diameter of 0.9 μm. The experiments were performed at the ID13 beamline (ESRF, Grenoble) at a wavelength of λ= 0.097 nm [4]. The crack was aligned parallel to the incoming beam (see fig.2.2b), because the footprint of the x-ray beam on the surface is extended to 0.9$\times$52.4 μm due to the fixed incident angle α_i=0.983^o.

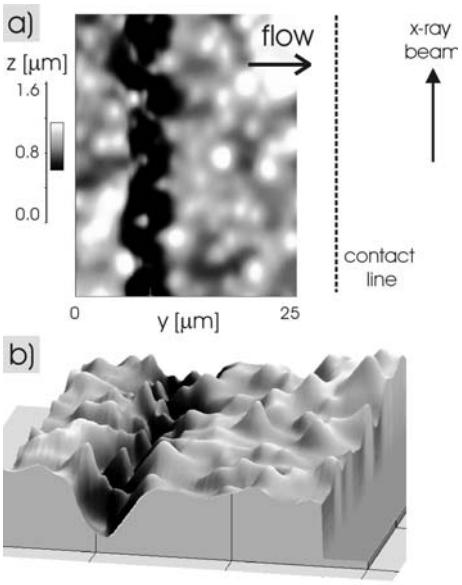

Figure 2.2:
AFM pictures (scan range $25 \times 40 \mu$m^2) of the topology as observed after toluene evaporation. In the elsewhere continuous film a micro-crack has formed. The blend surface is covered with small drops. a) In the sub-microbeam GISAXS experiment the crack was aligned parallel to the incoming x-ray beam. b) The crack nearly extends down to the substrate surface.

By shifting the sample perpendicular to the incoming beam in steps of $\Delta y = 1\mu$m the crack and the surrounding film were scanned. Instead of presenting the resulting 2d GISAXS pattern, fig. 2.3a comprises the detector scans as a function of the sample position y. We have chosen the contour plot presentation to emphasize on the changes in the amplitude of the Yoneda peak. In the region of the micro-crack (see fig. 2.3) the Yoneda peak has a much lower intensity as compared to the surrounding blend film. Internal and surface roughness induced by the phase separation of the blend cause an increased Yoneda scattering. In contrast, in the crack region the film obviously

appears to be smoother. Smooth polymer films as well as the Si surface result in a very low Yoneda scattering [4].

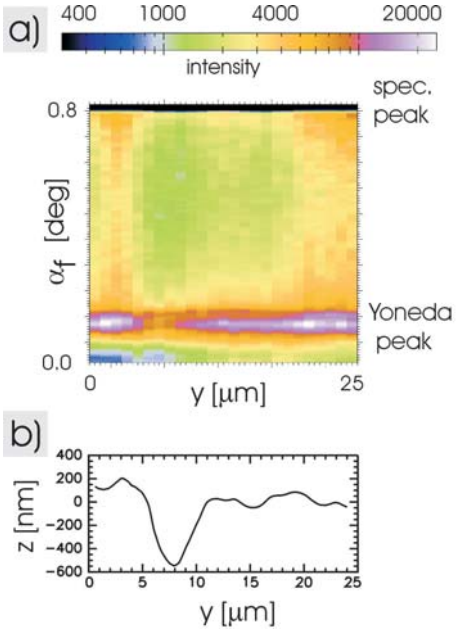

Figure 2.3:
a) Close-up of the ($y\alpha_f$)-mapping in the region around the Yoneda peak: With the sub-microbeam GISAXS experiment a region of 25 μm was scanned in steps of Δy=1 μm. b) Representative line from the AFM data visualizing the micro-crack.

This work was financially supported by the DFG Schwerpunktprogramm SPP 1164 *Nano- and Microfluidics* (Mu1487/2).

[1] P. Müller-Buschbaum, Anal. Bioanal. Chem. **376**, 3 (2003)

[2] P. Müller-Buschbaum, S.V. Roth, M. Burghammer, A. Diethert, P. Panagiotou, C. Riekel; Europhys. Lett. **61**, 639 (2003)

[3] S.V. Roth, M. Burghammer, C. Riekel, P. Müller-Buschbaum, A. Diethert, P. Panagiotou, H. Walter; Appl. Phys. Lett. **82**, 1935 (2003)

[4] P. Müller-Buschbaum, S.V. Roth, M. Burghammer, E. Bauer, S. Pfister, C. David, C. Riekel; Physica B **at press**

Stability of thin polymer film on rough substrates

P. Volodin [1], M. Stamm [1], P. Müller-Buschbaum

[1] Leibniz Inst. f. Polymerforschung, Dresden

The stability of thin polymer films on solid substrates is an interesting phenomenon from the technological and scientific point of view. Polymeric coating, paints, lubrication of thin films, lithography, dielectric layers are often used in different modern technologies.

Despite its relevance for application, the influence of substrate roughness on thin polymer film stability is still not well understood. Whereas within the past years the theoretical understanding of dewetting has increased significantly [1, 2] and a large body of experimental work was performed devoted to this topic [3, 4], less attention was paid to substrate roughness [5]. Within the present

investigation we address this question within a simple model system. The homopolymer polystyrene (PS) is investigated upon rough silicon substrates. The silicon substrates have a thick oxide layer on top to ensure an instability of the PS film even in the case of small surface roughness. The substrate roughness was controlled by a wet chemical etching of the silicon prior to the oxidation.

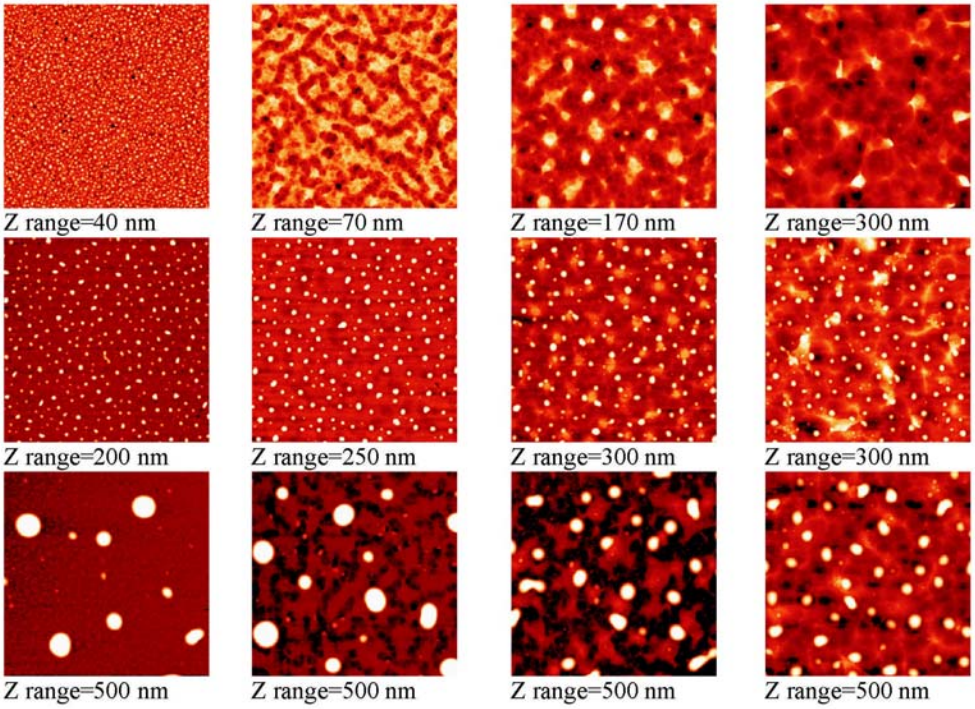

Figure 2.4:
AFM measurements of bare rough oxidized substrate surfaces (top row) and the final dewetted state of the PS films with 10 nm (middle row) and 31 nm (bottom row) thickness. The scan range is 50x50 μm.

The etching procedure was carried out in a 20 % potassium hydroxide solution in methanol at $(60 \pm 5)^o$C in an ultrasound bath. The samples were etched in the solution for a defined time (up to 25 min). After the etching, the samples were cleaned in sulfuric acid peroxide solution (piranha solution) and in ammonium peroxide solution. The rms-surface roughness of the etched samples varied from 5 up to 70 nm depending on the detailed process with a high sensitivity. In order to increase the silicon oxide layer thickness of the substrates, the etched samples were annealed in oxygen atmosphere at 1100^{o}C for 135 min (performed at Forschungszentrum Rosendorf). After the annealing an oxide layer thickness of about 200 nm thickness on top of the silicon (100) surface is installed. PS films were spin coated on top of the substrates from a solution of polystyrene (M_w=11225 g/mol, M_w/M_n=1.343, synthesized in Mainz) in toluene. In order to obtain different film thicknesses, the concentration of the solution and spinning speed were varied. The thickness of the films were monitored by ellipsometric measurements. Next the spin coated films were annealed above the glass transition temperature of the PS (T_g=94^{o}C) at 150^{o}C for 24 h.

The film stability was investigated with atomic force microscopy using a DI-3100 (Digital instruments Ins., Santa Barbara). After quenching the samples down to room temperature, the measurements were carried out in tapping mode with scan size 50x50 μm. Figure 2.4 shows the corresponding data of the original bare surface (top row), after annealing of 10 nm PS layer (middle row)

and after annealing of a 31 nm PS layer (bottom row). As indicated in the figure the z-range was chosen for each figure separately to emphasize on the surface features of different hight. From the left to the right the rms-surface roughness increases (6.6±0.3, 9.3±3, 27±1 37±1 nm). The given error bar accounts for the variation of the surface roughness at different position along the sample surface, picturing the heterogeniety of the installed roughness.

The polystyrene films dewetted on top of the rough substrates as well as dewtting occurs on flat silicon oxide surfaces. In the final state, the dewetted films formed drops. In order to characterize the resulting film patterns after dewetting, a mean first neighbor distance (FND) between the drops was calculated. In case of the 10 nm PS film thickness, the distance between the drops is almost the same on all of the rough substrates (see middle row in figure 2.4). The calculated FND is close to the theoretically calculated dominant spinodal wavelength of the PS film (2.66 μm). In contrast, in case of the 31 nm PS film thickness, the distance between the resulting drops depends on the rms-surface roughness and is not constant. In addition, it is significantly smaller as compared to the theoretically calculated spinodal wavelength (26 μm). In figure 2.5 the calculated FND are shown as a function of the rms-surface roughness. In addition, the FND of the bare substrates are added to this plot, assuming a mountain-like structure of the surface in a first order approximation. As visible from figure 2.5 for substrates with large roughness, the distance between the dewetted drops is closer to the lateral substrate structure. This pictures the influence of surface roughness in terms of amplitude (rms-roughness) and lateral roughness component (FND) on the dewetting process.

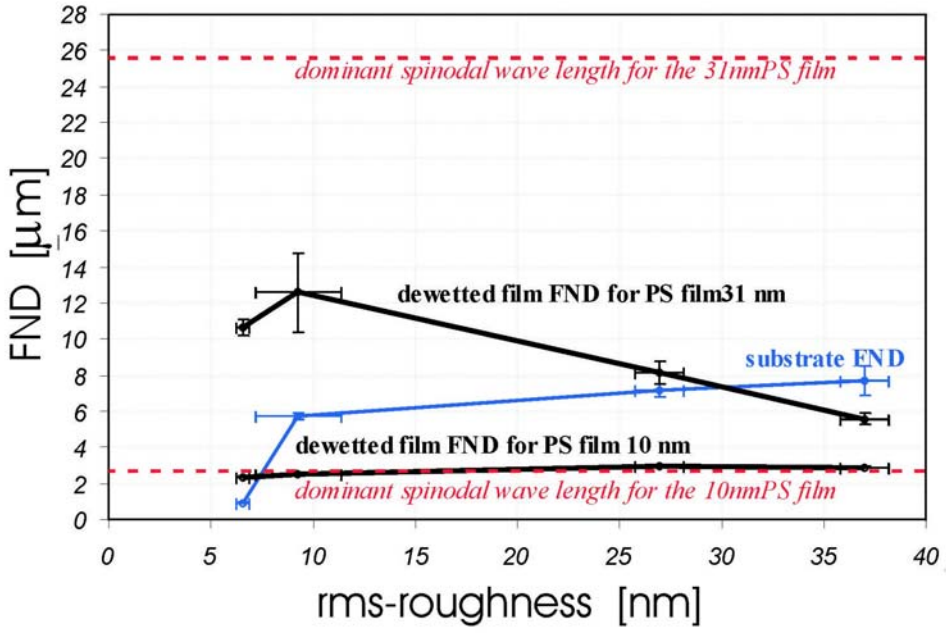

Figure 2.5:
Mean first neighbor distance (FND) of the PS drops (black lines) as a function of the rms-surface roughness of the substrates for two different PS films thicknesses. For comparison the theoretically calculated spinodal wavelengths are ploted with dashed lines and the data of the bare substrate are added (blue line).

This work was financially supported by the DFG Schwerpunktprogramm SPP 1052 *Benetzung und Structurbildung an Grenzflächen.*

[1] F. Brochard-Wyart, J. Daillant; Can. J. Phys. **68**, 1084 (1990)
[2] K. Kargupa, R. Konnur, A. Sharma; Langmuir **16**, 10243 (2000)
[3] K. Kargupa, A. Sharma; Langmuir **18**, 1893 (2002)
[4] R. Seemann, S. Herminghaus, K. Jacobs; Phys. Rev. Lett. **86**, 5534 (2001)
[5] P. Müller-Buschbaum; J.Phys.Condens.Matter **15**, R1549 (2003)

Structure of silica in polydimethylsiloxane: A GISAXS study

G.J. Schneider [1], P. Müller-Buschbaum, T. Pöpperl [1], R. Gehrke [2], D. Göritz [1]

[1] Institute of Physics, Regensburg
[2] HASYLAB, Hamburg

Filler-rubber systems define a large class of materials which are of high interest with respect to many applications. It it is wellknown, that fillers are predominantly responsible for the mechanical reinforcement of the filler-rubber system. Despite numerous investigations, the influence of structure on the mechanical properties of elastomers has not been understood in detail up to now. Previous investigations [1] showed that silicas could be interpreted as fractal objects with a hierarchical structure with structure sizes from a few nanometers up to length scales of micrometers. To cover such a wide interval of length scales the advanced scattering technique named grazing incidence small angle x-ray scattering (GISAXS) appears to be advantageous. However, up to now GISAXS has been only applied to thin film samples. Within the presented investigation we focused on the possibilities to overcome this limitation and apply GISAXS to macroscopically thick samples. First results addressing samples with a thickness on the order of 1 mm are shown in the figures. As samples we choose silica in polydimethylsiloxane (PDMS) provided by Bayer Silicones, with two different filler degrees.

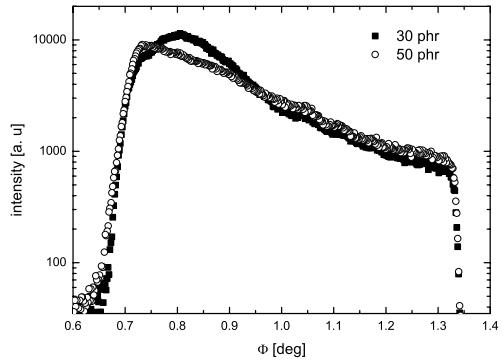

Figure 2.6:
Vertical slices of intensity as a function of the detector angle $\Phi = \alpha_i + \alpha_f$ cut out of the 2d intensity mapping recorder for a fixed angle of incidence α_i. The investigated samples differ in the degree of filling as explained in the text.

The GISAXS measurements were performed using beamline BW4 of the DORIS III storage ring at the synchrotron radiation facility HASYLAB/DESY at Hamburg, Germany. The selected wavelength was $\lambda = 0.138$ nm and the sample-detector distance was 12765 mm. Within the utilised reflection geometry, the sample was placed horizontally on a two circle-goniometer attached on a z-translation table with a fixed angle to the incident beam. The complete pathway of the beam was evacuated and a beam stop was installed. The Gabriel detector with an array of 512x512 pixel

was used to record the specular intensity as well as the Yoneda peak. From this two-dimensional intensity distribution typical vertical (so-called detector) and horizontal (so-called out-of-plane) cuts were sliced. The position of the q_y cuts, which is the wave vector component parallel to the surface and perpendicular to the scattering plane, was selected according to the critical angle of the filler material SiO_2. As a consequence, the structure imposed by the filler material is under investigation [2].

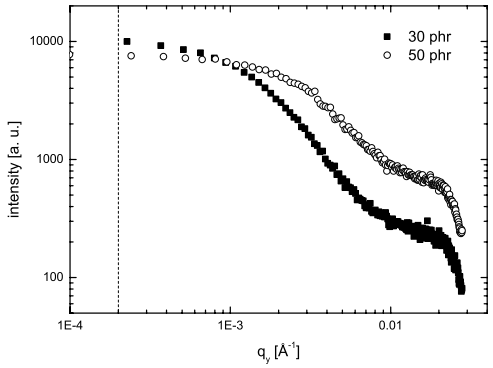

Figure 2.7:
Horizontal slices of intensity as a function of the lateral wave vector q_y, which is oriented perpendicular to the scattering plane. The investigated samples differ in the degree of filling as explained in the text.

As visible in figure 2.6 and 2.7 the change in the degree of filler material yields significant changes of the scattered intensity. These changes can be attributed to changes in the structure of the silica embedded in the PDMS matrix. In the out-of plane scan two marked features in the intensity are well resolved (resolution limit shown by the dashed line in figure 2.7). These features correspond to two lengths which differ by more than one order in magnitude.

Although the quantitative processing of the data is still not finished, it can be stated that GISAXS experiments are appropriate to probe the structure of silica embedded in macroscopically thick samples. Compared to standard USAXS/SAXS experiments the available range for the scattering vector is significantly enlarged towards larger length scales. Therefore the GISAXS-technique provides an alternative for transmission experiments, such as for example small angle neutron scattering experiments.

[1] D. W. Schaefer, K. D. Keefer, Phys.Rev.Lett. **56**, 2199 (1986)
[2] P. Müller-Buschbaum; Anal. Bioanal. Chem. **376**, 3 (2003)

Kinetics of ternary polymer blend films investigated with neutron reflectometry

P. Panagiotou, E. Maurer, R. Cubitt[1], P. Müller-Buschbaum

[1] ILL, Grenoble (France)

Blending polymers with different properties in terms of their molecular weight, their glass transition temperature and ratio of mixture immiscibility can be achieved and new structures are observable.

In the present investigation three different polymers with various glass transition temperature T_g were used, polyisoprene (PI, $T_g = -59^\circ$ C), deuterated polystyrene (PS, $T_g = 57^\circ$ C) and poly(α-methylstyrene) (PαMS, $T_g = 98^\circ$ C) [1]. All polymers were solved at a given mass concentration in toluene and afterwards blended at a weight fraction of PI : PS : PαMS = 4 : 5 : 1. This given polymer solution were then spin coated onto a prior cleaned Si(100) wafer for 33 sec at 2000 rpm at ambient temperature.
After further preparation based on annealing and swelling in solvent vapor the morphology can undergo kinetic transformations. These kinetic changes of the system have been investigated in-situ in the neutron reflectometry D17 at ILL [2]. With its horizontal plane scattering geometry set-up and its time-of-flight (TOF) mode synchronous detection of both specular and off-specular signals could be carried out using a position-sensitive wide-angle detector [3, 4].

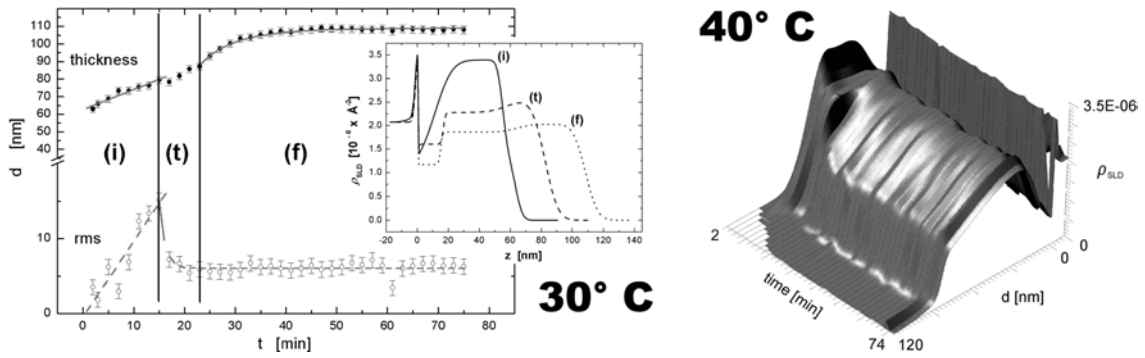

Figure 2.8:
left: thickness and roughness progress during swelling procedure at 30° C. Inset illustrates for all three regime representative reflectivity curves with the substrate-polymer interface at $z = 0$ nm. right: 3d SLD profile simulated (with Parratt32) out of the single measured reflectivity curves with ρ_{SLD} versus swelling time ($2 - 74$ min).

By applying the TOF-mode an in-situ investigation with a high time resolution of 60 sec for each measurement become possible. The investigated time domain amounts to 74 min. The measured range of the momentum transfer q_z perpendicular to the sample surface was restricted to (0.008 - 0.052) Å^{-1}. The samples were placed in a constantly tempered cell (at 30° C, 40° C and 50° C) with a saturated vapor atmosphere of toluene. During the swelling process the polymer undergoes a phase separation caused by the toluene atmosphere. The toluene molecules migrates into the film and decrease the viscosity of the polymer chains in such a manner that the mobility of the swollen component can rise. Due to the significant interaction parameter χ for polymers the miscibility of the individual polymer components changes with increasing swelling temperature and diffusion is taking place. The annealing temperature is below the glass transition temperature T_g of deuterated PS and PαMS which would stay immobile without the addition of toluene, while PI is mobile even without swelling [6].
From a fit of the reflectivity curves for each temperature and time interval (separately with Parratt32) by assuming a three layer model, the rms-roughness of the upper polymeric layer and the total thickness were extracted. In the left plot of fig. 2.8 the thickness progress in the upper curve is illustrated, while the bottom curve shows the changes in the rms-roughness of the top polymer layer during swelling at 30° C. Three distinguish regime are observed [7]. In the initial state (i) the roughness increases fast to its maximum value while the total thickness grows slow. The transient regime (t) shows a fast decay of the surface roughness, while in the final stadium (f) the total thickness approaches an asymptotic maximum at a constant rms-roughness. The inset shows for

each of the three regimes (i), (t) and (f) a representative scattering length density (SLD) profile. The right diagram shows a 3 dimensional SLD profile evolution of the simulated thickness depending on the swelling time ($2 - 74$ min) and the change of the scattering length density ρ_{SLD} at 40° C in saturated toluene atmosphere.
In contrast to the surface tensions PI ($\gamma = 31.0$ mN/m) diffuses towards the substrate interface and the less mobile component PS ($\gamma = 39.3$ mN/m) tends to the surface. At the initial state (i) PS shows a high and narrow distribution at the substrate with respect to its high scattering length density of $\rho_{SLD} = 5.99 \cdot 10^{-6}$ Å^{-2} which is lowered up by the presence of the other components. During swelling the deuterated PS layer is displaced from the bottom of the film towards the surface. The total thickness of the blend film increases due to the embedded solvent molecules. Moreover the surface roughness decreases and the distribution of PS broadens in the final swelling state (f). As three different swelling temperature were investigated, a time dependance of the final thickness was observed. While for 30° C the final thickness under swelling condition is 177% as compared to the thickness in the beginning, respectively at 40° C the final thickness has swollen only to 155% [4].

In summing, a faster kinetics and diffusion process with increasing swelling temperature was observed on the basis of the change of thickness in the swelling.

This work was supported by the BMBF (Förderkennzeichen 03MBE3M1).

[1] M. Geoghegan, R. A. L. Jones, D. S. Sivia, J. Penfold, A. S. Clough: Phys. Rev. E **53** (1), 825(1996)
[2] R. Cubitt, G. Fragneto: Appl. Phys. A **74**, 329 (2001)
[3] T. P. Russell: Physica B **221**, 267 (1996)
[4] A. P. Y. Wong, A. Karim, Ch. C. Han: Physica B **221**, 301 (1996)
[5] A. Budkowski, F. Scheffold, J. Klein, L. J. Fetters: J. Chem. Phys. **106**, 719 (1997)
[6] P. Müller-Buschbaum, J. S. Gutmann, R. Cubitt, M. Stamm: Colloid and Polymer Science **277**, 1193 (1999)
[7] H. Wang, R. J. Composto: J. Chem. Phys. **113** (22), 10386 (2000)

Surface morphology of thin immiscible ternary polymer blend films investigated with GISAXS and AFM

P. Panagiotou, N. Hermsdorf[1], T. Titz, M. Dommach[2], S. S. Funari[2], S. Cunis[2], R. Gehrke[2], P. Müller-Buschbaum

[1] Henkel KgaA, Düsseldorf
[2] HASYLAB, Hamburg

By the use of polymer additional characteristics of materials for industry purposes can be established. Moreover development expenses can be reduced by introduction of polymer blends, concerning their key parameters, which in turn is of fundamental interest for science. So does the structure of a polymeric film affect its properties. Thin films shows unlike bulk systems different behaviour.

For this purpose a ternary polymer blend was introduced: namely polystyrene (PS), poly(α-methylstyrene) (PαMS) and polyisoprene (PI) with different glass transition temperatures T_g depending on the molecular weights M_w. These polymer components were separately diluted at a

given mass concentration. The individual polymer solutions were mixed together with the weight ($wt\%$) fraction of PαMS : PS : PI = 1 : 5: 4 (system ***A***) and the polymer 5 : 1 : 4 (system ***B***), respectively.

For removing basically organic impurities and getting a reproducible surface chemistry of the substrate, Si(100) with its native oxide layer was cleaned in a piranha bath at 80° C for 15 min. After rinsing the wafers several times with deionised water and drying them with nitrogen there were immediately spin-coated with the prepared blend solutions ***A*** or ***B*** to a thin film. This results in a spatial confined arrangement of the polymer chains. For each ratio of mixing 2 appropriate thin films were prepared. Afterwards one sample of system ***A*** and ***B*** was annealed for 500 min yielding in a relaxation of the individual polymer component towards equilibrium in the morphology by phase separation of the film [1 - 4]. The annealing temperature was chosen in such a manner, that according to their molecular weight of the components is above the glass transition temperature T_g of PS ($T_g = 57^{\circ}$ C) and of PI ($T_g = -59^{\circ}$ C) but below the one of PαMS ($T_g = 98^{\circ}$ C). Which in terms leads to an immobility of PS and PI while PαMS gets mobile during annealing procedure. The sample ***A*** consist in minority ($10\, wt\%$) of the immobile matrix (PαMS), while the system ***B*** is composed of $50\, wt\%$ of the mobile phases formed by PS and PI.

To detect the most prominent surface structures ξ in the topology atomic force microscopy (AFM) measurements were performed up to $95\, x\, 95\, \mu$m^2 in the scanned area. In addition grazing incidence small-angle x-ray scattering (GISAXS) was employed [5]. GISAXS measurements were performed at the BW4 and at the A2 beamline in the synchrotron radiation facility HASYLAB/DESY (Hamburg). The sample was mounted horizontally on a z-translation table provided with a two circle-goniometer to allow a fixed angle of incident. The complete pathway of the beam was evacuated and a beam stop was installed. For recording the specular intensity as well as the yoneda peak a 2-dim detector was used: A Gabriel detector with an array of ($512\, x\, 512$) pixels at the BW4 and an image plate with an array of ($1024\, x\, 1024$) pixels at A2 respectively. The used wavelength λ, the resolution limit q_y and the sample-detector distance d at BW4 was $\lambda = 1.38$Å, $q_y = 2.840 \cdot 10^{-2}$ nm^{-1} and $d = 13$ m , for A2 $\lambda = 1.5$ Å, $q_y = 1.995 \cdot 10^{-2}$ nm^{-1} and $d = 2$ m respectively. Out of these 2-dim intensity distributions typical vertical and horizontal (also called out-of-plane) cuts were extracted at the critical angle α_c(PS)$= 0.15^{\circ}$ to obtain the structures formed by PS domains.

AFM measurements were performed at ambient conditions with the AutoProbe CP from Thermomicroscope in the non-contact mode to prevent degradation of the sample surface. Out of the scanned real space images a radial averaged 2-dim Fourier transformation of the height distribution was calculated. These power spectral density functions (PSD) were compared with the GISAXS data as a function of the annealing temperature and the ratio of mixture for system ***A*** and ***B***. Hence it can be deduced if ξ appears either in the inner part of the film or in addition on the surface.

During the spin coat process solvent evaporates and freeze the polymer component in its non-equilibrium state indicated by a morphology with varying length scale. By annealing the mobile components can relax and diffuses as a function of the annealing time towards an equilibrium.

By comparison of the AFM images with the GISAXS data an understanding of the kinetic phase separation process can be made for following plots:
Plot 1: Peak I shows a length scale exclusive at the surface but not in the GISAXS curves. This indicates a domain not formed by PS. Unlike peak II shows a structure by PS on the surface and in the inner film, while peak III is a hint of a hidden PS domain underneath the surface.
Plot 2: All observed structures except peak II can be seen on top of the surface and in the inner film.

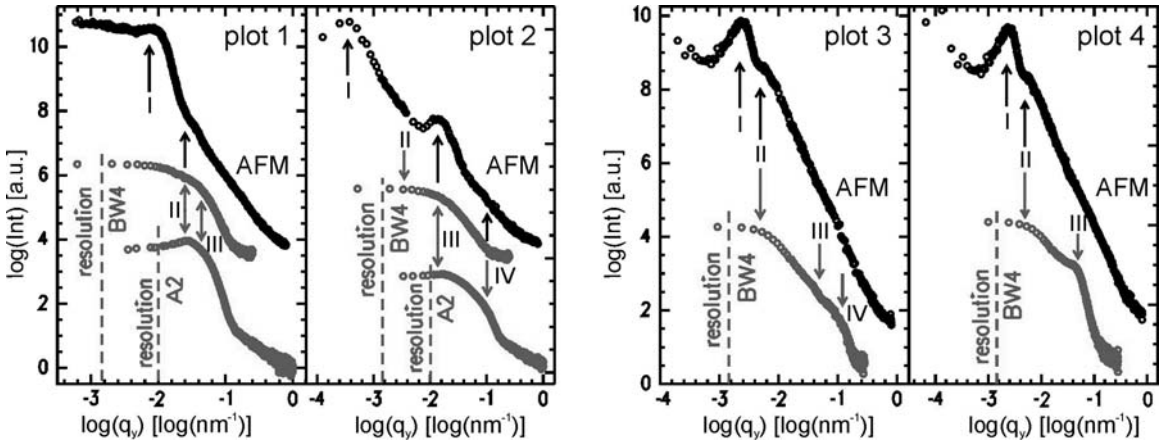

Figure 2.9:
GISAXS cuts are grey and compared with the black PSD curves of the AFM scans. Peak I, II, III and IV indicate the in-plane length scales ξ marked with arrows. Plot 1+2 figures measured system ***A***, plot 3+4 shows system ***B***. Plot 1+3 indicates sample as prepared and plot 2+4 annealed films for 500 min respectively.

Compared to plot 1 the structures are shifted. In the case of peak I, II and III the structures have grown, while the last peak IV is assumed to have been generated during the annealing process.
Plot 3: The peak I exist only on the surface. While peak II can be seen in the AFM images and in the GISAXS. Peak II exist in both curves, while peak III and IV contribute only in the inner part of the film. This gives arise that the structures are build up by PS domains.
Plot 4: Peak I compared to the peak I of plot 3 is not shifted, the domains didn't change. Like in plot 3 the peak II consists of PS domains. Peak III is formed by PS domains in the inner film.

The annealing temperature was chosen in such a manner to keep PαMS rigid according to its glass transitions temperature T_g, so its mobility is restricted, while PS and PI show mobility annealing. Depending on the annealing temperature and the mixing ratio of the components multiple length scales ξ reveal, which appear either on top of the surface, the inner part of the film or in both positions. According to the $50\,wt\%$ of the immobile component (PαMS) in system ***B*** the peaks didn't shift much from the as-prepared to annealed stadium. The mobility of the components is hindered. In contrast, in system ***A*** the length scales changed to bigger structures due the phase separation in the annealed sample which indicate a higher diffusivity due to the little fraction of the immobile phase ($10\,wt\%$).

This work was supported by the BMBF (Förderkennzeichen 03MBE3M1).

[1] K. Binder: Journal of Chemical Physics **79**, 6387 (1983)

[2] G. Krausch: Material Science and Engineering **R14**, 1 (1995)

[3] P. Müller-Buschbaum; J. S. Gutmann; M. Stamm: Macromolecules **33**, 4886 (2000)

[4] S. Walheim; M. Ramstein; U. Steiner: Langmuir **15**, 4828 (1999)

[5] P. Müller-Buschbaum; J. S. Gutmann; R. Cubitt; M. Stamm: Colloid and Polymer Science **277**, 1193 (1999).

Phase separation of pressure sensitive adhesive blend films

K. Schlögl, E. Maurer, P. Müller-Buschbaum

For a wide range of applications in industry and in everyday life the adhesion between different materials, e.g. between polymers or polymer and non-polymeric surface, is of great interest. Pressure sensitive adhesives (PSA) play an important role as substances which can combine the ability of high tackiness with the fact to be removable. The process of bond formation between a PSA and a non polymer material can be easily achieved by pressure or contact of the surfaces as the name already implies [1]. Other parameters the adhesion properties rest on are contact pressure and time, temperature and debonding rate. Therefore a central aspect for understanding this bearing lies in the characteristics of the sticky material. In general, PSA flow under stress like a viscous liquid and on the other hand they comport like soft, elastic solids. One possibility to adjust this behaviour is by tuning the chemical composition. Homo-, copolymers or polymer blends are used to design PSA depending on the latter application with effect of the surface morphology and roughness.

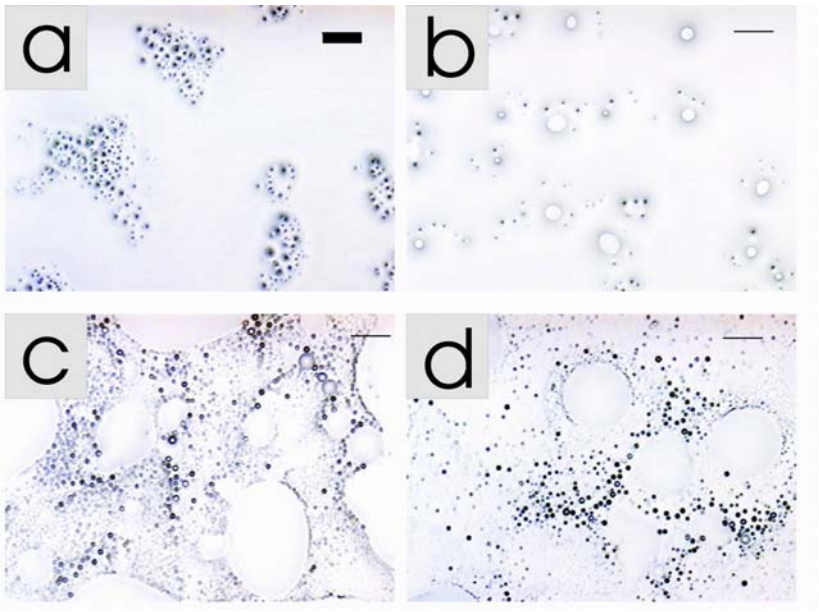

Figure 2.10:
Optical micrographs of a P(EHA-stat-MMA) and PMMA blend film with different compositions of P(EHA-stat-MMA):PMMA: (a) 95:5; (b) 90:10; (c) 45:55; (d) 10:90. All the pictures were recorded with a magnification of five. The bar denotes a size of 200 μm.

In this research field copolymers are of major scientific value due to the fact that different types of monomers in the same polymer chain can be used to tune the interchain friction and the dissipative processes in the material [2]. By adding another polymer component it should be possible to alter the part responsible for the cohesion more precisely. To reach the desired surface behaviour we investigate blends of copolymers (P(EHA-stat-MMA)) and a monomer (PMMA) already incorporated in the copolymer chain by varying the blending ratio.

The samples were prepared on acidic cleaned and with compressed nitrogen dried glass substrates. A defined amount of the corresponding polymeric solution was smoothly spread over the glass surface. After evaporation of the solvent the surface of the films was macroscopically studied via

microscopy (figure 2.10). We have observed different phase separation morphologies depending on the blend composition. They already occur at small ratios of PMMA up to 1 %, whereas with an increasing amount of PMMA the formed structures increase in size.

This work was supported by the BMBF (Förderkennzeichen 03CO333).

[1] H. Lakrout, Adhesion **69**, 307 (1999)
[2] C. Gay, L. Leibler, Physics Today **52**, 48 (1999)

Optically inaccessible structures of polymeric pressure sensitive adhesive films

E. Maurer, S. Loi, E. Bauer, T. Mehaddene, P. Müller-Buschbaum

Pressure sensitive adhesives (PSA) are based on polymers. They adhere by simply applying pressure to a huge variety of materials. In many PSA applications a controlled release of the adhesive bond is desired. One of the most prominent examples in daily life are stick-on notes, making use of the ability to undergo several cycles of bonding and detaching. Scientifically, the quality of adhesion is quantified in the so called tack test [1]. A probe punch, like a flat-ended cylinder, is pressed with a defined force onto a PSA film. After maintaining the force for a controlled time the punch is withdrawn from the surface with a fixed velocity (see fig. 2.11 A). During the process the force needed to sustain the constant retraction velocity is probed as a function of the film-punch distance. Usually, the resulting curves show characteristic features such as a maximum force followed by a force plateau. Even at film-punch distances of multiple film thicknesses the formerly glued interfaces remain locally connected by a fibrillar structure.

PSA debonding during the tack test was in detail analyzed by optical microscopy from both underneath, through a transparent substrate, and from the side [2]. In early debonding stages macroscopic cavities appear locally, introduced into the former homogenous film by hydrodynamic stress [3]. With proceeding tension they grow in number and size until the former contact area is almost completely covered. Finally, the polymeric material located at the partition walls separating cavities is elongated in direction of tension. Thereby numerous fibrils are formed. Nevertheless, investigations by conventional microscopy are restricted towards small length scales by the optical resolution limit. In order to overcome this limit we applied in-situ ultra small angle x-ray scattering (USAX) during the tack test [4, 5].

Within the presented investigation the PSA model system is a statistical copolymer of 80 % 2-ethyl hexylacrylate (EHA) and 20 % methyl methacrylate (MMA). Films (thickness 30 μm) were prepared upon float glass slides by solution casting. The USAX experiments were performed at HASYLAB at beamline BW4 operating a two-dimensional position sensitive detector. The direct beam, which had a diameter of approximately 400 mm, was shadowed by a beam stop. At a wavelength of 0.138 nm and a sample detector distance of 13.2 m structures between 25 nm and 400 nm were resolvable. The PSA film was placed parallel to the incident beam shadowing only a small part of the beam. While film and beam remained solidly attached the punch was retracted in the direction perpendicular to both, film surface and incoming beam (see fig. 2.11 B). In-situ to the tack experiment, thereby yielding the force-distance information, at several film-punch distances 2D scattering patterns were recorded. In addition to the USAXS signal, the observed scattering pattern contain also diffuse scattering from the PSA surface.

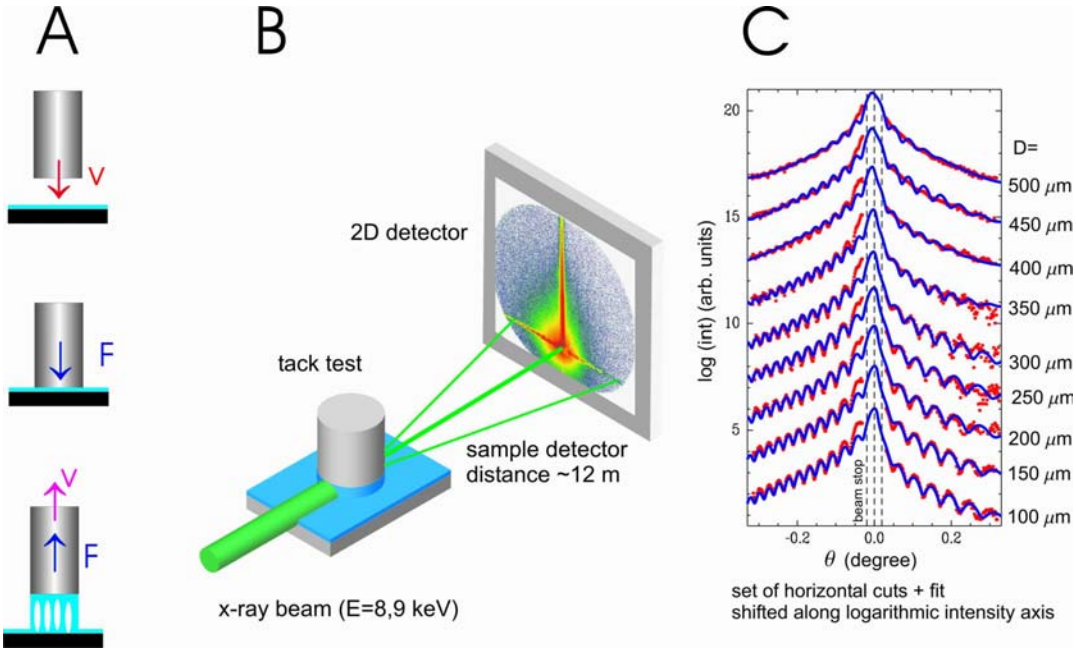

Figure 2.11:
A: In the tack test a flat-ended cylindrical punch is pressed onto a PSA film and later again retracted. A fibrillar structure between the punch and the PSA develops. **B:** In-situ to the tack test the created fibrillar structure is investigated by ultra small angle scattering. A typical scattering pattern on the two-dimensional position sensitive detector is shown in the sketch. **C:** Scattering data (dots) for a set of different film punch distances D displayed together with the corresponding fits (solid lines) based on the model explained in the text. Towards small scattering angles the resolution is limited by the beam stop (dashed lines).

Within a first analysis we focus on the structure which is present between the film and the punch and not on the surface structures. As a consequence, we address simply the USAX signal and thus we restrict ourselves to horizontal cuts out of the 2D intensity map. These horizontal cuts were selected through the direct beam position and parallel to the PSA film surface ($q_z = 0$) to fulfill the USAX condition. In fig. 2.11 C the resulting curves are displayed for several film-punch distances. The cuts show extremely well pronounced, multiple fringes. With increasing distance the amplitude of the modulation in intensity decays. A further eye-catching feature is the strong asymmetry of the curves with respect to the scattering angle. Both intensity and angular positions of the fringes depend on the sign of the scattering angle. This type of asymmetry of the scattered intensity with respect t o $q_y = 0$ does not allow for the commonly performed addition of the $-q_y$ and the q_y signals. Accordingly, the simplest standard models used for the interpretation, such as objects of a symmetrical shape with a defined distance to neighboring objects [4], can no longer be used.

One simple model to explain the latter aspect is scattering at an one-dimensional grating of small voids. In order to account for the asymmetry each void, displayed with respect to the neighboring one by D_y in direction perpendicular to the beam, is in addition also shifted by D_x in beam direction. In this case the ratio $\eta = D_x/(2\,D_y)$ can be considered as a parameter governing the degree of asymmetry in phase. In detail $42 < \eta < 50$ holds for all scattering curves in fig. 2.11 C. In the context of adhesive debonding the grating of voids could be embodied by a regular, linear

arrangement of nano-bubbles embedded in the partition walls separating macroscopic cavities. Independently of a detailed geometrical interpretation in real space the well pronounced fringes prove that structure creation extensively studied in a macroscopic range by optical microscopy is also proceeded on a microscopic level [5].

This work was supported by the BMBF (Förderkennzeichen 03CO333).

[1] A. Zosel: Coll. Polym. Sci **263**, 541 (1985)
[2] H. Lakrout, P. Sergot, C. Creton: J. Adhesion **69**, 307 (1999)
[3] C. Creton, H. Lakrout, J. Polymer Sci, Polym. Phy. **38**, 965 (2000)
[4] P. Müller-Buschbaum, T. Ittner, W. Petry, Europhys. Lett. **66**, 513 (2004)
[5] E. Maurer, S. Loi, D. Wulff, N. Willenbacher, P. Müller-Buschbaum, Physica B (at press)

Comparative analysis of nanostructured diblock copolymer films

P. Müller-Buschbaum, E. Bauer, E. Maurer, M. Cristofolini [1], S.V. Roth [2], R. Gehrke [2]

[1] School of Chemistry, Cardiff University (UK)
[2] HASYLAB, Hamburg

Future generations of microelectronic devices will require both, ever-decreasing critical dimensions and shrinking tolerance on those dimensions. The rising costs and complexity associated with lithographically created structures at the nanometer length scale opened opportunities for alternative techniques. Following this track, self-assembly in physical systems might play a key role in future technological applications. Self-assembling materials are characterized by spontaneous formation of nanometer-scaled structures. In addition long-range order or domains are installed.

The self-assembly based nanofabrication process is especially attractive because of its simplicity. The basic preparation procedures involve only a few preparation steps: substrate cleaning, thin film creation and nanostructure creation. Despite all the efforts in creating new types of surface structures, the quality of the self-organized nanostructures is rather limited due to the currently applied experimental analysis techniques [1]. Mostly, experiments are based on local techniques such as atomic force microscopy (AFM) or scanning electron microscopy (SEM). As compared to the desired large scales to be structured these techniques probe only very limited surface areas. To obtain a statistically significant information scattering is a helpful tool. With the advanced scattering technique of grazing incidence small-angle scattering (GISAS) lateral lengths from molecular to micrometer-size are covered. Thus the addressed range is quite comparable to AFM or SEM, but the probed surface area is macroscopic instead of microscopic [2]. In the aplied gazing incidence geometry the beam footprint is strongly increased due the extremely small angle of incidence.

Based on the example of dewetted poly(styrene -block- paramethylstyrene) diblock copolymer (molecular weight 230k, symmetric block ratio and narrow molecular weight distribution 1.08) P(Sd-b-pMS) films the possibilities and limitations of GISAXS are enlightened within this investigation. Research is directed towards the host surface structures created by dewetting, because this enables a direct comparison with real space analysis techniques such as AFM or SEM. This opens the opportunity to test modelling of the scattering data. The internal contrast between the styrene and paramethylstyrene block is very low and thus in a good approximation the diblock copolymer

can be understood as a simple homopolymer with respect to the scattering signal using x-rays. The grazing incidence small angle x-ray scattering (GISAXS) measurements were performed at the BW4 USAX beamline of the DORIS III storage ring at HASYLAB/DESY in Hamburg. The selected wavelength was 0.138 nm. The scattered intensity was recorded with a two dimensional detector which consists of a 512x512 pixel array. Due to the sample-detector distance of 12.1 m a high resolution was achieved. The beam divergence in and out of the plane of reflection was set by two entrance cross-slits. At one fixed angle of incident the two-dimensional intensity distribution can be cut in several vertical and horizontal slices with respect to the sample surface. Vertical slices contain mainly scattering information from structures perpendicular to the sample surface, whereas horizontal slices contain only scattering contributions with an in-plane information.

Figure 1a shows a typical two-dimensional GISAXS scattering pattern as measured in case of a sample stored for 4 hours under toluene vapour. Since an incident angle α_i= 0.534^o larger than the critical angle of the polymeric material was chosen, the specular and the diffuse scattering contributions are well separated along the vertical detector direction and thus easily separated. The specular peak in the top of figure 2.12a is shielded by a beam stop (resulting in a staggered looking intensity) to protect the array detector, because the specular scattering is orders of magnitude larger compared to the diffuse scattering.

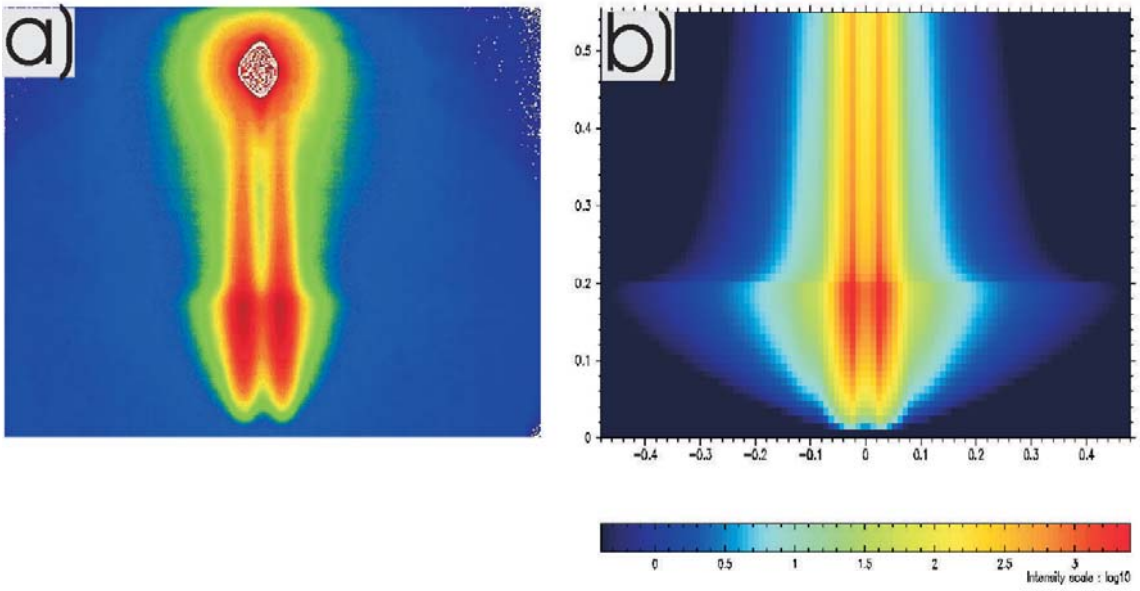

Figure 2.12:
a) Typical two-dimensional GISAXS scattering pattern measured at BW4 in case of 4 h storage under toluene vapour atmosphere. b) Calculated two-dimensional GISAXS scattering patterns using the program IsGISAXS as described in the text. Both two-dimensional intensity mappings cover a range of -0.48^o $< \psi <$ 0.48^o in horizontal direction and 0.0^o $< \alpha_f <$ 0.55^o in vertical direction. The intensity is shown on a logarithmic scale. The colour coding was chosen to emphasize on the features in the diffuse scattering (blue=low and red=high intensity). [4]

In many cases the data analysis is restricted to a comparison with other experimentally determined data, based on a statistical interpretation of the data [2]. Care has to be taken, because either the reflection-refraction effects in the simple Born approximation or the interplay between interference function and form factor or the particle size distributions might be of importance.

Reflection-refraction effects will become significant in the region of total external reflection, e.g. if the incident angle of the GISAXS experiment is chosen close to the critical angle. Moreover, concerning particle size, the coupling between the interference function and form factor greatly increases the complexity of the analysis and prevents the use of classical Guinier or Porod approaches. Therefore, direct modelling of the data can provide further insights. With the program IsGISAXS [3] the simulation of off-specular scattering in the GISAXS geometry is accessible. A detailed description of the possibilities offered by this program can be found in reference [3]. For the modelling basically the form and structure factor have to be chosen.

Because the polymeric material probed within this investigation is placed on top of the solid support the model of supported particles is well suited. In first approximation the form factor of the host structure is chosen to obey a cylinder type and the structure factor to behave like a one-dimensional paracrystal [5]. To elucidate the possibilities and limits of the modelling based on IsGISAXS we restrict us to this model assumption [6]. The two-dimensional intensity mappings shown in figure 2.12 cover exactly the same angular range. The colour coding was adapted to match. Since only the diffuse scattering is modelled, no specular peak is present in figure 2.12b. As a consequence the comparison can mainly focus to the region around the Yoneda peaks. On a first view, basic features of the measured two-dimensional intensity mapping are captured by the modelling. In general, the agreement covers the split-up Yoneda peaks in their positions and shapes. Most deviations are originated from a missing background in the modelled data and effect the regime of large ψ (or q_y) values [4, 6].

This work was supported by the BMBF (Förderkennzeichen 03DU03MU).

[1] C. Harrison, P.M. Chaikin, D.A. Huse, R.A. Register, D.H. Adamson, A. Daniel, E. Huang, P. Mansky, T.P. Russell, C.J. Hawker, D.A. Egolf, I.V. Melnikov, E. Bodenschatz; Macromolecules **33**, 857 (2000)

[2] P. Müller-Buschbaum; Anal. Bioanal. Chem. **376**, 3 (2003)

[3] R. Lazzari; Appl. Cryst. **35**, 406 (2002)

[4] P. Müller-Buschbaum, N. Hermsdorf, S. V. Roth, J. Wiedersich, S. Cunis, R. Gehrke; Spectrochimica Acta Part B: Atomic Spectroscopy **59**, 1789 (2004)

[5] R. Hosemann, W. Vogel, D. Weick; Acta. Cryst. A **37**, 85 (1981)

[6] P. Müller-Buschbaum, E. Bauer, E. Maurer, M. Cristofolini, S.V. Roth, R. Gehrke; to be published

Creation of channelled polymer films by selective removal of one block out of a diblock copolymer film

P. Müller-Buschbaum, P. Busch [1], M. Stamm [1], B. Smarsly [2], C. Egger [2], H. Schlaad [2]

[1] Leibniz Inst. f. Polymerforschung, Dresden

[2] Max Planck Institute of Colloids and Interfaces, Potsdam

Channelled substrates are of growing interest with respect to application as well as to basic research. For the preparation of channels several different techniques have been developed. Today's leading edge lithography tools are using 193 nm excimer lasers to produce commercial chips at the 90 nm technology node. And 193 nm tools are expected to carry on into the 65 nm node -and with the little help of water - even into the 45 nm. A shift in laser wavelength gains in reduction of

feature sizes and with extreme ultraviolet lithography 13 might become reachable. Alternatively, nano-imprinting offers the creation of linewidths beyond the 10 nm mark without the use of complex light sources and reduction optics [1]. However, despite its potential to return litographers to a simpler time, nanoimprinting requires a stamp to be used. Thus in addition, the use of diblock copolymer films still remains a promising candidate for the preparation of channelled substrates. While phase separated surface structures in polymer blend films are typically of micrometer size, micro-phase separation in diblock copolymer systems is well known to offer nanostructures in the bulk as well as in thin films. Diblock copolymers arranging in perpendicularly to the substrate surface oriented lamellae are well suited precursor systems for the creation of a lateral patterning. Recently, the epitaxial self-assembly of block copolymers on lithographically defined nanopatterned substrates was shown to improve the long-range order of the lamellar structure significantly (see figure 3) [2]. The resulting patterns are defect-free, are oriented and registered with the underlying substrate and can be created over arbitrarily large areas. These structures are determined by the size and quality of the lithographically defined surface pattern rather than by the inherent limitations of the self-assembly process.

In the present investigation diblock copolymers with a synthetic polymer block and a polypeptide block (for a review see [3] and references therein) were used for the creation of channelled substrates. Triggered by the different architectures of the diblock copolymer different superstructures can form. Basic origin of the differences in the formed superstructure can be attributed to the differences in the spatial extension and volume fraction of components [3]. Using polystyrene-poly(Z-L-lysine) block copolymers a lamellar structure results in the bulk [4]. In case of linear block copolymers due to the dipole moment of the polypeptide block the lamellae is perpendicularly arranged with respect to a defining surface. The lamellar order extends over large surface areas on the order of several micrometers. This was illustrated by transmission electron microscopy (TEM). Thin films have been prepared out-of a THF solution onto pre-cleaned Si(100) substrates by spin-coating. From a variation of the concentration used for the spin-coating, a change in the resulting film thickness results. After the spin-coating the peptide is removed completely with a solution containing 30 % hydrogen bromide in glacial acetic acid. In order to characterize the resulting volume structures inside the film as well as the surface structures, grazing incidence small angle x-ray scattering (GISAXS) was applied.

The GISAXS measurements were performed at the beamline A2 of the DORIS III storage ring at HASYLAB/DESY in Hamburg. The selected wavelength was 0.154 nm. The scattered intensity was recorded with a two dimensional detector (MARCCD) which consists of a 2048x2048 pixel array. Due to the sample-detector distance of 0.95 m a relaxed resolution was achieved which enabled the detection of lateral structures between 1 and 300 nm. This fits well to the typical regime expected for polymeric lamellae. The beam divergence in and out of the plane of reflection was set by two entrance cross-slits. At one fixed angle of incident the two-dimensional intensity distribution can be cut into several vertical and horizontal slices with respect to the sample surface. Vertical slices contain mainly scattering information from structures perpendicular to the sample surface, whereas horizontal slices contain only scattering contributions with an in-plane information.

Figure 2.13 shows the example of 4 different concentrations used for the spin-coating (increasing from the top to the bottom). The specular peak (shielded with a beam stop) and the Yoneda peak are well separated due to the chosen angle of incidence well above the critical angle of the related materials. In figure 1a to 1d the data of the diblock copolymer films without the removal of the peptide are shown. In comparison, figure 1e to 1h shows films of same concentration but after having removed the peptide and thus resulting in channelled substrates. Obviously, the removal of

the peptide increases the internal contrast and thus changes the 2d scattering pattern significantly.

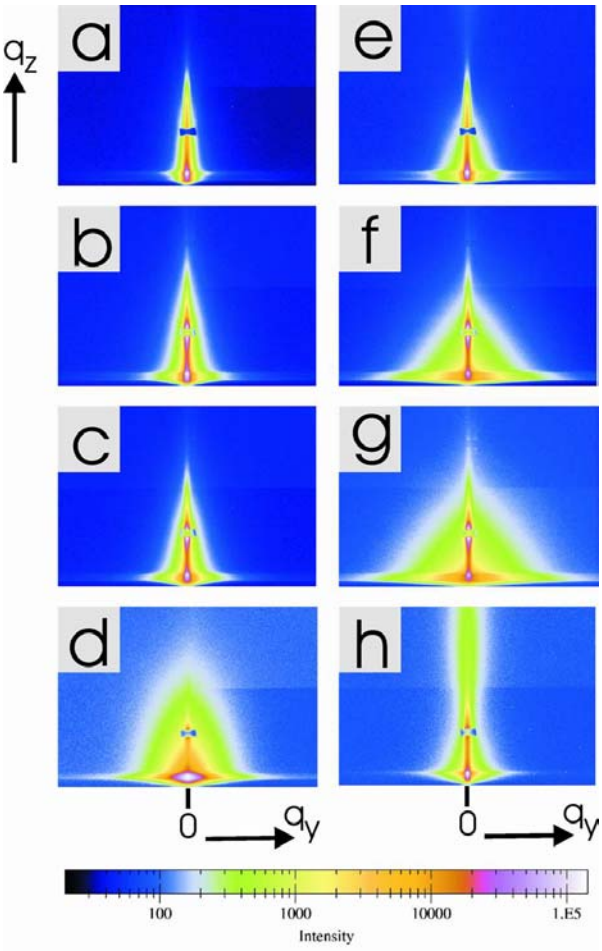

Figure 2.13:
Typical two-dimensional GISAXS scattering pattern measured at beamline A2: a-d) diblock copolymer films and e-h) channelled substrates resulting from the removal of the one block. The specular peak is shielded with a beam stop to enable the detection of the diffuse scattering, which is orders of magnitude lower than the specular. The intensity is shown on a logarithmic scale. The colour-coding was chosen to emphasize on the features in the diffuse scattering (black=low and white=high intensity).

The absence of typical lattice rods well known from surface sensitive scattering at surface gratings, depicts the absence of a resolvable, defined lateral spacing perpendicular to the incoming x-ray beam. With respect to the creation of channeled substrates this does not imply the absence of well ordered channels.

This work was financially supported by the DFG Schwerpunktprogramm SPP 1164 *Nano- and Microfluidics* (Mu1487/2).

[1] A. Hand; Semiconductor Intern. **27**, 40 (2004)

[2] S.O. Kim, H.H. Solak, M. P. Stoykovich, N.J. Ferrier, J.J. de Papblo, P.F. Nealey; Nature **424**, 411 (2003)

[3] H. Schlaad, M. Antonietti; Eur. Phys. J. E **10**, 17 (2003)

[4] H. Schlaad, H. Kukula, B. Smarsly, M. Antonietti, T. Pakula; Polymer **43**, 5321 (2002)

Orientation behavior of lamellae forming blends of diblock copolymers with low molar mass additives

P. Busch [1], A. Sidorenko [1], M. Stamm [1], S.S. Funari [2], P. Müller-Buschbaum

[1] Leibniz Inst. f. Polymerforschung, Dresden

[2] HASYLAB, Hamburg

Diblock copolymers represent a versatile class of materials because of the high flexibility to incorporate different material properties into the same material, simply by the covalently linkage of two chemically different polymers. Furthermore, mostly the two blocks are not miscible, and phase separation occurs. Due to the connectivity of the different blocks, this phase separation can only occur on a mesoscopic length scale and highly ordered structures like lamellae, cylinders or spheres are formed. The typical repeat period of these structures lies between 10 and 100 nm. The narrow polydispersity of this repeat period makes these materials suitable candidates for thin film technology, as they can be used as templates for lithography or nanopatterned surfaces.

The selective incorporation of low molecular weight additives into one of the two blocks opens not only the way to tune the length scale to a desired value or to change the morphology of the block copolymer. It has also been shown that they can be removed resulting in nanoporous materials which can be either used as membranes [1] or precursors for the fabrication of nanodots or nanowires [2]. For many of these applications it is required that the orientation of the cylinders or lamellae is perpendicular with respect to the film interfaces. However, usually they tend to align parallel, due to preferential absorption of one of the two blocks to the interfaces and major efforts have to be applied like creating neutral interfaces or applying electric fields [3, 4].

Recently it has been shown that in a thin film of a blend of Polystyrene-*b*-poly-4-vinylpyridine (PS-*b*-P4VP) diblock copolymer with 2-(4'hydroxybenzene-azo)benzoic acid (HABA) the orientation of cylinders can be controlled by the exposure to different solvent vapors [2]. HABA is dissolved as an additive in the P4VP-block, which forms cylinders in a PS-matrix. If chloroform – which is a good solvent for both blocks – is used for the vapor exposure, the cylinders orient parallel to the film surface. If dioxane is used – which is a good solvent for the polystyrene-matrix, but a bad solvent for the P4VP-cylinders – a perpendicular orientation was observed. Even though the driving forces and the mechanism of the switching behavior have not been clarified in detail it could be shown that it is fully reversible. From the perpendicular oriented cylinders the HABA additive can be extracted by methanol, resulting in cylindrical pores, which can be loaded by metals [2].

In the present experiment we have extended this experiment to the case of lamella forming blends of PS-*b*-P4VP and HABA. Three films have been prepared under different conditions and have been investigated by grazing incidence small-angle x-ray scattering (GISAXS) at A2. The films have been illuminated by a well collimated incident beam (300 μm height) under an incident angle α_i = 0.99°. The scattered intensity was recorded by a two-dimensional CCD-detector with a pixel array of 2048×2048 and a pixel distance of 79 μm at a distance of 960 mm from the sample.

Most of the intensity is reflected specular and had to be covered by a beamstop. The off-specular intensity gives than information about the internal structure of the copolymer films [5].

The PS-*b*-P4VP block copolymer had the number average molar masses of 32.9 kg/mol for the PS-block and 8.08 kg/mol for the P4VP-block, respectively. The weight fraction of HABA was 31.2% with respect to the copolymer and the bulk lamellar thickness of the blend was 34 nm as determined by SAXS. Thin films were prepared by dip coating from dioxane solution and had an initial film thickness of 40 nm. One film was investigated without further processing (A), one film was washed with methanol to remove the additive (B) and one film was exposed to chloroform vapor and afterwards washed with methanol (C). According to Ref. [2] it was expected, that the two films (A) and (B) show a perpendicular orientation of the lamellae, while film (C) should show a parallel orientation. Consequently, only for the first two films strong out of plane scattering was expected.

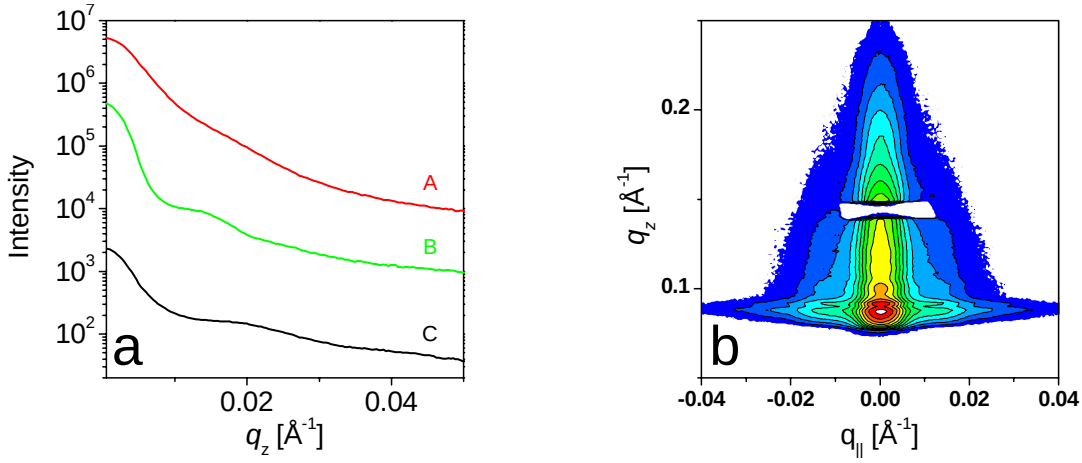

Figure 2.14:
(a) Horizontal cuts of the films processed under different conditions. The curves are shifted for clarity. The processing conditions are given in the text. (b) Two-dimensional GISAXS-map of the film C, which was exposed to chloroform vapor and extracted with methanol.

Fig. 2.14a shows horizontal cuts of the three films. For film (A) no out of plane scattering could be observed. In contrast, the two films, where the additive was extracted by methanol weak peaks point to a laterally order inside the films, pointing to perpendicular lamellae. In Fig. 2.14b the two-dimensional GISAXS-map for film (C) supports the weak out-of plane scattering. Thus, for lamellae forming blends of PS-*b*-P4VP and HABA the response to different solvents is differs significantly from cylinder forming blends.

[1] O. Ikkala, G. ten Brinke, Science **295**, 2407 (2002)

[2] A. Sidorenko, I. Tokarev, S. Minko, M. Stamm, J. Am. Chem. Soc. **125**, 12211 (2003)

[3] E. Huang, T. P. Russell, C. Harrisson, P. M. Chaikin, R. A. Register, C. J. Hawker, J. Mays, Macromolecules **31**, 7641 (1998)

[4] T. Thurn-Albrecht, J. Schotter, G. A. Kästle, N. Emley, T. Shibauchi, L. Krusin-Elbaum, K. Guarini, C. T. Black, M. T. Tuominen, T. P. Russell, Science **290**, 2126 (2000)

[5] P. Müller-Buschbaum; Anal. Bioanal. Chem. **376**, 3 (2003)

Dynamic scattering effects in grazing incidence small-angle X-ray scattering experiments

P. Busch [1], C.M. Papadakis, M. Stamm [1], S.S. Funari [2], P. Müller-Buschbaum

[1] Leibniz Inst. f. Polymerforschung, Dresden
[2] HASYLAB, Hamburg

Diblock copolymers are frequently used materials in thin film technology. Due the connectivity of two chemically different blocks they are able to undergo phase separation on a mesoscopic length scale and self assemble into highly regular structures of e.g. lamellae or cylinders with a repeat period of typically 10 – 100 nm. Due to the narrow polydispersity of the structures formed they can be used as membranes or templates in photolithography [1, 2].

A major challenge is the control of the orientation of the mesoscopic structures formed, as lamellae or cylinders can either orient parallel or perpendicular to the film interfaces. Recently, grazing incidence small-angle X-ray scattering (GISAXS) has been developed as a nondestructive tool to investigate the orientation of diblock copolymers in thin films [3, 4]. In contrast to traditional SAXS, where the incident beam passes a bulk sample and the scattering of the transmitted intensity is probed, GISAXS experiments are carried out in reflection geometry on thin films on a highly reflective substrate. The incident beam impinges on the film surface under a grazing angle (typically 1° or lower), where most of the intensity is specular reflected. However, a small part of the incoming intensity can be also scattered off-specular, in particular in the case of an internal structure of the film itself.

In the last few years this technique has been used mainly to investigate laterally structured films like perpendicular cylinders [1, 2] or lamellae [3, 5], as in this case the momentum transfer parallel to the film plane $\mathbf{q}_{||}$ is directly related to the repeat period D by $\mathbf{q}_{||} = 2\pi/D$. This allows for a relative straightforward characterization of laterally structured films.

GISAXS investigations on films with a structure along the film normal – e. g. with lamellae parallel to the film normal – are rather scarce [5, 6]. This might be due to mainly two reasons. First of all the scattering along the film normal is affected by both refraction, when the incident beam enters the film surface and reflection from the substrate. In this case kinematic scattering theory fails to describe the scattering and approaches including dynamic scattering theories have to be applied. Second, many of the experiments performed so far were conducted at incident angles α_i close to the critical angles of the polymer film α_cP and the substrate α_cS in order to increase the off-specular scattered intensity or to vary the indentation depth by changing α_i. As it is difficult to vary α_i and adjust a circular beamstop with respect to the specular reflected beam, a rod like beamstop is usually used which covers most of the incident plane. However this has the drawback, that most of the intensity along q_z is blocked by the beamstop.

In a forthcoming publication we will present a dynamic scattering theory, which is able to explain the scattering at angles close to the critical angle of total reflection in the context of the distorted wave Born approximation [7]. In this theory it is expected, that the refraction and reflection effects are most pronounced at angles around the critical angle for total reflection and for large α_i kinematic scattering can be assumed. Experiments performed at low α_i confirm this approach, even though a rod like beamstop has been used and only the tails of rather broad peaks could be observed. In general the diffuse scattering at $\mathbf{q}_{||} = 0$ Å$^{-}1$ contains the same information than the

specular reflectivity. However, in specular reflectivity one has to scan over many incident angles which can be very time consuming, while in GISAXS the experiment can be performed in a single shot.

In order to test the theory developed in Ref. [7] we investigated the same film as in Ref. [7] at larger α_i. The lamellar Polystyrene-polybutadiene block copolymer had a molar mass of $\bar{M}_n = 22.6$ kg/mol and a lamellar thickness of $D_{lam} = 197$ Å. The film was prepared by spin coating from toluene solution and had a film thickness of 1570 Å, which is 8 times the lamellar thickness.

Fig. 2.15a shows the two-dimensional GISAXS-map at α_i = 0.99°. Several peaks can be observed in the scattering plane ($\mathbf{q}_{||} = 0$ Å^{-1}). This can also be seen in figure 2.15b, were a cut at $\mathbf{q}_{||} = 0$ Å-1 is shown. In Figure 1c the peak positions expected from the calculations in Ref. [7] are shown in dependence of the incidence angle α_i and the experimental peak positions from figures 2.15a and b are drawn as circles. The two peaks at $q_z \approx 0.1°$ can be understood as the first and second order peaks, respectively. However, for the second order peak the q_z-position is highly affected by refraction and appears at nearly the same value as the first order peak. Thus, even at values of α_i which are much larger than α_{cP} dynamic scattering cannot be neglected for the length scales typically covered by diblock copolymers.

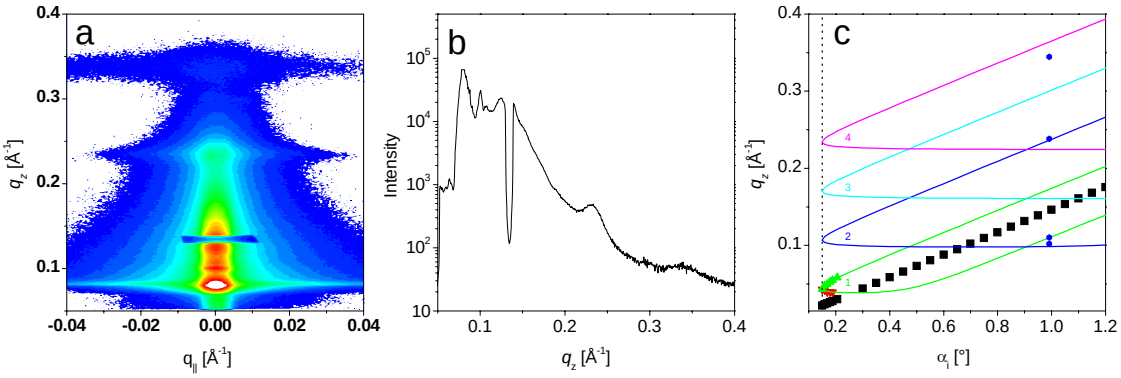

Figure 2.15:
(a) GISAXS-map of a block copolymer film with lamellae oriented parallel to the films interfaces.(b) Vertical cut at $\mathbf{q}_{||} = 0$ Å^{-1} of the GISAXS-map in (a). (c) q_z-positions of the diffuse peaks in dependence on α_i. Squares: specular reflected beam, circles: $q_z$positions of diffuse peaks in (a), lines: peak positions predicted by Ref. [7], the orders are given as numbers in the graph. The vertical line denotes α_{cP}. For comparison, the peak positions observed in Ref. [7] are included as triangles.

[1] M. Li, K. Douki, K. Goto, X. Li, C. Coenjarts, D.-M. Smilgies, C. K. Ober, Chem. Mater. **16**, 3800 (2004)

[2] P. Du, M. Li, K. Douki, X. Li, C. B. W. Garcia, A. Jain, D.-M. Smilgies, L. J. Fetters, S. M. Gruner, U. Wiesner, C. K. Ober, Adv. Mater. **16**, 953 (2004)

[3] D.-M. Smilgies, P. Busch, C. M. Papadakis, D. Posselt, Synchr. Rad. News **15**, 35 (2002)

[4] P. Müller-Buschbaum, Anal. Bioanal. Chem. **376**, 3 (2003)

[5] C. M. Papadakis, P. Busch, D. Posselt, D.-M. Smilgies, Adv. Sol. State Phys. **44**, 327 (2004)

[6] P. Müller-Buschbaum, M. Stamm, Macromolecules **31**, 3686 (1998)

[7] P. Busch, D. Posselt, M. Rauscher, D.-M. Smilgies, C. M. Papadakis,to be publisched

Morphology of annealed gold nanoparticle thin films: Influence of film thickness and annealing time

S.V. Roth [1], H. Walter [2], R. Gehrke [1], P. Müller-Buschbaum

[1] HASYLAB, Hamburg
[2] CSEM SA, Zürich (Switzerland)

Controlling the morphology of noble metal nanoparticle layers is of high technological and scientific interest. The broad field of application of such layers includes solar cells, bio-recognition and optocelectronic devices. This is due to the plasmon resonance in noble metal nanoparticles leading to strong absorption bands in the visible light. The plasmon resonance can be considered as a collective motion of the free electron gas. It depends strongly on the nanoparticle layer structure and morphology. A very simple route to structuring is low-temperature annealing [1]. We investigated a two-layer system consisting of a gold nanoparticle layer on top of a glass substrate. In this study we focussed on the evolution of evaporated gold nanoparticle layers as a function of two parameters: 1. nanoparticle layer thickness, ranging from 3 nm to 8 nm and 2. annealing time at 300^{o}C (for 0-24h).

Whereas a local surface information is easily obtainable with atomic force microscopy (AFM), a statistically more significant characterization of the large scale samples becomes accessible with scattering techniques. Although gold is a strongly scattering material and might give rise to a weak signal in a transmission geometry already, by the use of a reflection geometry the surface sensitivity is enhanced [2].We investigated the samples using grazing incidence small-angle x-ray scattering (GISAX) using the ultra-small angle option uniquely offered at the BW4 beamline [2]. This combination of reflection geometry and USAX setup is especially suited to investigate structural and morphological changes at length scales up to larger than 1 μm. The GIUSAX measurements were carried out at the beamline BW4 of HASYLAB. The wavelength used was 0.138 nm and a sample-to-detector distance 12.87 m with an angle of incidence α_i= 0.631^o. The beam size was 400x400 μm^2, defined by two high-quality entrance cross-slits ensuring a high signal-to-background ratio. Most part of the scattering pathway was under high vacuum conditions to reduce background by air scattering. Samples were placed in the special designed GISAXS chamber and measured ex-situ for different annealing times and film thickness, respectively.

The two-dimensional GIUSAX signal can be characterized by two perpendicular line cuts, the so-called detector- and out-of-plane scan. In the detector-scan, the behavior of the signal along the line (α_i constant, α_f variable) is followed. Here correlations perpendicular to the sample surface can be investigated. One remarkable feature is the Yoneda peak, which occurs at the critical angle of the material under consideration at α_i,α_f=α_c. In the out-of-plane scan the signal is characterized as a function of the out-of-plane scattering vector $q_y = 2\pi/\lambda \sin(\psi)$ with 2ψ being the out-of-plane scattering angle. Here, correlation parallel to the sample surface are detected.

Fig. 2.16A shows a detector-scan of the 8nm gold nanoparticle layer as a function of annealing time. For comparison, data from the bare substrate have been included in the plot as well (bottom) to picture the influence of the added gold layer. With increasing annealing time of 0, 10, 20 minutes and 1, 3, 7 and 24 hours (curves shifted from the bottom to the top along the intensity axis for clarity) the scattering pattern is altered. The Yoneda peak at 0 min at Φ=1.05^o can be attributed to the gold nanoparticle layer. With increasing annealing time the Yoneda maximum approaches the

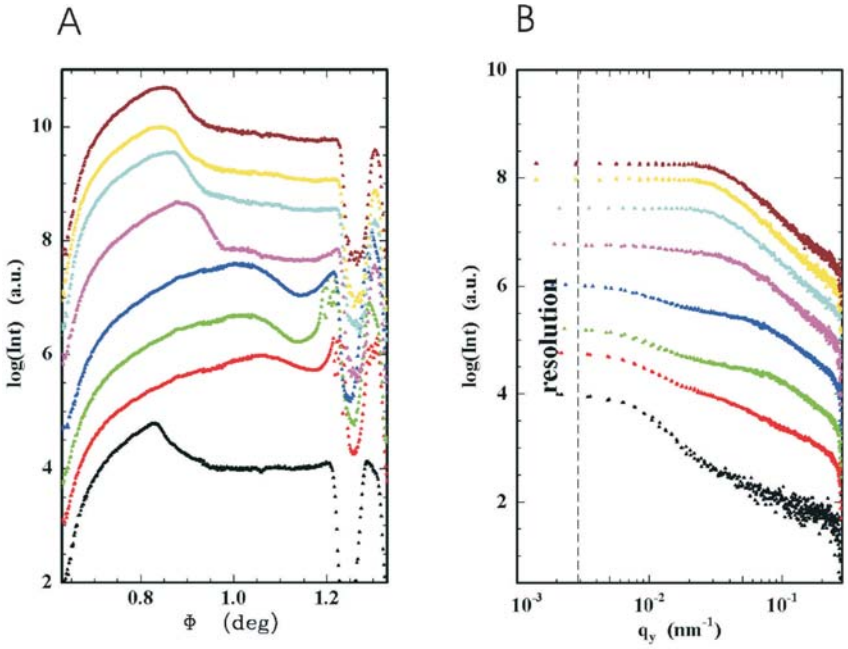

Figure 2.16:
GISAX data of the 8nm gold nanoparticle layer: Detector-scans (A) with the detector angle Φ and out-of-plane scans at 0.43^o (B) are displayed as a function of annealing time. From the bottom to the top the data result from the bare substrate and gold films annealed for 0 min, 10 min, 20 min, 1 h, 3 h, 7 h and 24 h. The curves are shifted along the intensity axis for clarity. In the detector scans the specular peak is absence due to the use of moveable beamstop shadowing the strong specular signal The dashed line in B shows the resolution limit.

Yoneda peak of the substrate. Fig. 2.16B shows the corresponding out-of-plane scans at α_f=0.43^o (critical angle of gold at the chosen wavelength). Again data of the bare substrate are included in figure 2.16B (bottom) to demonstrate the absence of most prominent in-plane lengths in the simple substrate. Without annealing already a weak shoulder is present in the data, corresponding to a small but less well defined lateral structure. With increasing annealing time the shoulder shifts to smaller q_y-values, indicating an increasing most-prominent in-plane length $\xi = 2\pi/q_y$. These results are compatible with an increased coarsening of the nanoparticle layer, e.g. induced by a coalescence of the nanoparticles. Additional optical interferometric measurements allow to correlate the temperature dependance with a shift in the plasmon resonace frequency [3]. A more detailed data analysis is in progress, including a fitting of 2d intensity data [4].

[1] J.C. Hulteen, C.J. Patrissi, D.L. Miltner, E.R. Crosthwait, E.B. Oberhauser, C.R. Martin; J. Phys. Chem. B **101**, 7727 (1997)

[2] P. Müller-Buschbaum et al.; Europhys. Lett. **40**, 655 (1997)

[3] S.V Roth, H. Walter, R. Gehrke, P. Müller-Buschbaum; to be published

[4] P. Müller-Buschbaum, N. Hermsdorf, S.V. Roth, J. Wiedersich, S. Cunis, R. Gehrke; Spectrochimica Acta Part B: Atomic Spectroscopy **59**, 1789(2004)

Internal structure of lamellar composites films with big nanoparticles

V. Lauter-Pasyuk, H. J. Lauter [1], M. Jernenkov [1], A. Petrenko [2], P. Müller-Buschbaum, W. Petry

[1] ILL, Grenoble (France)
[2] Joint Institute for Nuclear Research, Dubna, (Russia)

Diblock copolymers microphase separate into spatially periodic structures. Upon annealing the polymers self-organized in lamellar, cylindrical, spherical or more complicated mesophases [1] depending on their symmetry. In the present investigation, nanocomposite thin films consist of a diblock copolymer and nanoparticles. Nanoparticles can self-assemble within ordered structures of block-copolymers in periodic arrays. The morphology of such hybrid system depends on the properties of the copolymer and on the size and volume fraction of the nanoparticles. The phase diagram as a function of the nanoparticle size and the length of the polymer chain was studied theoretically [1]. However, experimental studies of such systems are still scanty.

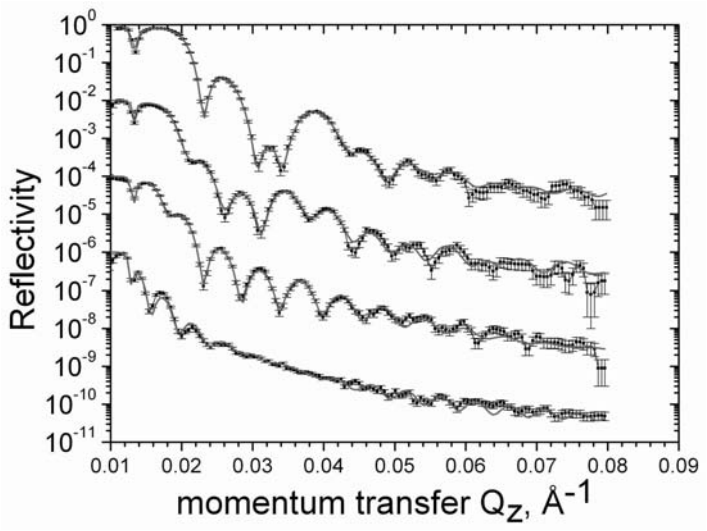

Figure 2.17:
Experimental reflectivity data (filled circles) extracted from the measured 2-dimensional (μp_f-maps of scattered intensity for samples with v_f = 5, 10, 20, 40% (from top to bottom), the fitted reflectivities are shown with solid lines.

We used symmetric poly(styrene-deuterated-block-buthylmethacrylate), denoted P(Sd7-b-BMA), diblock-copolymer films as a matrix for the nanoparticle arrangement. [2-4]. The molecular mass of P(Sd7-b-BMA) was M_w = 187 kg/mol. Magnetite Fe_3O_4 nanoparticles were coated with short chains of sulfonated α-lithium polystyrene, providing the affinity of nanoparticles to the PS layers. The mean size of the nanoparticles as determined with light scattering is 10 nm. Via a self-organization process we succeeded to produce nancomposite lamellar films with the concentrations of nanoparticles ranging from 5 to 40%.

For the synthesis of the composite, the control over the structure of the host matrix as well as over the spatial distribution of the nanoparticles inside the composite is required. Here we used

neutron reflectometry, which yields simultaneously in specular reflection the depth profile and in off-specular scattering the lateral structure of the nanocomposite film.

The experiments on neutron specular reflection and off-specular scattering were performed on the D17 reflectometer at the Institut Laue Langevin at Grenoble, using the time-of-flight method with the wavelength band $\Delta\lambda$ from 0.2 to 2.0 nm and a fixed incident angle α_i = 1.4 deg. The data were recorded with a position sensitive detector in a wide range of incoming and outgoing wave vectors k_i and k_f . The reflected and scattered intensities were normalized for the detector efficiency and for the intensity distribution of the incident beam. The data are present in a two-dimensional intensity map as a function of p_i and p_f, where $p_i = 2\pi \sin\alpha_i/\lambda$ and $p_f = 2\pi \sin\alpha_f/\lambda$ are the components perpendicular to the sample surface of the incoming and outgoing wave vectors, respectively.

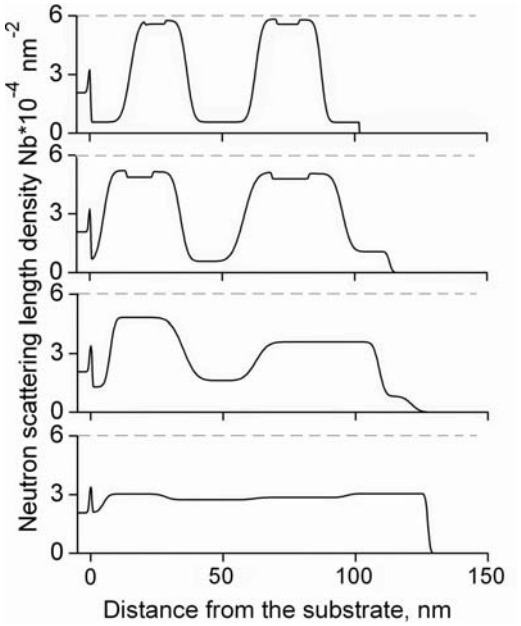

Figure 2.18:
Neutron scattering length density profile Nb (solid lines) obtained from the fit to the data is shown as a function of the distance from the substrate for increasing v_f = 5, 10, 20, 40% (from top to bottom). Deuterated PS layers have high Nb. 'Grooves' in the Nb of PS lamellar correspond to the positions of the nano-sheets averaged over the whole area of the sample.

The evolution of the reflectivity profiles extracted from these scattered intensity maps for all samples with different volume fractions of nanoparticles is depicted in figure 2.17. The data show that the increasing particle volume fraction causes a shift of the Bragg peaks to smaller values of momentum transfer q_z. So the thickness L of the lamellar period increases. This periodic and expanding structure persists up to v_f= 20%. The absence of the Bragg peaks for a very high volume fraction of nanoparticles v_f= 40% shows that the lamellar structure is absent. The transverse structure of the composite films obtained after the fit to the data is presented in figure 2.18. For v_f= 5 and 10% the films are organized into a well ordered lamellar structure with the particles concentrated around the central part of the PS layers. For the volume fraction of v_f= 20% nanoparticles are distributed through the PS layers. With further increasing of the volume fraction up to v_f= 40 % the lamellar structure cannot survive.

In conclusion, we investigated the buried structure of self-assembled block-copolymer nanocomposite films with high volume fractions of nanoparticles. The films are organized in a well-ordered structure, with nanoparticles concentrated within the polystyrene layers of the polymer matrix up to 20 % of the volume fraction of nanoparticles.

We acknowledge the support by the BMBF (grant No 03DU03MU).

[1] F. Bates, G. Fredrickson, Phys. Today **52**, 32 (1999)

[2] J.Y. Lee, R.B. Thompson, D. Jasnow, A.C. Balazs, Phys.Rev.Lett. **89**, 155503 (2002)

[3] B. Hamdun, D. Ausserre, S. Joly, Y. Gallot, V. Gabuil, C.J. Clinard, J. Phys.II France **6**, 493 (1996)

[4] V. Lauter-Pasyuk, H. Lauter, D. Ausserre, Y. Gallot, V. Gabuil, E.I. Kornilov, B. Hamdun, Physica B bf 241-243, 1092 (1998)

[5] V. Lauter-Pasyuk, H. Lauter, D. Ausserre, Y. Gallot, V. Gabuil, E.I. Kornilov, B. Hamdun, Physica B **248**, 243 (1998)

[6] V. Lauter-Pasyuk, H. Lauter, G.P. Gordeev, P. Müller-Buschbaum, B.P. Toperverg, M. Jernenkov, W. Petry, Langmuir **19**, 7783(2003)

Larmor Precession Reflectometry

H. J. Lauter [1],V. Lauter-Pasyuk, A. Petrenko [2], B.P. Toperverg [3], W. Petry, V. Aksenov [2]

[1] ILL, Grenoble (France)
[2] Joint Institute for Nuclear Research, Dubna, (Russia)
[3] PNPI, Gatchina, (Russia)

The spin-echo (SE) techniques for improving resolution of small angle neutron scattering (SANS) experiments have been applied to reflectometry and SANS at grazing incidence (GISANS) and have been summarized in Ref.1. SE-SANS is based similar to classical SE on encoding of the incident beam by the Larmor Precession (LP) phase by means of the polarization vector **P** and subsequent decoding by the 'echo'.

We show that a LP-device encodes the wavelength in time-of-flight (TOF) spectra by intensity oscillations. We also demonstrate how the LP technique is used for 3D vector polarization analysis to study magnetic layered structures.

The first studies of the LP-device have been proposed and carried out on the reflectometer REMUR [2] in TOF [3]. The LP-device in figure 2.19a is placed inside the reflectometer set-up using polarized neutrons with velocity $v_n(\lambda)$ (λ, the neutron wavelength) and neutron-spin analysis (A) in (+) direction in front of the linear PSD (D). The LP-device itself consists of two current sheets (CS) with a magnetic field H_{LP} in between them. The first CS starts the Larmor precession providing spin rotation in the x-z plane. The CS-current is adjusted such that the effective magnetic field in front of the CS (being composed of the field from the CS and H_{LP}) is at $\pi/2$ to the one behind the CS and thereby LP is initiated. The second CS, adjusted as the first CS, turns the rotation plane into the x-y plane for analysis [4]. The wavelength encoding is given by the accumulated phase F between the CS's with $\Phi = -\gamma H_{LP} L/v_n(\lambda)$ [1] (γ is - (2π)2916.4 Hz/G and L the distance between the CS's).

A thin polymer multilayer film (PS-PBMA with nanoparticles [4]) was used as a sample and was positioned in front of the CS's. The 2-dimensional (2D) intensity map in figure 2.20 shows the intensity of the direct beam as well as the intensity from the reflected beam as $f(\lambda)$ and the detector pixel position. The direct beam appears due to over-illumination. Off-specular scattering accompanies the reflected beam and crosses the high intensity spots of the Bragg-peaks. The figures 2.20a and b show the spectra with the LP-device switched off and on, respectively. So, intensity modulations being equidistant in λ are created over all the range shown in figure 2.20b. The period Φ of this structure originates from the LP between the current sheets and represents

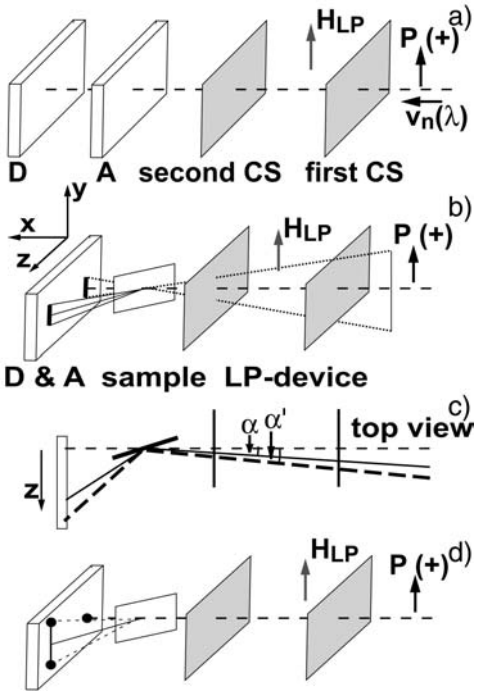

Figure 2.19:
Larmor precession set-up. a) The neutrons precess with the Larmor frequency between the first and second CS. The Larmor precession is made visible as intensity oscillations in the detector D through the effects of the second CS and the analyser A (see Fig.2). Guide fields are outside the LP device. b) Reflectometry set-up. c) Two beam case in reflectometry. d) GISANS set-up.

the encoding of the wavelength with period $\Phi = 6.2(2\pi)/\mathring{A}$ (L= 0.473 m and H_{LP} = ∼18G), in agreement with the number of oscillations per unit wavelength in figure 2.20b.

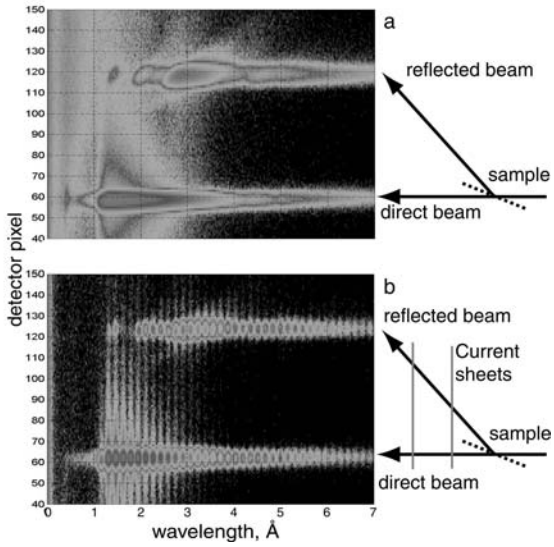

Figure 2.20:
2-dimensional intensity maps as a function of the linear PSD pixel position and the wavelength λ in TOF. a) The top map was obtained with the LP-device switched off and the bottom map with the active LP device (incoming beam with (-) polarisation). The arrows indicate the direct beam and reflected beam position.

The intensity profiles of the direct and reflected beam are displayed in figure 2.21 (here $H_{LP} \sim$ 20Gs, so that $\Phi = 6.6(2\pi)/\mathring{A}$). The division of the reflected by the direct beam intensity leads to the reflectivity curve without oscillations. Thus, the LP has no influence on the scattering process with the sample in front of the LP-device. The effect of a different path length of the neutrons through the LP-device in the direct beam direction and the reflected beam direction is too small to be recognized. This effect can be significantly enhanced by turning the CS's [5]. The same effect, which increases the angular sensitivity of the field integral between the CS's, was obtained in using a triangular shaped magnetic field in addition to H_{LP} (not shown here). This angular

encoding is intended to be used to separate in GISANS measurements the specular and scattered intensity with the aim to obtain high resolution [6].

Here an other very important application of the wavelength encoding in reflectometry (see figure 2.19b with direct and reflected beam) is outlined in the following. If aiming a gain in intensity the incoming beam is focused onto the sample and then each direction of incidence results in its own reflectivity curve $R(\alpha, \lambda)$ for each incident angle a. A simplification, the 2-beam case, is shown in figure 2.19c. From the two incident directions two reflectivity curves are obtained. However, off-specular scattering will overlap (see figure 2.20a, if one takes here as the 2 beams the direct beam and reflected beam). Encoding made in figure 2.20b can solve the problem of separation by the difference in the phase of the intensity oscillations due to a different path length in the LP field of the beams at α and α' in figure 2.19c.

An other promising application of the encoding method is envisaged for GISANS outlined in figure 2.19d. If a size distribution of the objects, from which the scattering originates in a film, is expected, then the two 'diffraction points' smear out to a distribution in y-direction. The incoming beam has to be collimated along z and y to provide the necessary resolution. However, wavelength encoding can be used in y-direction to collect intensity from an incoming beam spread in y-direction like in figure 2.19b. to gain appreciably intensity in GISANS. The LP-device in figure 2.19d has to be turned by 90^o in order to be sensitive in y-direction.

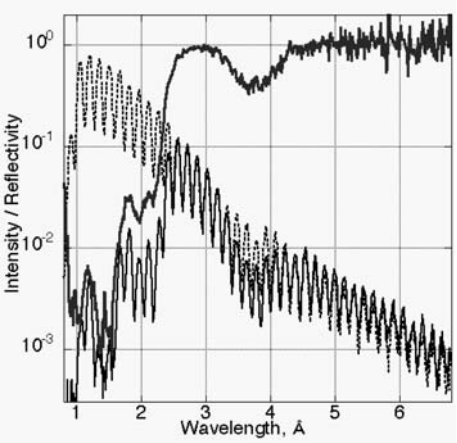

Figure 2.21:
Intensities from a reflectometry set-up with LP-device as a function of wavelength. Dotted curve: direct beam profile (with (+) polarisation); Full line with oscillations - reflected signal from polymer sample. The part of the curve joining at large wavelength λ the direct beam profile is the total reflecting region. Both curves show intensity oscillations due to LP. The third curve is the reflectivity obtained by division of the reflected intensity by the direct beam intensity. The critical wavelength λ_c is at $\sim 4.3\mathring{A}$.

We acknowledge the support by the BMBF (grant No 03DU03MU).

[1] R.Pynn et.al., Rev.Sci.Instrum. **73** 2948 (2002)

[2] Reflectometer REMUR (http://www.jinr-ru)

[3] H.J. Lauter, B.P. Toperverg, V. Lauter-Pasyuk, A. Petrenko, V. Aksenov, Physica B **350**, E759 (2004)

[4] private communication of V. Bodnarchuck and E. Dokukin

[5] V. Lauter-Pasyuk, H. Lauter, G.P. Gordeev, P. Müller-Buschbaum, B.P. Toperverg, M. Jernenkov, W. Petry, Langmuir **19**, 7783(2003)

[6] M.T. Reckveldt, Physica B **234** 1135 (1997)

[7] G.P. Felcher, 'SERGIS' Proc. of SPIE, **4785** 164 (2002)

3 Liquid dynamics

Al-Ni and Al-Ni-Ce melts: short range order and diffusion

S. Mavila Chathoth, A. Meyer

We have shown that in dense hard-sphere like liquids transport mechanism become highly collective and the packing density dominate in the mass transport[1-2]. The liquid Al-Ni and glass forming Al-Ni-Ce alloys exhibit a prepeak in the static structure factor. The prepeak indicate that the liquids are no longer random hard sphere mixtures. In a neutron scattering experiment[3], it was shown that the chemical short range order in the liquid appear as a prepeak in the structure factor at an intermediate length scale around 1.8Å^{-1}. To understand, how CSRO affect the mass transport, we studied the composition dependence of the CSRO and Ni self-diffusion in Al-Ni melts.

The alloys were prepared from a mixture of pure elements by arc melting in an Argon atmosphere. The liquidus temperature measured by differential scanning calorimetry and are in excellent agreement with the phase diagram[4]. For neutron time of flight experiments thin walled Al_2O_3 containers has been used that provide a hollow cylindrical sample geometries of 22mm diameter and 0.7 to 1.3mm wall thickness. For the chosen geometries and neutron wavelengths the samples scatter less than 5%. Therefore, multiple scattering which would alter the data especially toward low q only has a negligible effect.

The incident neutron wavelength λ = 5.1Å give an accessible wavenumber range q = 0.2 to 2.0Å^{-1} at zero energy transfer. Regarding the scattering cross sections of the individual elements, with the first structure maximum at $q_0 \cong 3.0$ Å^{-1} our spectra are dominated by incoherent scattering from nickel, since the incoherent scattering cross section of Al is negligible. The alloys were measured at room temperature to obtain instrumental energy resolution function. In the liquids, data were collected at different temperatures with a duration of 2 to 3 hours each. At each temperature, empty cell run was also performed. In order to obtain scattering law $S(q,\omega)$ (Fig.1), the raw data were normalized to a vanadium standard, corrected for self absorption and container scattering, interpolated to constant q and symmetrized with respect to energy with the detailed-balance factor.

Structural information on an intermediate length scale can also be obtained from inelastic neutron scattering by integrating the scattering law $S(q,w)$ over the quasielastc line. The figure 1.1 displays this quasielastic structure factor $S_{qu}(q)$ for Al-Ni melts at 1795K. For Al rich alloys the spectra exhibit a prepeak. Its intensity increases with increasing Ni content, its position shifts from $\simeq$1.6Å^{-1} in $Al_{80}Ni_{20}$ to $\simeq$1.8Å^{-1} in $Al_{62}Ni_{38}$. In $Al_{90}Ni_{10}$ nearly no prepeak is visible anymore. The quasielastic structure measured at 1525 K shows similar characteristic. On Ni rich side the $Al_{25}Ni_{75}$ $S_{qu}(q)$ also exhibit a prepeak. This prepeak is much broader and it has a maximum approximately 1.5Å^{-1}.

In the hydrodynamic limit for $q \rightarrow 0$ one expects that the mean relaxation time $\langle\tau_q\rangle$ are indirectly proportional to the momentum transfer q square. The 1/q^2 dependence of the mean relaxation time demonstrates that structural relaxation leads to long range atomic transport with a diffusivity D = $[\langle\tau_q\rangle q^2]^{-1}$. The figure 1.2 shows the Ni self-diffusion coefficients as a function of composition at 1525K and 1795K. At 1795K the value range from 3.95$\pm$0.10$\times$10^{-9}m^{2}s^{-1} in $Al_{25}Ni_{75}$ to 10.05$\pm$0.11$\times$10^{-9}m^{2}s^{-1} in $Al_{90}Ni_{10}$. The Ni self diffusion coefficient in $Al_{25}Ni_{75}$ is equal to the value in pure liquid Ni with D = 3.80$\pm$0.06$\times$10^{-9}m^{2}s^{-1}[2]. Substitution of 25% Ni by Al

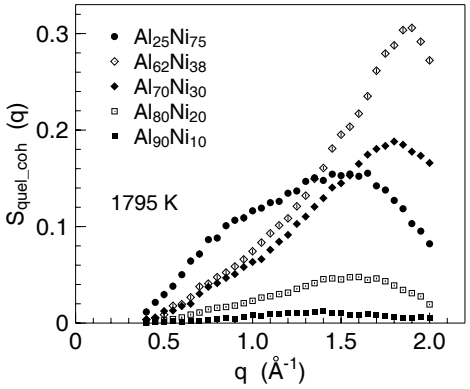

Figure 3.1:
$S_{qu}(q)$ of Al-Ni alloys at 1795K and is obtained by subtracting incoherent contribution from Ni. The coherent contributions from the CSRO in the liquids appears as a prepeak in the structure factor.

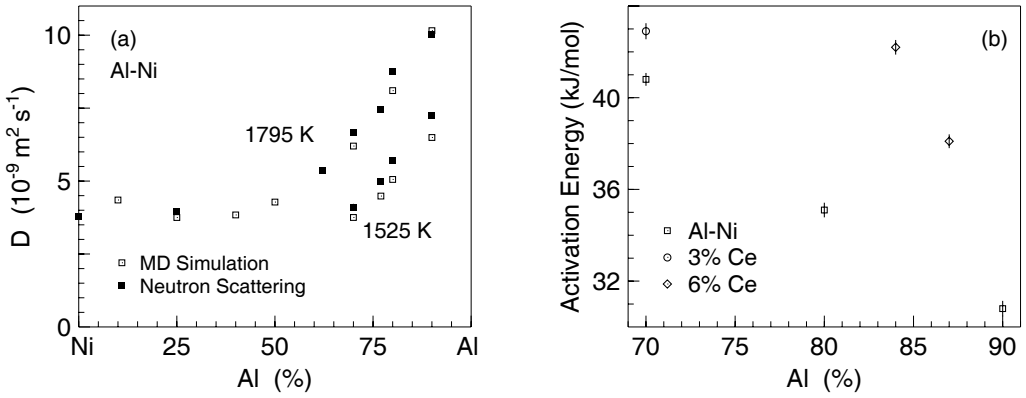

Figure 3.2:
(a): Ni self-diffusivities in Al-Ni melts (MD simulation by S.K. Das and J. Horbach[5]) and (b): Activation energy for Ni self-diffusion in Al-Ni and Al-Ni-Ce melts as a function of Al concentrations

does not affect the diffusion coefficient significantly. In contrast, on Al rich side diffusion shows a pronounced increase with increasing Al content.

The Al-Ni alloy displays a non linear behavior in the atomic volume and hence a nonlinear packing. It shows that the decrease in Ni diffusivity while increasing the Ni content is essentially a packing effect. Addition of Ce in Al-Ni shows a similar prepeak intensity but change in its maximum. The prepeak position is shifted toward a higher q values. Also, the addition of Ce increases the activation energy for the self-diffusion of Ni, higher the Ce content higher is the activation energy at a given Al concentration.

[1] A. Meyer, Phys. Rev. B. **66**, 134205 (2002)

[2] S. Mavila Chathoth, A. Meyer, M. M. Koza, F. Juranyi, App. Phys. Lett. **85**, 4881 (2004)

[3] M. Maret, T. Pomme, A. Pasturel and P. Chieux, Phys. Rev. B. **42**, 1598 (1990)

[4] B. Predel, edited by O. Madelung, *Phase Equilibria of Binary Alloys* (Springer, Berlin, 2003)

[5] S. K. Das, J. Horbach, M. M. Koza, S. Mavila Chathoth, A. Meyer, App. Phys. Lett. (in press)

Diffusion mechanism in sodium borates investigated by light scattering

E. Longueteau, F. Kargl, A. Meyer

Understanding of ionic diffusion in strong glasses is of main interest for theoretical and industrial points of view. Our motivation is thus to study the mechanism for ion diffusion in glasses and melts.

Neutron experiments [1,4] and molecular dynamic simulations [2,3,4] on sodium silicates showed that sodium atoms diffuse via diffusion channels in the static structure. A decoupling between sodium and glass matrix α-relaxations was observed. The sodium relaxation time was found to be 100 times smaller than the one corresponding to the matrix [5]. A β-relaxation which is associated to the motion of an atom into a cage formed by the neighbouring atoms was measured. However, for instrumental reasons, no decoupling of sodium and structure β-relaxations have been pointed out. This leads the question about the mode coupling theory suitability for multicomponent systems.

Now, we investigate wether the ion transport mechanisms of sodium-silicates can be applied to sodium-borates or sodium-germanates as well. Beside quasielastic neutron scattering, in the transparent systems light scattering with its extended dynamic range can be used as well.

Signals measured in depolarised light scattering are very weak. In sodium diborate, it has been measured in range of $5.10^{-3} photons/second.channel$ with a resolution function in range of 150 MHz (high resolution configuration). To obtain such a result the tandem Fabry-Perrot interferometer (FPI) had been optimised by realigning the internal and external optics. Measurements of ethanol spectra before and after the realignment show an enhancement of the signal by a factor greater than 10 over the full range for both polarised and depolarized configurations. More over, in order to make long acquisition durations possible, we have bought and adapted a new mirror controlling electronics for the FPI. Now, up to 6 days of stabilisation can be planned.

We designed a vertical tube furnace allowing the spectrum measurement of liquid glasses in backscattering configuration. A mirror and a 10-cm focal doublet located on the top of the furnace deviate the beam vertically, focus the incident laser beam on the sample and collect the scattered light with a numerical aperture of 0.32. An infrared filter is inserted between the lens and the furnace to reduce the black body emission. Otherwise this could damage the interface glue of the doublet and could again enhance noise on the measurement.

Figure **??** is a plot of the depolarised light scattering susceptibility of the sodium-diborate at $300°C$, $400°C$, $500°C$, $700°C$, $800°C$, $900°C$ and $1000°C$. As the glass transition temperature is around $480°C$, it was not possible to measure $600°C$ because of sample crystalization. Each curve consists of 3 single spectrum measurements at different resolutions. The adjustment have been achieved by overlapping their common parts.

From $700°C$ to $1000°C$, the high frequency tail of an α-relaxation is clearly visible. We had to fit these data with mode coupling theory to dissociate sodium and matrix relaxations. For the low temperature and low frequency range, one can observe broad structures in the susceptibility which are not expected. This perturbation is due to an indetermination of incident wave-vector resulting from the reflexion of the beam on the platinium sample holder. This hinders us to measure the sodium α-relaxation which is supposed to be present below the glass transition.

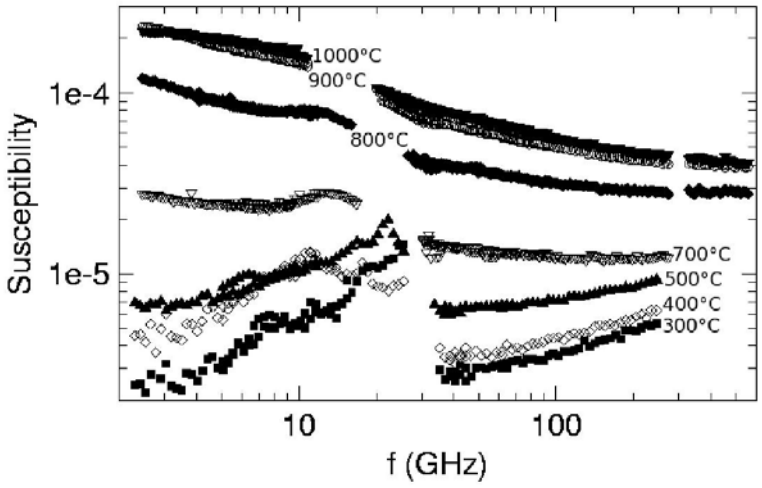

Figure 3.3:
High frequency tail of sodium-diborate α-relaxation for various temperatures.

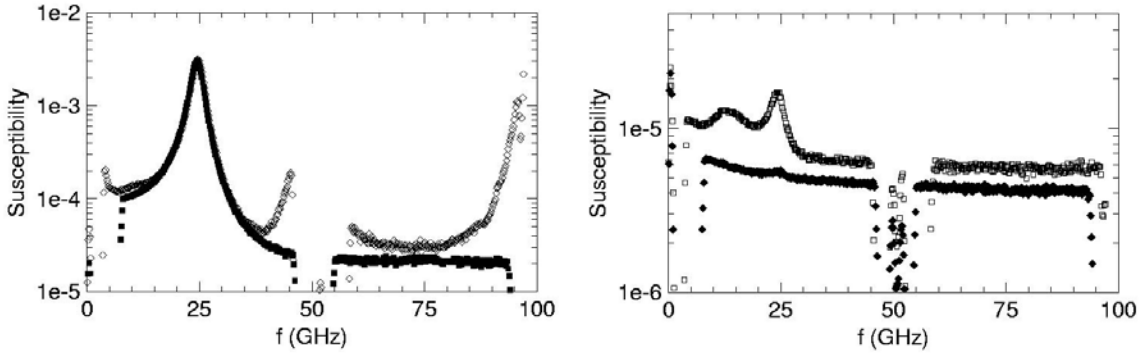

Figure 3.4:
Polarized (left) and depolarized (right) susceptibility of sodium-diborate measured in a crucible shape sample holder (empty symbols) and in the wire loop (filled symbols) at $700°C$. The polarized wire loop susceptibility has been divided by 2 to compare the shape of Brillouin peaks.

To bypass this problem one can use a wire loop sample holder: by capillarity the liquid state sample is holded in the center of a platinium wire loop. This technique avoids the presence of platinium in the beam path. This wire loop will be inserted in the tube furnace.

Figure 3.4 shows the comparison between signals collected in the crucible shape sample holder and in the wire loop at $700°C$. One can observe the quasi-total disappearence of the low frequency perturbations on the VH wire loop data and a gain of a factor 2 in intensity for the VV configuration. This has been observed also for lower temperatures ($350°C$ an $550°C$). Thus the wire loop technique will provide a powerfull set-up to investigate the decoupling of relaxation in alkaline glasses.

Systematic investigations on the dynamics in sodium-borates and sodium-silicates over a broad temperature and frequency range are now feasible with E13 light scattering set-up.

[1] A. Meyer, H. Schober, D.B. Dingwell, Europhys. Lett. **59**, 70 (2002)

[2] P. Jund, W. Kob, R. Jullien, Phys. Rev. B **64**, 134303 (2001)

[3] J. Horbach, W. Kob, K. Binder, Phys. Rev. Lett. **88**, 125502 (2002)

[4] A. Meyer, J. Horbach, W. Kob, F. Kargl, H. Schober, Phys. Rev. Lett. **93**, 27801 (2004)

[5] F. Kargl, A. Meyer, Chem. Geol. **213**, 165 (2004)

Structural and Dynamical Properties of Hydrous Silica(tes)

M. Pöhlmann, A. Meyer, A. Müller, H. Schober[1], T. Hansen[1], G. Cuello[1], M. Benoit[2], and W. Kob[2].

[1] Institut Laue-Langevin, Grenoble, France

[2] Laboratoire des Verres, Université Montpellier II

The presence of water drastically alters the physical properties of silica(tes). The decrease in viscosity plays, e.g., a decisive role in explosive volcanic eruptions [1]. The use of water as defect passivant in SiO_2 used in semiconductor devices [2] is another example for the relevance of the mentioned systems. In silicates, water can dissolve to SiOH groups. In addition to OH groups, molecular water may be present. So far the water-induced microscopic mechanisms leading to the modification of the macroscopic properties of silicates like viscosity and electric conductivity are not understood well. We combine first-principles molecular dynamics computer simulations with neutron scattering techniques in order to understand the influence of water on the mass transport in silica(tes) as well as their electric properties. For the exploration of mechanisms associated to explosive volcanism, it is of course necessary to come to a common picture for the liquid state. Note that such an idea was recently obtained for sodium silicate systems [3], also using molecular dynamics computer simulations and neutron scattering. Due to the chemical analogy of the systems $(1\text{-}x)SiO_2+xH_2O$ and $(1\text{-}x)SiO_2+xNa_2O$ ($0\leq x\leq 1$), it can be assumed that both systems have similar mechanisms for mass transport. However, hydrous silicates are much more challenging to investigate:

- *Experiments are currently limited to the glassy state.* Since no pressure equipment is currently available for neutron scattering instruments at high temperatures, experimental data can only be obtained up to temperature where water is released from the silicate. This is the case above the glass transition temperature of the mixtures at several hundred Kelvin. (Note that more than 1000 K at several kbar are required in order to bring the mixtures in equilibrium at the sample preparation.)

- *Simulations are in principle limited to the liquid state.* A suitable interatomic potential as for sodium silicates does not exist for hydrous silica. Therefore the only way to perform computer simulations for hydrous silica are first-principle methods. Today's available computer power puts clear limits to the *ab initio* equilibration of viscous liquids. For the used system size of about hundred atoms, the time limit is at some tens of pico-seconds (these are six orders of magnitude less than in the classical approach used for sodium silicates). The lowest temperature at which equilibration can be achieved is 3000 K. Information on the glass can only be obtained from samples based on ultra-rapid quenches.

The setup and the main results of the simulation for the liquid state of a system with the composition SiO_2+11.8mol%H_2O were recently described in [4,5]. Also structural information on quenched

samples has been obtained from experiments [6]. It is remarkable that even at the temperature of 3500 K and 3000 K the silica tetrahedral network is preserved. Also during an ultra-fast quench with a quench rate of the order of 10^{14} K/s the tetrahedral network is not destroyed (in agreement to other studies [7] and hence the structure at ambient temperature obtained from the computer simulation should be realistic. Indeed this can be demonstrated for the neutron scattering structure factor. Figure 3.5 shows the simulated neutron scattering structure factor for dry and hydrous silica at ambient temperature in comparison to the same quantity recorded at the ILL diffractometer D20.

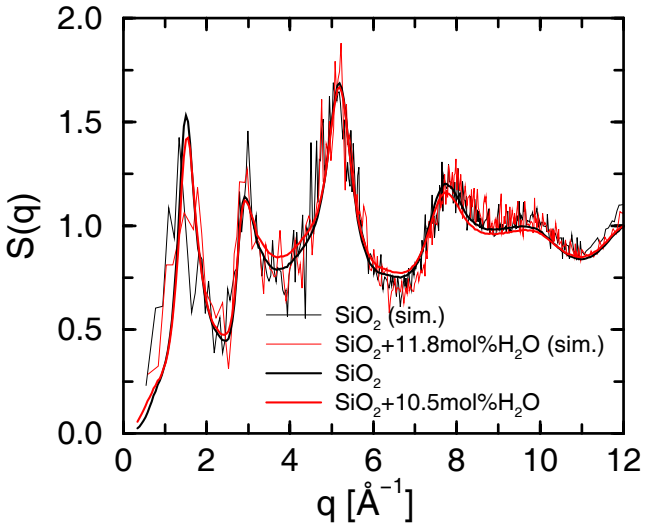

Figure 3.5:
Neutron scattering structure factor of pure and hydrous silica at 300 K as obtained from the experiment (bold lines) and the simulation (thin lines).

Generally the experimental and simulated curves are in rather good agreement. Deviations occur only for very low q and between 9 Å^{-1} and 12 Å^{-1}. At low q the deviations from the simulation to the experiment can be ascribed to the rapid cooling rate in the simulation. The deviations between 9 Å^{-1} and 12 Å^{-1} arise most likely from bad corrections of the experimental data. However, it should be recognized that -for a first main result- from the experimental and from the simulation side there are no indications that water affects the silica tetrahedral network considerably. In the context of the comparison to sodium silicates, it is interesting to note that the influence of sodium oxide on the structure of silica is much higher than the influence of water. This effect is predominantly related to the different sizes of the hydrogen and the sodium atom [5].
The neutron scattering structure factor S(q) is one of the few ways to validate the simulation and thereafter we believe more in the details of the simulation. Due to the *ab initio* character of the simulations, they are able to reveal electronic features of the system [8]. In particular the simulations were able to confirm predictions made many years ago on states in the electronic band gap that lead to (electronic) conductivity [9]. Note that such states may -for example- be responsible for the breakdown of semiconductor devices. Together with investigations of the protonic conductivity with neutrons, the simulations are able to investigate such concerns of the semiconductor industry.

[1] D. B. Dingwell. Science **273**, 1054 (1996)

[2] C. R. Helms and E. H. Poindexter. Rep. Prog. Phys. **57**, 791 (1994)

[3] A. Meyer, J. Horbach, W. Kob, F. Kargl, and H. Schober. Phys. Rev. Lett. **93**, 027801 (2004)

[4] M. Pöhlmann, A. Meyer, M. Benoit and W. Kob in *High Performance Computing in Science and Engineering, Munich 2004*. Transactions of the Second Joint HLRB and KONWIHR Result and

Reviewing Workshop, March 2nd and 3rd, 2004, Technical University of Munich. Springer-Verlag, Berlin, Heidelberg, New York, p. 199 (2004).

[5] M. Pöhlmann, M. Benoit, W. Kob. Phys. Rev. B. **70**, 184209 (2004), in press

[6] M. Pöhlmann, A. Meyer, A. Müller, H. Schober, T. Hansen, Submitted to Phys. Rev. B

[7] K. Vollmayr, W. Kob, and K. Binder. Phys. Rev. B **54**, 15808 (1996)

[8] M. Pöhlmann, H. Schober, M. Benoit and W. Kob in *Proceedings of the 2004 Nanotechnology Conference and Trade Show, Boston (Ma), USA*, Vol. III, p. 73. The Nano Science and Technology Institute, Cambridge (2004)

[9] J. Robertson in *The physics and technology of amorphous* SiO_2. R. Devine (Ed.). Plenum Press, New York, 1988

Evolution of ion dynamics in silica based melts

F. Kargl, A. Meyer

Sodium silicate glasses and melts are widely used materials in glass technology. Properties of silica glasses are highly dependent on composition. Viscosity, a characteristic measure for the elastic response of a system on deformation, changes by orders of magnitude in a relatively narrow temperature range. Viscosity and its evolution with temperature is affected by the composition. In binary alkali silicates viscosity at a fixed temperature decreases by up to 10 orders of magnitude upon addition of small amounts of the alkali modifier to pure silica [1]. Recent investigations using inelastic neutron scattering revealed a prepeak in the elastic structure factor indicating medium range order [2,3]. The prepeak was studied depending on Na concentration in Na silicate melts. Its position is unaffected in the range of 20 mol% to 33 mol% Na_2O concentration. In addition fast Na dynamics on a 10 picosecond scale in the melt at temperatures of 1200 K to 1600 K was revealed. The Na ion relaxation was found to be decoupled by still three orders of magnitude in the melt.

A comparison with recent MD simulations performed by groups in Mainz and Montpellier revealed similar behaviour concerning ion dynamics and structure [3,4,5]. The prepeak in the structure factor was attributed to Na rich microchannels embedded in the static structure. These microchannels were identified to be responsible for the fast Na ion transport. Thus Na is clearly inhomogeneously distributed in the SiO matrix. Na disrupts the Si-O matrix and triggers formation of channels for ion conduction. The inhomogeneous distribution could explain the viscosity concentration behaviour in alkali silicates and the fast diffusion of Na.

In order to clarify whether the structural results found in Na silicates are general features of alkali silicates further experiments were performed on binary silicates depending on the alkali modifier species. Results of these investigations are discussed in more detail in the second report.

Our main effort in this report is guided towards the dynamical behaviour of Na silicates. One of the remaining puzzles which could not be solved within the very early performed measurements two years ago was whether all Na atoms participate in the fast diffusion process and whether this is long range type. Thus we performed an experiment on Na disilicate on the time-of-flight spectrometer IN5 allowing for smaller wavenumbers and timescales up to 100 ps due to the extremely smooth Gaussian type resolution function. The experiment was performed in the melt from 1100 K to 1600 K in steps of 100 K. Fast Na long range diffusion was observed. From the spectra diffusion coefficients were derived. A comparison of Na self diffusivities measured by means of

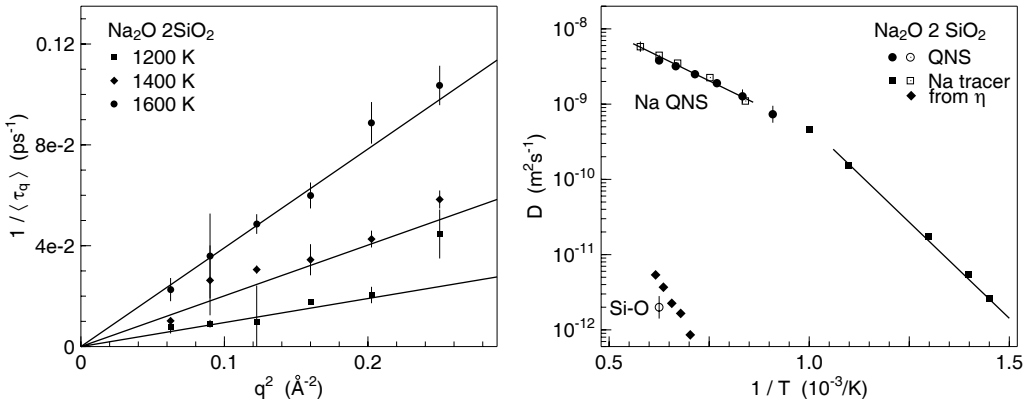

Figure 3.6:
Left: Relaxation rate versus momentum transfer squared. The relaxation rate features a q^2 dependence indicative for long range diffusion. Right: Arrhenius diagramm of diffusivities. Important are Na diffusivities by means of tracer diffusion [6] and by means of quasielastic neutron scattering.

tracer diffusion and our neutron scattering results revealed that the self diffusivities in the melt coincide within the experimental error. Thus we have experimental evidence that all Na atoms are participating in the fast process. We performed as mentioned above experiments on other binary alkali silicates. In K silicates due to the extremely low incoherent cross section of K we were not able to derive diffusivities from neutron scattering data. In case of lithium incoherent scattering is reduced by almost a factor of 3. The data obtained was not conclusive. However we observed that Li relaxation is on a shorter timescale as compared to Na for the same composition and temperature [7].

Macroscopic investigations revealed an increase in viscosity upon addition of Al_2O_3 corroborating that alumina might as a network former stiffening the disrupted Si-O matrix [8]. Partial substitution of the network modifier Na_2O by the network former Al_2O_3 resulted in an increase of the relaxation times by up to one order of magnitude at the same temperature in the melt [9]. In addition the prepeak is also decreasing. Thus we have experimental evidence that the network former Al_2O_3 obviously stiffens the network and disrupts the structure of ion conducting channels resulting in a decrease in Na mobility.

[1] R. Knoche, D. B. Dingwell, F. A. Seifert, S. L. Webb, Chem. Geol. **116**, 1 (1994).

[2] A. Meyer, H. Schober, D. B. Dingwell, Europhys. Lett., **59**, 708 (2002).

[3] A. Meyer, J. Horbach, W. Kob, F. Kargl, H. Schober, Phys. Rev. Lett., **93**, 027801 (2004).

[4] J. Horbach, W. Kob, K. Binder, Phys. Rev. Lett., **12** 125502 (2002).

[5] J. Horbach, W. Kob, K. Binder, J. Phys.: Cond. Matt., **15** S903 (2003).

[6] Y. P. Gupta, T. B. King, Trans. Met. Soc. AIME, **239**, 1701 (1967); J. R. Johnson, R. H. Bristow, H. H. Blau, J. Am. Ceram. Soc., **34**, 165 (1951).

[7] F. Kargl, A. Meyer, M. M. Koza, H. Schober, Phys. Rev. B (to be submitted)

[8] M. J. Toplis, D. B. Dingwell, T. Lenci, Geochim. Cosmochim. Acta, **61** 2605 (1997).

[9] F. Kargl, A. Meyer, Chem. Geol., **213**, 165 (2004).

Intermediate range order in binary alkali silicate glasses and melts.

F. Kargl, A. Meyer, M. M. Koza[1], H. Schober[1]

[1] Institut Laue-Langevin, Grenoble, France

In this report we focus on the evolution of the medium range order found in sodium silicate glasses with the network modifier species. Main aim of the study was to reveal whether the prepeak indicating intermediate range order is a general feature in alkali silicate melts. We replaced Na by K and Li. The enriched Li disilicate sample was provided by Paul Heitjans. In earlier studies of the static structure factors of silicate glasses and melts no prepeak indicating medium range order was revealed in the structure factor [1]. Main reason was that in these investigations an as large as possible momentum transfer range was used to allow for calculations of the real space correlator via Fourier transformation.

We performed investigations on sodium silicate glasses and melts up to 1600 K by means of inelastic neutron scattering [2,3]. Time-of-flight spectroscopy was performed on IN6 at ILL for various binary compositions [2,3,4]. Time-of-flight spectroscopy allows for investigations of the elastic structure factor. We use only five to eight percent scatters reducing multiple scattering down to a minor event. In addition even at high temperatures the elastic structure factor is not spoiled by multiphonon contributions as it would be the case for a direct measurement of the static structure factor. The elastic structure factor is obtained by integration over the instrumental resolution function. It is in good approximation proportional to the static structure factor times the Debye-Waller factor. Data was normalized to a vanadium standard. The background was subtracted and self absorption was taken into account. Thus, a direct comparison of the elastic structure factors of different compositions on an absolute scale is possible within an error of $\simeq 10$ %.

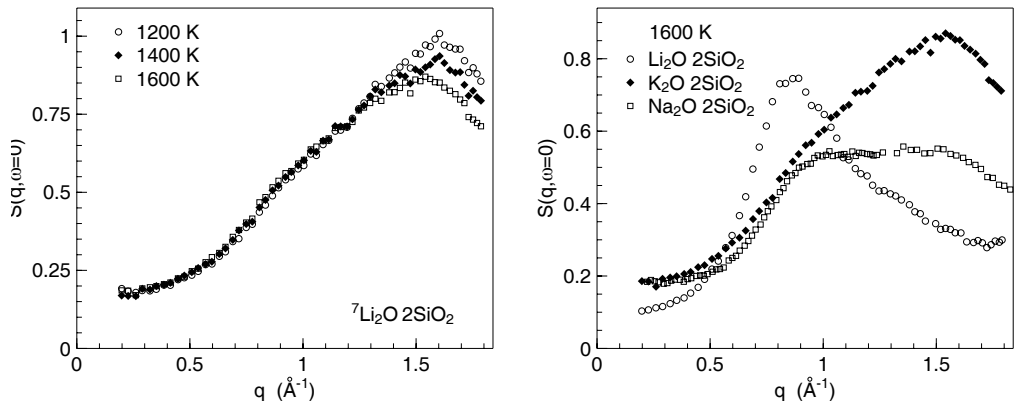

Figure 3.7:
Elastic structure factor of Li disilicate at three different temperatures in the melt (left). Comparison of the elastic structure factors of alkali disilicate melts at 1600 K containing potassium, sodium and lithium (right taken from [4]).

In case of the enriched lithium disilicate sample a slight loss of material during heating and the partial crystalline nature of the sample at room temperature lead to an error of about 20 % on an absolute scale. The height of the elastic structure factor was estimated by comparing our data with diffraction measurements performed on lithium disilicate glass [5].

In the lithium disilicate sample we observed only a preshoulder around 1.2Å^{-1} in the melt in the range of 1200 K to 1600 K. This preshoulder is almost constant in height. A decrease of the first sharp diffraction peak (FSDP) around $1.7\,\text{Å}^{-1}$ with the Debye-Waller factor similar to the sodium silicates is also found. The FSDP reflects typical SiO tetrahedra distances.

We compare the elastic structure factors of potassium disilicate, sodium disilicate and lithium disilicate at 1600 K. We observe a strongly pronounced prepeak in potassium silicate at 0.8Å^{-1}. This prepeak changes slightly position with increasing temperature and is also increasing in height (the latter is not shown). A first sharp diffraction peak related to characteristic distances of Si-O tetrahedra is absent in this sample. Thus, we conclude that the larger ion potassium disrupts even more the silica network. The position of the prepeak (preshoulder) shifts to larger q values with decreasing size of the modifier ion. The height of the FSDP decreases at the same temperature with increasing size of the modifier ion.

Intermediate range order is a general feature in binary alkali silicate melts and glasses. The SiO network is more disrupted the larger the modifier ion is. The medium range order present in these material could account for the fast modifier diffusion. A comparison with results provided from MD simulations on sodium silicates, we have an hint that the network of channels for fast ion conduction is present in all alkali silicates.

[1] Y. Waseda, H. Suito, Trans. Iron Steel Inst. Japan, **17**, 82 (1977).

[2] A. Meyer, J. Horbach, W. Kob, F. Kargl, H. Schober, Phys. Rev. Lett., **93**, 027801 (2004).

[3] A. Meyer, H. Schober, D. B. Dingwell, Europhys. Lett., **59**, 708 (2002).

[4] F. Kargl, A. Meyer, M. M. Koza, H. Schober, Phys. Rev. B, (submitted).

[5] N. Kitamura, K. Fukumi, M. Mizoguchi, M. Makihara, A. Higuchi, N. Ohno, T. Fukunaga, J. non Cryst. Sol., **274**, 244 (2000).

4 Dynamics of ordered and disordered solids

Martensitic transitions and single crystal growth of NiTi and NiAlMn shape memory alloys

T. Mehaddene, J. Neuhaus, W. Petry

There has been a growing interest in the study of Martensitic Transitions in shape memory alloys. Owing to its low transformation temperature and its biocompatibility, the NiTi system is among the most studied. The thermal, as well as, the mechanical properties of a nearly stoichiometric NiTi alloys have been the topic of several theoretical and experimental works. However, many high-temperature applications of the shape memory effect require a higher transition temperature than commercially available NiTi alloys. Currently, there are only a few experimental shape memory alloys known to exhibit martensitic transition temperatures well above room temperature, among them the ternary alloy NiAlMn. To get more insight on the physical behavior of the martensitic transition, well known as a phonon driven mechanism, information on the microscopical scale are needed. For this purpose, we are aiming at a single crystal growth, prerequisite to measure the normal modes of vibration, from which informations on the interatomic potential can be deduced.

In view of the preliminary Differential Scanning Calorimetry (DSC) measurements in NiAlMn, we have attempted to grow a stable $Ni_{50}Al_{22}Mn_{28}$ single crystal using the floating zone technique [1]. Starting rods of 10 cm in length and 6-10 mm in diameter were prepared by arc-melting of pure elements under Argon atmosphere. Several re-melts were carried out to insure a homogenous composition. The rod diameter and growth speed have been varied, however, the low surface tension made extremely difficult an accurate control of the molten charge. The Bridgman technique has been used with Alumina crucible of 6-8 mm in diameter. Pulling speeds of 10-15 mm/h led to samples containing a handful of small grains. Relatively large grains have been obtained using very low speeds e.g. 1-3 mm/h. Typical grain-size of 10-15 mm were obtained along the growth direction, but they do not extend over the whole cross section. We are now trying to cut out a reasonable large grain from the rod but the small grains on the outer parts of the rod make the task quite complicated. In the same time, we are planning to perform the Czochralski technique in which the solid-liquid interface is free on any contact.

In the case of NiTi, preliminary measurements of the martensitic transition temperatures have been performed using the DSC. Ni_xTi_{100-x} alloys with x =50.2, 50.6 and 50.8 were prepared by arc-melting of pure elements under Argon atmosphere. All samples were solution annealed for 1 hour at 1273 K under Argon atmosphere and subsequently water quenched. The measured Martensitic start temperatures (M_s) are in the range of 190-220 K and slightly sensitive to the thermal cycling as previously reported by Matsumoto [2]. A two-step transformation has been seen in the case of $Ni_{50.2}Ti$, in which case a slight departure of M_s from the expected line reported in the literature [3] is observed (Fig 4.1). Based on those results, first attempts to grow $Ni_{50.2}Ti$ and $Ni_{50.8}Ti$ single crystals have been made using the floating zone technique. Rods of 8-10 mm in diameter have been pulled at different speeds e.g. 15-20 mm/h. Transversal cross-sections have been cut, mechanically polished and etched to get optical micrographs. An example is shown in Fig. 4.2. Surprisingly, the micrograph shows a martensitic texture signature of a martensitic transition occurring well above the indicated temperature from the preliminary measurements. For seek of completeness, DSC measurements have been performed on as-prepared samples of NiTi. They all show a single-step transition above or around the room temperature. The measured

M_s for the different Ni content is reported in Fig. 4.1 for the quenched and as-prepared samples. In order to avoid the *in-situ* single crystal growth, higher Ni concentration have been investigated to lower M_s. A transition temperature of 268 K has been found for x =51. $Ni_{51}Ti$ rods of 8 mm in diameter have been pulled along 5-6 cm at 12 mm/h. Grain-size of 2-3 mm have been obtained. Thinner rods and lower pulling speeds are thus needed to get a reasonable large single crystal.

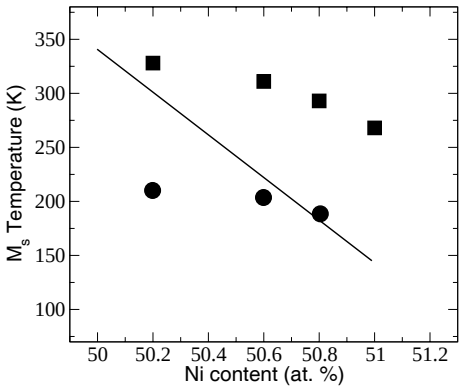

Figure 4.1:
Martensitic start temperature (M_s) of Ni_xTi_{100-x} alloys as a function of nominal Nickel composition for quenched samples (filled circles) and as-prepared samples (filled squares). The line shows the reported M_s variation versus temperature for quenched samples in the literature [3].

Figure 4.2:
Optical micrograph of a transversal cross-section of the $Ni_{50.2}Ti$ pulled rod showing that the sample did undergo a martensitic transition around or above the room temperature.

[1] T. Flottmann, W. Petry, R. Serve and G. Vogl, Nuclear Instruments and Methods in Physics Research **A260**, 165 (1987).

[2] H. Matsumoto, Journal of Alloys and Compounds **350**, 13 (2002).

[3] K. Otsuka, X. Ren, in *Materials Science Forum* **394-395**, 177 (2002).

Vibrational Dynamics of Glasses using Nuclear Inelastic Scattering: Collective Nature of the Boson Peak and Universal Transboson Dynamics

A. I. Chumakov[1], I. Sergueev[2], U. van Bürck, W. Schirmacher, T. Asthalter[3], R. Rüffer[1], O. Leupold[1], W. Petry

[1] ESRF Grenoble
[2] ESRF Grenoble and TU München, E13
[3] Physikalische Chemie, Universität Stuttgart

Using probe molecules with resonant nuclei and nuclear inelastic scattering we have measured the density of states exclusively for collective motions with a correlation length of more than ~ 20Å [1]. Such spectra exhibit an excess of low-energy modes (boson peak) which behaves in the same way as that observed by conventional methods, e.g. inelastic neutron, X-ray or Raman light scattering. When a probe is embedded in a glass matrix, it obviously must follow the

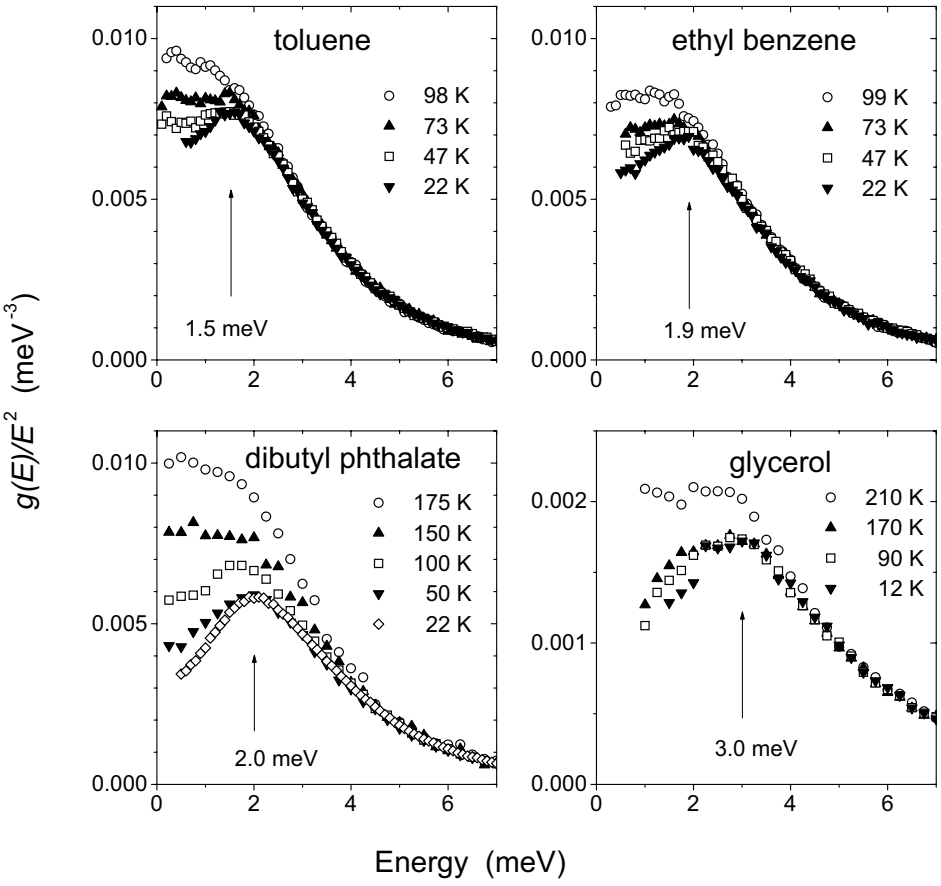

Figure 4.3:
Reduced DOS of collective motions in toluene, ethylbenzene, dibutylphthalate, and glycerol glasses. Arrows indicate the energy of the boson peak estimated from the data at lowest temperature.

collective motions of the glass with a correlation length larger than the probe size. On the other

hand, the vibrational spectrum of the probe is insensitive to local eigenmodes of the host, as long as the probe is not chemically bound. This insensitivity is confirmed by our experimental data. In order to monitor the motions of the probes, we used the isotope-selective technique of nuclear inelastic scattering (i.e. resonant inelastic scattering of x rays via low-energy nuclear transitions) and probe molecules with a resonant nucleus in the center of mass. With this approach, one monitors exclusively the motions of the central resonant nucleus. Furthermore, in this way one selects pure translational motions of the probes: Rotation is disregarded because the spectator nucleus is in the center of mass; the few intra-molecular modes are separated in energy. Therefore, the selected pure translational motions of the probe give a "density of states of collective motions" (CDOS) of the glass matrix.

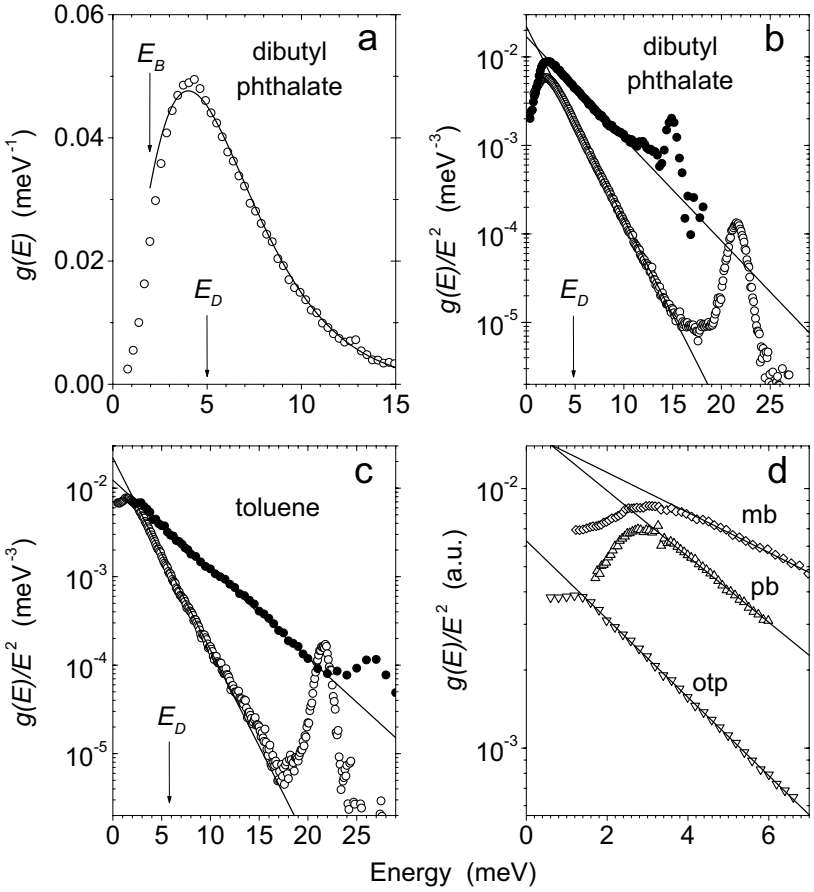

Figure 4.4:
(a) DOS of collective motions in dibutylphthalate at 22 K. Reduced DOS of collective motions in (b) dibutylphthalate and (c) toluene at 22 K (○) in comparison to reduced total DOS (●) from neutron data [2,3]. The neutron data are scaled to match our data at lowest energy. (d) Reduced total DOS from neutron data for orthoterphenyl (otp, ▽) [4], polybutadiene (pb, △) [5], and myoglobin (mb, ◊) [6]. Solid lines show the fit according to Eq. (4.1) The arrows indicate the Debye energy E_D and the boson peak energy E_B.

The CDOS in toluene, ethylbenzene, dibutylphthalate, and glycerol glasses was measured at the Nuclear Resonance beamline ID18 [7] of the European Synchrotron Radiation Facility with a 0.5 meV-bandpass inelastic spectrometer. The studied glasses cover a substantial range of Angell

fragility m from very fragile (toluene, *m*=105), fragile (dibutylphthalate, *m*=85), and intermediate (glycerol, *m*=53) glass formers. The probes were neutral ferrocene molecules with the central resonant ^{57}Fe nucleus for the three first glasses and $^{57}Fe^{2+}$ ions for glycerol. The size of the ferrocene probe (7.3Å) is close to those of the host molecules (7.0, 7.3, and 9.5Å for toluene, ethylbenzene, and dibutylphthalate, respectively). To follow the collective motions of the glass, the probe should experience correlated forces at least from the nearest molecules. Thus, it is sensitive to the collective modes with a correlation length of more than $\sim$20Å. The concentrations of the probes for the above mentioned glasses were 2.5, 2, 5, and 1% (mol). The probes did not cause noticeable changes in the glass properties. For instance, no changes in the static structure factor and in the calorimetric glass transition temperatures were revealed. Furthermore, lowering the probe concentration had no influence on the experimental results.

The reduced CDOS $g(E)/E^2$ clearly exhibits a boson peak for all studied glasses (Fig. 4.3). The positions E_B of the peak are consistent with the boson peak energies E_{Btot} in the total DOS from neutron and light scattering data. The temperature evolution of the boson peak (Fig. 4.3) shows the same features as observed with conventional methods: It is temperature independent at low temperatures, becomes less pronounced at higher temperatures and disappears when approaching the glass-liquid transition. This clear manifestation of the boson peak in the CDOS shows that a significant part of the modes constituting the boson peak must be delocalized collective motions with a correlation length of more than $\sim$20Å.

Concerning the frequency regime beyond the boson peak we find the astonishing result that all the low-temperature data can be precisely represented as

$$g(E)/E^2 \propto \exp(-E/E_0), \tag{4.1}$$

This is most easily seen from Fig. 4.4, where the data are represented semilogarithmically. We have also included data obtained from incoherent neutron scattering.

These findings can be explained using the mean-field theory of Schirmacher and co-workers [8] (see also the next contributions in this section). Within this theory it can be shown that the parameter E_0 is inversely proportional to the spatial extent of the probe atom or molecule. This explains the fact that the exponentials obtained in our experiments are steeper than those obtained from neutron scattering data.

[1] A. I. Chumakov, I. Sergueev, U. van Bürck, W. Schirmacher, T. Asthalter, R. Rüffer, O. Leupold, W. Petry, Phys. Rev. Lett. **92**, 245508 (2004)

[2] E. Duval *et al*., J. Non-Cryst. Sol. **307-310**,103 (2002)

[3] I. Tsukushi *et al*., J. Phys. Chem. Sol. **60**, 1541 (1999)

[4] R. A. Tölle *et al*., Eur. Phys. J. B **16**, 73 (2000)

[5] R. Zorn *et al*., Phys. Rev. E **52**, 781 (1995)

[6] W. Doster, S. Cusack, W. Petry, Phys. Rev. Lett. **65**, 1080 (1990)

[7] R. Rüffer and A. I. Chumakov, Hyperfine Interact. **97-98**, 589 (1996)

[8] E. Maurer and W. Schirmacher, J. Low-Temperature Physics, **137**, 453 (2004)

Comparison of Two Models for the Boson Peak

Walter Schirmacher, Edith Maurer

In order to study the vibrational properties of harmonic disordered solids we have considered a Debye-like solid, which allows for longitudinal waves only. In this framework we considered two models for disorder: randomly fluctuating elastic constants (intrinsic disorder) and coupling to

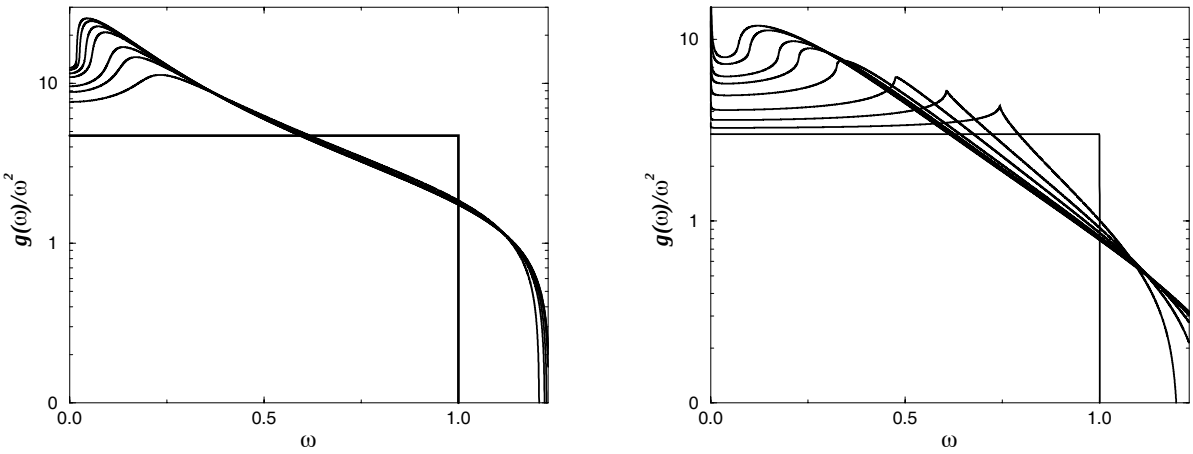

Figure 4.5:
Left: Reduced DOS $g(\omega)/\omega^2$ for the elastic disorder model with (from bottom to top) $\gamma = 0.0, 0.2, 0.3, 0.4, 0.45, 0.47, 0.49, 0.495$ in units of the Debye frequency.
Right: Reduced DOS $g(\omega)/\omega^2$ for the oscillator model with $g = 1, \omega_0 = 1$ and (from bottom to top) $\gamma = 0.0, 0.1, 0.2, 0.3, 0.4, 0.45, 0.47, 0.49, 0.495$

local oscillators (defects) with random eigen frequencies [1]. The first model has been treated in self-consistent Born approximation (SCBA), the second can be solved exactly. In both models an enhancement of the low-frequency vibrational density of states over that predicted by Debye is obtained ("boson peak") as a result of the presence of the disorder (Fig. 4.5). The disorder parameter γ is the variance of the fluctuating quantities, divided by the sqare of the mean. In both cases the system becomes unstable if the disorder is too strong. The boson peak is a percursor phenomenon of this instability. It marks the lower boundary of the frequency regime in which the disorder-affected states prevail. This regime becomes broader with increasing γ by virtue of the so-called level repulsion effect. Therefore the boson peak is shifted downwards in frequency with increasing disorder. From the figures it can also be seen that our theory reproduces approximately the experimental result [2], that in the "trans-boson" frequency regime the reduced density of states $g(\omega)/\omega^2$ decays exponentially, independent of the specific disorder model. From our theoretical expressions we find that such a law is obtained if the imaginary part of the disorder-induced complex sound velocity is of the same order as the real part and does not depend strongly on frequency. This regime coincides with the above-mentioned regime of the disorder-dominated vibrational states. Because the results are so similar, we are led to the conclusion, that perhaps any model, which involves coupled harmonic vibrations and disorder, may produce a boson peak and the associated exponential decay at higher frequencies. However, we consider the fluctuating-elastic-constant model to be superior to treatments with microscopic model assumptions because

it serves as a general explanation for the appearance of the boson peak in very different disordered solid materials.

[1] E. Maurer, W. Schirmacher, J. Low-Temp. Phys. **137**, 453 (2004)

[2] A. I. Chumakov, I. Sergueev, U. van Bürck, W. Schirmacher, T. Asthalter, R. Rüffer, O. Leupold, W. Petry, Phys. Rev. Lett. **92**, 245508 (2004). See also the previous contribution

Field-Theoretical Description of the Vibrational Dynamics of Disordered Solids, Including Transverse Degrees of Freedom

W. Schirmacher

The field-theoretical description of the vibrational dynamics of disordered solids which has been developed in our group in the last years [1] has been generalized to include transverse degrees of freedom. Within the previous approach only longitudinal waves were considered the sound velocity of which was assumed to fluctuate randomly in space. Within the present model we

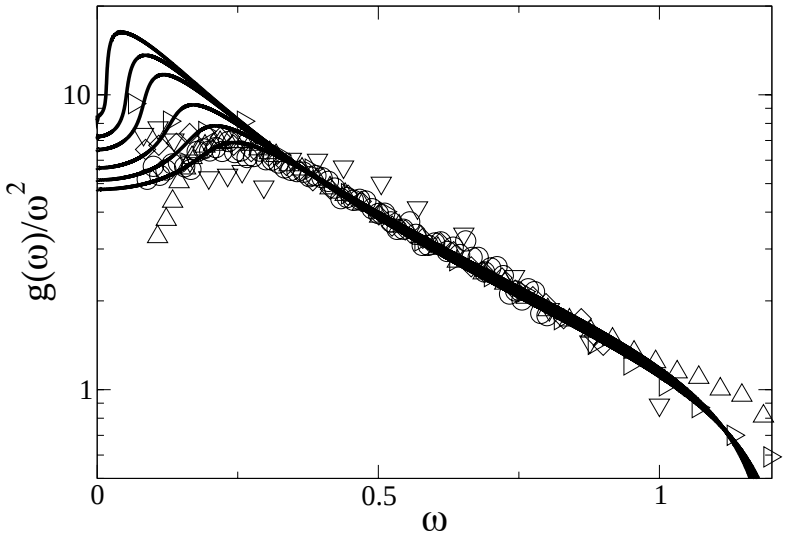

Figure 4.6:
Lines: Reduced DOS as calculated in SCBA for the disorder parameters (from bottom to top) $\gamma = 0.13, 0.14, 0.15, 0.16, 0.164, 0.1664$. In all calculations we use units in which c_T =1, k_D = 1, Θ_D = 1 (transverse sound velocity, Debye wave number, Debye temperature). The longitudinal sound velocity is set $c_L = \sqrt{2}c_T$. For this choice we have $\gamma_c = 1/6$.
Symbols: measured reduced density of states $g(\omega)/\omega^2$ for some glasses. The frequency has been scaled with a characteristic frequency, and the DOS has been multiplied with a scaling factor to obtain a "universal plot". ▷: simulated Lennard-Jones glass [2]; ○: metallic glass [3]; △: PMMA [4]; ◇: OTP [5]; ▽: SiO_2 [6].

consider the full vector degrees of freedom of elasticity theory, in which the longitudinal and transverse sound velocities $c_L^2 = (\lambda + 2\mu)/\rho$, $c_T^2 = \mu/\rho$ (ρ is the mass density) are represented in terms of the two Lamé coefficients λ and μ. We assume (in accord with experimental findings and theoretical considerations in the literature) that the dominant influence of the disorder comes

from the transverse elastic constant, i. e. we consider a spatially fluctuating $\mu = \mu(\mathbf{r})$. The parameter γ, which characterizes the disorder, is, again, given by the variance of the transverse Lamé coefficient μ, divided by the square of its mean. Applying the field-theoretical scheme used in our previous theory [1] to this case yields a generalized self-consistent Born approximation (SCBA), from which the vibrational density of states (DOS) can be calculated.

The results are quite similar to those of the previous theory [1]. However there is an interesting difference: In the "longitudinal" theory the system becomes unstable (due to the appearance of negative elastic constants) for a critical value of the disorder parameter $\gamma_c = 0.5$, whereas in the present model which includes the transverse degrees of freedom the instability occurs already for $\gamma_c \approx 0.17$. This means that the glass is much more sensitive to disorder in the transverse elastic constants, and, correspondingly, the boson peak is present already for quite small values of γ.

[1] E. Maurer, W. Schirmacher, J. Low-Temp. Phys. **137**, 453 (2004). See also the previous contribution in this annual report.

[2] A. Rahman, M. J. Mandell, J. P. McTague, J. Chem. Phys. **64**, 1564 (1976).

[3] A. Meyer *et al.* Phys. Rev. Lett. **80**, 4454 (1998).

[4] E. Duval *et al*., J. Non-Cryst. Sol. **307-310**,103 (2002).

[5] A. Tölle *et al*., Eur. Phys. J. B **16**, 73 (2000).

[6] U. Buchenau, N. Nücker, A. J. Dianoux, Phys. Rev. Lett. **53**, 2316 (1984).

The influence of the Boson peak on the thermal conductivity in disordered solids

W. Schirmacher

A theory of the frequency dependent diffusivity $D(\omega)$ has been developed on the basis of the mean-field approach describing the anomalous vibrational properties of disordered solids, which has been developed in our group [1,2]. In order to be able to evaluate the configurational average of the four-body correlation functions, that appear in the Kubo formula for $D(\omega)$, the fluctuations beyond the mean-field (SCBA) saddle point have been considered. This procedure yields for the diffusivity the result

$$D(\omega) \propto \ell_0(\omega)\omega^2/g(\omega) \quad . \qquad (*)$$

Here $\ell_0(\omega)$ is the scattering mean-free path, and $g(\omega)$ is the density of states, both to be calculated in mean-field approximation (SCBA). In order to calculate the thermal conductivity by summing over frequency with the proper quantum weight factor, one has to overcome a problem common to all harmonic theories of thermal conductivity, namely the fact that for small frequencies $D(\omega)$ diverges as $D(\omega) \propto \omega^{-4}$ (Rayleigh law). In reality this divergence is cut off by inelastic scattering. The contribution of inelastic scattering from two-level defects can be described as $D_{in}(\omega)^{-1} = C_{in}\omega$, where C_{in} is a constant, which does not vary much from material to material. For the thermal conductivity we have therefore

$$\kappa(T) \propto \int \mathrm{d}\omega g(\omega) \left[D(\omega)^{-1} + D_{in}(\omega)^{-1}\right]^{-1} (\omega/T)^2 \frac{e^{\hbar\omega/k_BT}}{[\exp\{\hbar\omega/k_BT\} - 1]^2} \quad . \qquad (**)$$

In Fig. 4.7 we compare several measured $\kappa(T)$ data versus the temperature, divided by the Debye temperature θ_D, as compiled by Freeman and Anderson [3]. It is clearly seen, how the boson

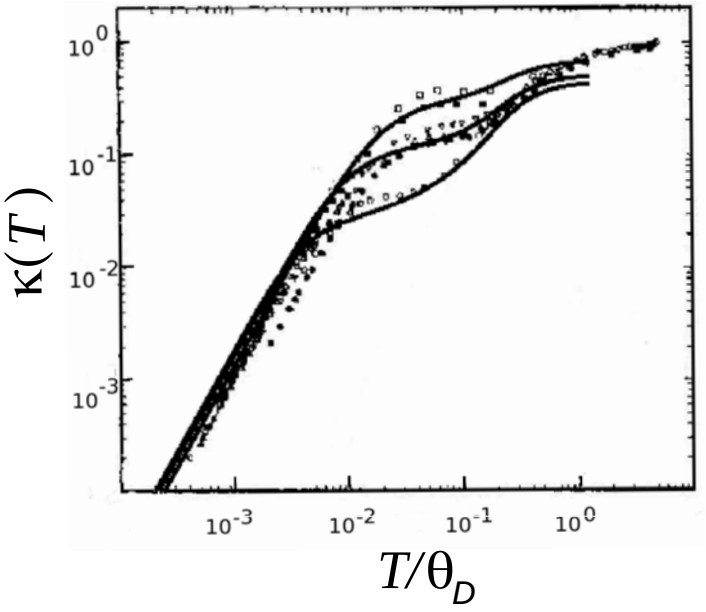

Figure 4.7:
Scaled thermal conductivity data of several glasses (from top to bottom): PB, PMMA, PET, B_2O_3, PS, SiO_2, as compiled by Freeman and Anderson [3] together with the calculations based on equations (*) and (**) using the SCBA density of state [2] for the following values of the disorder parameter: $\gamma_\mu = 0.15, 0.164,$ and0.1664.

peak [1,2] is related to the plateau: The plateau appears in a temperature regime that corresponds to the energy $\hbar\omega$ of the boson peak. It is shifted down in energy as the disorder increases. It is interesting to note that obviously SiO_2 is the material with the strongest disorder and that the Freeman-Anderson scaling may serve as a means to classify glassy materials with respect to their degree of disorder.

[1] E. Maurer, W. Schirmacher, J. Low-Temp. Phys. **137**, 453 (2004).

[2] W. Schirmacher, submitted to Phys. Rev. Letters (2005). See also the previous two contributions to this annual report

[3] J. J. Freeman and A. C. Anderson, Phys. Rev. B **34**, 5684 (1986).

Rotational and translational glass dynamics studied by nuclear resonant scattering of synchrotron radiation

I. Sergueev[1], U. van Bürck, A. I. Chumakov[2,3], T. Asthalter[4], G. V. Smirnov[3], H. Franz[5], R. Rüffer[2], W. Petry

[1] TUM, E13; ESRF, Grenoble
[2] ESRF, Grenoble
[3] Russian Research Center 'Kurchatov Institute', Moscow
[4] Institut für Physikalische Chemie, Universität Stuttgart
[5] Hasylab, Hamburg

The microscopic understanding of the liquid-glass transition remains a subject of contemporary debates. Whereas relaxation of the undercooled liquid state above the critical temperature T_c is well described by the mode coupling theory (MCT) [1], the dynamics below this temperature is still under discussion. Below T_c a characteristic feature observed in many experiments [1] is the decoupling of different relaxation processes. Such a decoupling could explain the origin of the slow β (Johari-Goldstein) relaxation [2], which might be due to molecular rotation remaining active even when translational motion of the molecules has been frozen out [3].

In order to understand the relaxational processes on a microscopic level and to distinguish between translational and rotational modes of motion we have applied Nuclear Forward Scattering (NFS) of synchrotron radiation (SR) and SR based Perturbed Angular Correlation (SRPAC) [4]. Both methods are sensitive to nuclear spin dynamics, which is coupled to the molecular rotations. In addition, NFS is also sensitive to translational motions on an atomic length scale. Thus the combination of NFS and SRPAC allows one to separate rotational and translational dynamics. NFS, as a spatially coherent scattering process, is bound to recoilfree scattering, whereas SRPAC, as an incoherent process, does not depend on recoil.

We applied NFS and SRPAC to investigate the dynamics of dibutyl phthalate (DBP) (glass transition temperature T_g=178K) using probe molecules of ferrocene (FC) enriched with ^{57}Fe [4]. Below and in the vicinity of T_g, the dynamics of DBP is described by α and slow β relaxation processes [5]. The FC molecule has an Fe atom in the center of mass between two cyclopentadienyl rings which produce an electric field gradient at the iron site and, correspondingly, a quadrupole splitting of the nuclear level. The molecular rotation does not change the position of the Fe atom and is seen only by the nuclear spin. The experiment has been carried out at the Nuclear Resonance beamline ID18 at ESRF. SRPAC was measured in the temperature range 100-330 K. Simultaneous NFS measurements were performed up to 210 K where the Lamb-Mössbauer factor vanishes.

The data evaluation has been performed assuming that the reorientation of the FC molecules proceeds via angular jumps with characteristic rate λ_r according to the strong collision (random angular jump) model [6,7]. The same model of molecular rotation was applied to treat the NFS data taking into account translational dynamics as well [8]. It was shown that in the slow relaxation regime the influence of dynamics leads to an additional decay of the NFS spectra with relaxation rate λ_{NFS} which is equal to the sum of λ_r and the translational relaxation rate λ_t. Using both SRPAC and NFS results we have obtained λ_r and λ_t separately. They are shown in Fig.4.8.

Reliable data for λ_r were obtained in a frequency range of $2 \cdot 10^6 - 4 \cdot 10^{10}$ Hz and a temperature range of 180-328 K. The rotational relaxation rate follows different temperature dependences abo-

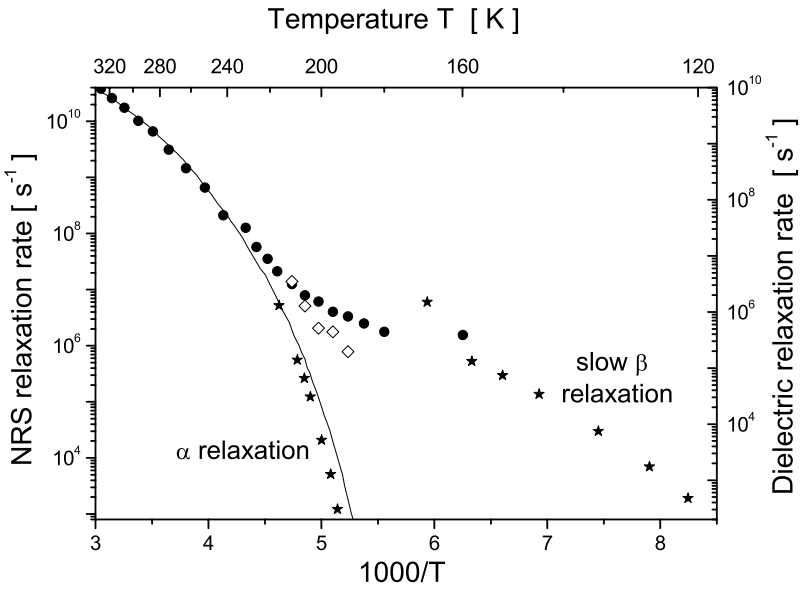

Figure 4.8:
Comparison of the rotational (●) and translational (◇) relaxation rates of the probe molecules (left side scale) to the DS data for pure DBP (right side scale) from [9] (solid line) and [5] (⋆).

ve and below 210 K. Below this temperature an Arrhenius dependence and above a viscous-like behaviour is observed. The translational relaxation rate λ_t has been obtained in the temperature range 190-210 K. Below 190 K the difference between λ_{NFS} and λ_r becomes smaller than the estimated error of these parameters. One can see that λ_t increases much faster with temperature than λ_r.

In the same Fig. 4.8 we compare our results for the dynamics of the probe FC molecule in DBP to data on pure DBP from dielectric spectroscopy (DS) [5,9]. The DS data were scaled to match our data at room temperature. In the undercooled liquid regime, the relaxation rate measured by DS consists of a single branch, which coincides with our data for the rotational relaxation of the FC probe molecule. Below 220 K, the DS data split into two branches. The branch of slow β relaxation is followed by our data on rotational dynamics, whereas the branch of α relaxation decreases approximately in parallel with our data on translational relaxation.

Thus, below 210 K, the dynamics of the probe decouples into two branches, similar to the dynamics of DBP. For the probe we have identified the branches with rotational and translational motion. The coincidence of the slow β relaxation branches for probe and DBP suggests that also in DBP the slow β relaxation is connected with rotational motion.

[1] W. Götze and L. Sjögren, Rep. Prog. Phys. **55**, 241 (1992)

[2] G. P. Johari and M. Goldstein, J. Chem. Phys. **53**, 2372 (1970)

[3] L. J. Lewis and G. Wahnström, Phys. Rev. E **50**, 3865 (1994)

[4] I. Sergueev, U. van Bürck, A. I. Chumakov, T. Asthalter, G. V. Smirnov, H. Franz, R. Rüffer, W. Petry: Ann. Report TUM Physik-Dep. E13, 39 (2001) and 7 (2002)

[5] S. A. Dzyuba and Yu. D. Tsvetkov, J. Struct. Chem. **28**, 343 (1987)
[6] S. Dattagupta, *Relaxation phenomena in condensed matter physics* (Academic Press, Orlando, 1987)
[7] I. Sergueev, PhD-thesis, TU-München (2004)
[8] S. Dattagupta, Phys. Rev. B **12**, 47 (1975)
[9] P. K. Dixon *et al.*, Phys. Rev. Lett. **65**, 1108 (1990)

SRPAC: application to a plastic crystal

T. Asthalter [1], U. van Bürck, I. Sergueev[2]

[1] Institut für Physikalische Chemie, Universität Stuttgart
[2] TUM E13; ESRF Grenoble

Synchrotron Radiation based Perturbed Angular Correlation (SRPAC) [1] has been proven to yield valuable information on molecular rotations in a glassy system [2]. In addition to the prospect to separate translational from rotational dynamics in combination with nuclear forward scattering (NFS), SRPAC yet has another advantage to offer: All systems having a negligible Lamb-Mössbauer factor, i.e. systems where both classical Mössbauer spectroscopy and (even more) NFS necessarily fail, are now amenable to dynamics studies provided they exhibit a hyperfine splitting.

We present new data on octamethyl-ethinyl-ferrocene (OMFA), a plastic crystal studied by us previously using NFS, powder diffraction, and differential scanning calorimetry (DSC) [3] as well as nuclear inelastic scattering [4]. Plastic crystals form a mesophase with translational symmetry but rotational disorder between the ordered crystalline and the liquid phase. Prominent examples are fullerene C_{60}, higher alkanes and Langmuir monolayers of surfactants. Supercooling of such mesophases, also called rotator phases, under freezing of rotational disorder may yield an orientational glass [5], whose dynamics provides partial insight into the physics of the glass transition [6].

Like some other highly substituted ferrocenes, OMFA exhibits a sharp decrease of the Lamb-Mössbauer factor far below the melting point T_m = 436 K [7]. This phenomenon was shown to be due to a first-order solid-solid phase transition to a nearly cubic rotator phase at $T_{pc} \approx 240$ K (as obtained from calibrated DSC) having a wide thermal hysteresis [3]. X-ray powder diffraction revealed that the rotation is most probably nearly free, however direct experimental evidence has been lacking so far.

Dielectric spectroscopy has been used extensively to study the dynamics of plastic crystals over a wide frequency range [8]. In the case of molecules with a small molecular dipole moment such as OMFA, however, X-ray or neutron scattering techniques are more promising. We therefore studied OMFA by SRPAC in order to learn more about the phase transition and the mechanism of the rotation. The experiment was carried out at the Nuclear Resonance beamline ID18 at the ESRF in single-bunch mode. A nested high-resolution monochromator yielding an overall energy resolution of 6 meV was used. The sample, a pressurized pellet of about 0.35 mm thickness, was mounted between thin Be sheets into a copper holder sealed with Kapton windows in a closed-cycle cryostat. Comparison of NFS spectra of the low-temperature phase during the first and subsequent heating cycles showed that the pressurizing process did not induce any noticeable texture that would affect the depth of the quantum beat minima.

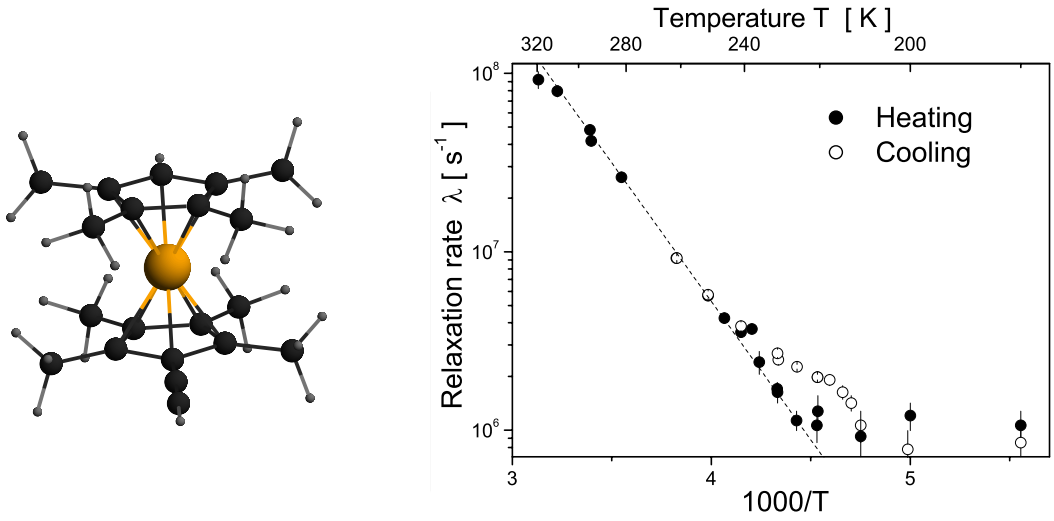

Figure 4.9: Molecular geometry (left) and rotational relaxation rate (right) of OMFA

The rotational relaxation rate λ of OMFA versus temperature was obtained through a full hysteresis cycle, as shown in Fig. 4.9 (right). For data fitting, the strong-collision model, which assumes unhindered random angular jumps [9,10], gave a satisfactory description of the time spectra over the entire temperature range. We can therefore conclude that SRPAC has provided us with the first direct evidence of quasi-free rotation in the rotator phase of OMFA. SRPAC is not very sensitive to mutual "gear-wheel"-type rotations of the two substituted cyclopentadienyl rings located at the same molecule, which were postulated in [11]. Instead, SRPAC provides us with a proof of reorientations of the EFG (which is oriented parallel to the ring–Fe–ring axis) and hence to reorientations of the entire OMFA molecule. Our method is therefore complementary to quasielastic neutron scattering, which "sees" both types of motion (see e.g. [12]).

It should be noted that on heating, rotational motion already sets in around 220 K, well below T_{pc}, where no trace of structural change appears in X-ray diffraction or DSC [3]. At $T = T_{pc}$, the dynamics shows no discontinuity but follows Arrhenius behaviour on heating (dotted line) with an activation energy of about 30 kJ mol^{-1} and a frequency factor of $8{\cdot}10^{12}$ s^{-1}. These values are roughly comparable with the ones found on formyl ferrocene [12].

On re-cooling, the Arrhenius plot of λ reveals a significant deviation from activated behaviour below T_{pc}; λ only drops to the low-temperature curve below the lower hysteresis point around 210 K. Deviations from Arrhenius behaviour and a Vogel-Fulcher-Tammann scaling of the relaxation rate have been described for some orientational glasses [8], where a slowing-down on cooling with respect to Arrhenius scaling was observed. In our case, the opposite is true, which rather suggests an incomplete energy transfer from the rotating OMFA molecules to their surroundings on cooling.

[1] I. Sergueev et al.: Ann. Report TUM Physik-Dep. E13, 39 (2001), Ann. Report TUM Physik-Dep. E13, 7 (2002), ESRF Highlights p.61 (2002)

[2] I. Sergueev et al.: ESRF Highlights p.12 (2003), Ann. Report TUM Physik-Dep. E13 (2004)

[3] T. Asthalter, H. Franz, U. van Bürck, K. Messel, E. Schreier, R. Dinnebier, J.Phys.Chem.Solids **64**, 677 (2003)

[4] T. Asthalter, U. van Bürck, H. Franz, E. Schreier, I. Sergueev, A. I. Chumakov, Ann. Report TUM Physik-Dep. E13, p.51 (2002)

[5] K. Adachi, H. Suga, S. Seki, Bull. Chem. Soc. Jpn. **41**, 1073 (1968)

[6] M. A. Ramos, S. Vieira, F. J. Bermejo, J. Davidowski, H. E. Fischer, H. Schober, M. A. González, C. K. Loong, D. L. Price, Phys. Rev. Lett. **78**, 82 (1997)

[7] R. H. Herber and I. Nowik, Hyperfine Int. **126**, 127 (2000)

[8] R. Brand, P. Lunkenheimer, and A. Loidl, J. Chem. Phys. **116**, 10386 (2002)

[9] S. Dattagupta and M. Blume, Phys. Rev. B **10**, 4540 (1974)

[10] I. Sergueev, PhD thesis, TU München (2004)

[11] H. Schottenberger, K. Wurst, and R. H. Herber, J. Organomet. Chem. **625**, 200 (2001)

[12] M. F. Daniel, A. J. Leadbetter, R. M. Richardson, J. Chem. Soc.: Faraday Trans. 2 **77**, 1851 (1981)

5 High-Pressure Biophysics: Stability of Molecular Assemblies

Wolfgang Doster

Hydrostatic pressure is used as a tool to probe molecular interactions in protein assemblies. Thermodynamic equilibra shift under pressure towards states of lower volume. During 2004 the equipment of the HP-group was further expanded: High pressure FTIR-spectroscopy using a homemade diamond anvil cell (N. Takeda), high pressure dynamic light scattering at different scattering angles (R. Gebhardt) and high pressure nano-second optical spectroscopy (X. Cai) are now in operation. Inelastic neutron scattering experiments at the ILL in Grenoble to study structural dynamics and unfolding of proteins under high pressure were performed.

Figure 5.1: Diamond anvil cell with condensor in FTIR spectrometer

The projects are supported by the DFG research group, 'High pressure treatment of food', a collaboration with groups of the Bioscience Center in Weihenstefan and the SFB 533, 'Light-induced Processes in Biopolymers'. In the context of food treatment we study interactions in casein micelles and oligomeric proteins by applying high pressure dynamic light scattering. The dissociation of Ca-phosphate nano-particles from phospho-serine with in-situ FTIR-spectroscopy in a diamond anvil cell was observed. The first bachelor theses is presently performed in E13 with FTIR in collaboration with the microbiology institut in Weihenstephan (R. Gänzle). A structural phase transition in the membranes of bacteria modified by carbohydrates is studied versus temperature and pressure [1]. The role of cavities in proteins is addressed in flash photolyis experiments monitoring the internal ligand migration in myoglobin and the effect of pressure on water penetration. Cavities in antenna proteins and how they modify the compressibility was investigated by optical spectroscopy with the group of P. Braun at the LMU. At the International High Pressure Conference on Bioscience and Biotechnology in Rio de Janeiro 2004 three contributions, on ligand binding kinetics, casein micelles and hemocyanin dissociation were presented. Solvent viscosity and protein dynamics was discussed at the International Conference on Biological Physics in Göteborg. With S. Longeville from the LLB in Paris we analyse protein diffusion in concentrated solutions, such as diffusion of hemoglobin inside blood cells. Apart from direct interactions, hydrodynamic forces play a major role. Further experiments on the technique of neutron elastic resolution spectroscopy were performed with V3 at the HMI in Berlin. This project, supported by the BMBF, terminated in 2004. N. Takeda left the group to take a position in Japan. Three invited review articles on 'Pressure-Temperature Phase Diagrams of Proteins' (with J. Friedrich) [2], 'Protein-Water Displacement Distributions'[3] and 'Proteins Dynamics'[4] were written.

[1] A. Molina Hoeppner, W. Doster, R. Vogel and M. Gänzle in Applied and Environmental Microbiology **70**, 2013 (2004)

[2] W. Doster and J. Friedrich, Pressure-temperature phase diagrams of proteins in: Handbook of Protein Folding, editors: Th. Kiefhaber and J. Buchner, John Wiley, 2005.

[3] W. Doster, Protein-water displacement distributions, Biochem.Biophys. Acta, Proteins and Proteomics, Special Edition (2004) submitted

[4] W. Doster, Protein Dynamics, in Neutrons for Biology, Methods and Applications, Ed. R. Gutberlet and J. Fitter, Springer (2004) submitted

Pressure Dissociation of Casein Micelles

R. Gebhardt, W. Doster, J. Friedrich [1] and U. Kulozik [2]

[1] TU München, Lehrstuhl für Physik, Weihenstefan

[2] Institut für Milchwissenschaften, TU Weihenstefan

Casein micelles are polydisperse particles, diameter 200 nm, which constitute 80% of the protein normally found in bovine milk. They mainly consist of a mixture of α-, β- and κ-casein in the ratio 5:4:1 and colloidal calcium phosphate particles. The physiological function of casein micelles is the transport of insoluble calcium salt to the neonates. Since casein proteins do not crystallize structural details of the quaternary structure of caseins – the casein micelle – are still under discussion. In the casein subunit model spherical sub-micelles (20 nm) are assumed. The dual binding model (Horn,2003), a representative of internal structure models, focus on specific interactions between the constitutents of the micelle. The individual casein molecules are considered as block copolymers interacting via hydrophobic and electrostatic forces. Pressure allows to probe the different contributions to stability by shifting equilibria towards compact states. Since molecular assemblies stabilized by hydrophobic forces require more volume than the monomers, they dissociate under pressure. Due to electrostriction also charges are stabilized by pressure.

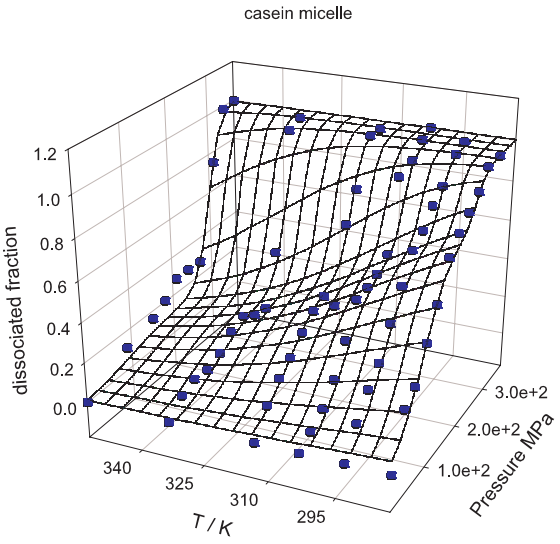

Abbildung 5.2: Pressure dissociation transition of casein observed by light scattering

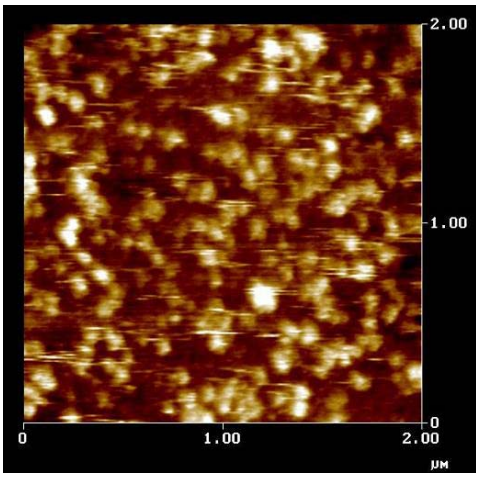

Abbildung 5.3: AFM-map of pressure-treated casein

Changes in size and molecular weight are recorded in situ with a dynamic light-scattering machine (ALV) equipped with a four window high-pressure cell. Since the casein solutions are generally turbid in native concentrations, experiments in extreme back-scattering geometry (177°) are performed. The casein micelle dissociate in two steps, as shown in fig. 1, depending on temperature, pH and calcium concentration. The stability increases with increasing temperature, Ca concentration and pH. A thermodynamic model assuming two micelle conformations accounts for the data, the fits are shown as lines in fig. 1. After pressure application the structure of the micelles was studied with AFM experiments in a liquid cell. Size distribution functions were determined based on AFM maps taken across the transition. A compact micelle was observed as a new intermediate induced by pressure treatment (Fig. 2).

Support from the DFG-research group Hochdruckbehandlung von Lebensmitteln is gratefully acknowledged.

[1] R. Gebhardt, W. Doster, U. Kulozik, Pressure dissociation of casein micelles, the effect of temperature, J.B.Biol.Med. (2004) submitted

Pressure-Effects on the Quaternary Structure of Hemocyanins

R. Gebhardt, W. Doster, H. Decker [1]

[1] Universität Mainz, Lehrstuhl für Biophysik

Hemocyanins are large multisubunit protein complexes which are dissolved in the haemolymph of arthropods. The physiological task is to store and transport oxygen. Figure 1 shows a schematic view of the hemocyanins. One single kidney-shaped subunit (a) of the hemocyanin oligomer has a molecular weight in the 75 kDa range. Three subunits associate to form trimers and hexamers (b). Depending on species or physiological conditions hexamers combine to multiple hexamers (2-8 x 6). For our investigations we studied a 12-meric lobster and a 24-meric spider

hemocyanin. The hemocyanin of the lobster Homarus americanus (940 kDa) has a dodecameric subunit structure (c) organized from two basic hexameric units. The 24-meric hemocyanin of the tarantula Eurypelma californicum (d) consist of four identical dodecamers with an estimated total molecular mass of about 1.8 MDa.

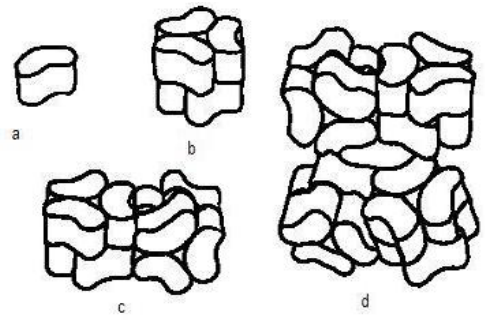

Figure 5.4:
Schematic view of arthropods hemocyanins. a) Subunit, b)hexamer, c) dodecamer of the lobster Homarus americanus, d) 24-mer of the tarantula Eurypelma californicum (Lamy et.al.(1981)

The hemocyanins exhibit high cooperative oxygen binding. In addition oxygen binding is regulated by allosteric effectors such as protons, L-lactate and urate analogues. Beside protons which decrease oxygen affinity (Bohr effect) all other effectors increase the oxygen affinity. A specific arrangement of the subunits within the 12- and 24-meric complexes is necessary for the full biological activity.For lack of a crystal structure functional and stability measurements have to be done to understand how this giant molecules work. Arthropod hemocyanins can be dissociated by various procedures such as increasing pH, removing divalent cations, dialysis against urea or by use of hydrostatic pressure. Stability studies which use Hofmeister salts and denaturants such as urea and GdnCl propose a sequential dissociation for the dodecameric crustacean hemocyanin (Herskovits, 1981) whereas the 24-meric tarantula hemocyanin dissociate completely in its monomers without any intermediates (Hübler et.al, 1998). It was found that the subunits are connected via hydrophilic and polar interactions. We have used pressure dependent static and dynamic light scattering to observe changes in the molecular weight and size distribution during the dissociation process. The pressure stability under similar conditions of the 24meric spider hemocyanin was measured in comparison to the dodecameric lobster hemocyanin. Furthermore the influence of the ligand carbon monoxide and the effector L-lactate on the stability of the dodecameric hemocyanin was tested.

The pressure dependent dissociation curves of the 12-meric crustacean hemocyanin are biphasic. The first step can be attributed to the dodecamer-hexamer equilibrium, the second step to the hexamer-monomer equilibrium. For the dissociation of the 24meric tarantula hemocyanin no intermediate such as dodecamers or hexamers could be observed. Both results are in accordance with the stability measurements by (Herskovits, 1981) and (Hübler, 1998). Extending the dodecamer-hexamer-monomer dissociation model of (Herskovits, 1981) by a pressure dependent free energy term, dissociation constants and volumes could be estimated. In case of the 24meric tarantula hemocyanin a 24mer-monomer equilibrium was assumed. Additionally by measuring intensity correlation functions radii distributions were estimated along the dissociation process.

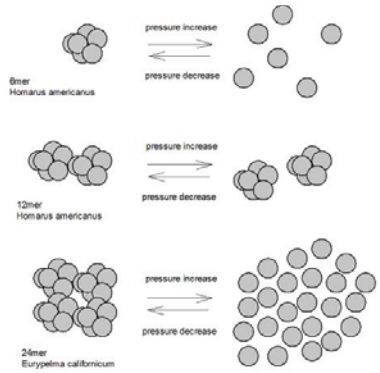

Figure 5.5:
Tested dissociation mechanisms for the hexamer, dodecamer and 24mer of arthropod hemocyanins

A new model was necessary to explain the dissociation of the dodecameric lobster hemocyanin under the influence of L-Lactate.

Das Projekt wird im Rahmen der DFG-Forschergruppe, Hochdruckbehandlung von Lebensmitteln gefördert.

[1] Lamy J., Bijholt M.M.C., Sizaret P-Y, Lamy J., van Bruggen E.F.J. (1981) Biochemistry, 20, 1849-1856

[2] Herskovits T.T., San George R.C., Erhunmwunsee L.J. (1981) Light-Scattering Investigation of the Subunit Dissociation of Homarus americanus Hemocyanin. Effect of Salt and Ureas. Biochemistry, 20, 2580-2587

[3] Hübler R., Fertl B.,Hellmann N., Decker H. (1998) On the stability of the 24-meric hemocyanin from Eurypelma californicum. BBA, 1383, 327-339

[4] Van Holde K.E., Miller K.I. (1995) Hemocyanins. Adv.Protein Chem. 47, 1-81 Gebhardt R., Decker

[5] R. Gebhard and W. Doster, Pressure-Effects on the Quaternary Structure of Hemocyanins, to be published

Spectroscopy and Kinetics of Myoglobin under High Pressure

X. Cai and W. Doster

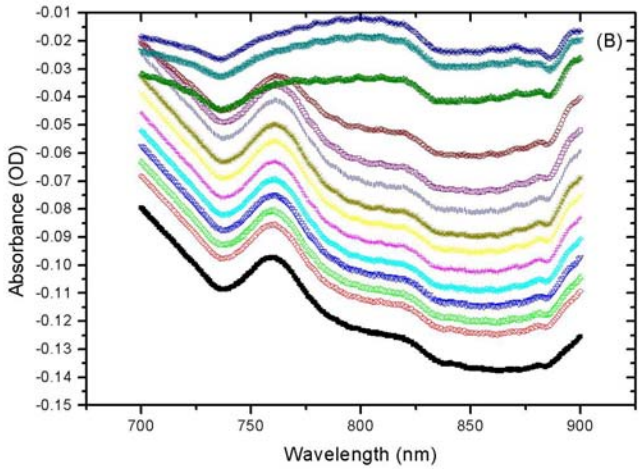

Abbildung 5.6:
Spectrum of the charge-transfer band III at 760 nm versus pressure, the broadening indicates unfolding

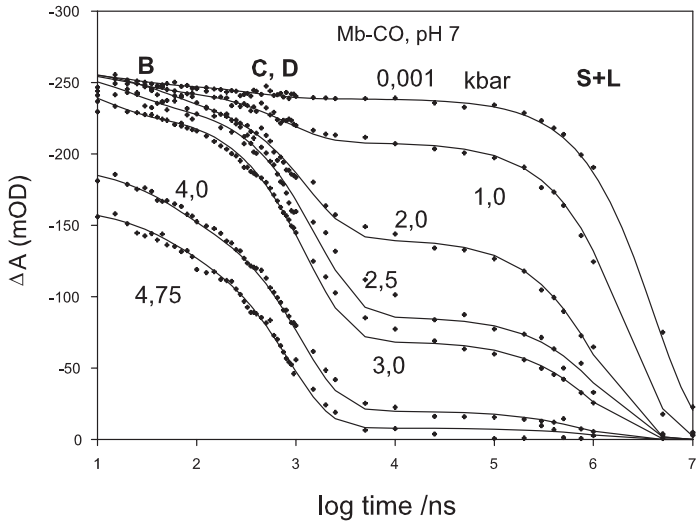

Abbildung 5.7: Kinetics of CO-binding to myoglobin under pressure

Pressure is an efficient tool to explore the active site of proteins. Pressure-dependent research has several advantages with respect to conventional temperature-studies: (1)Changing the pressure one varies the volume without affecting the thermal energy of the system, with temperature one varies both, (2) experiments can be done in aqueous solution down to -20 C (2 kbar) due to the freezing point depression, and (3)pressure-induced denaturation of proteins is different from heat denaturation.

Structure-sensitive absorption spectra under high pressure are also useful to interpret kinetic data. For deoxy-myoglobin, the intensity of the spectrum of the charge-transfer band (III) at 760 nm is sensitive to the heme-iron displacement(1): The closer the iron to the heme plane, the stronger the intensity of the band III. The intensity of band III shows only small changes at low pressures (Figure 1), while a nonlinear increase is observed at higher pressure. The nonlinear relationship between intensity and pressure and the change in linewidth indicates structural changes, where the heme group is exposed to the solvent. Fig. 2 shows the kinetics of CO-binding to myoglobin at various pressures using flash photolyis. The most drastic change concerns the amplitude of the slow process, which is the ligand escape fraction. Ligand transfer to the solvent involves the creation of a cavity (32 ml/mol) and a corresponding cavity energy which increases with the pressure increased. From the data one can extract the volume changes of the reaction, in particular two water molecules exchanged with the CO-ligand. The internal ligand migration steps are much less affected by pressure, indicating a low protein compressibility.

The project is supported by the DFG (SFB 533), Light-Induced Processes in Biopolymers.

[1] Stefan Franzen, Stacie E. Wallace-Williams, and Andrew P. Shreve, Heme charge-transfer band III is vibronically coupled to the Soret Band, J. Am. Chem. Soc. (2002). 124: 7146-7155

[2] A.B.P. Lever, Harry B. Gray. Iron porphyrins. Addison-wesley publishing company. 1982